

**Laboratory Investigations on the Applicability
of Triphenoxymethanes as a New Class of Viscoelastic Solutions
in Chemical Enhanced Oil Recovery**

By the Faculty of Geosciences, Geotechnics, and Mining
of the TU Bergakademie Freiberg

approved

DOCTORAL THESIS

to attain the academic degree of

Doktor-Ingenieur

Dr.-Ing.

by Dipl.-Ing. Christin Dieterichs
born on 25 April 1989 in Stendal

Assessors: Prof. Dr.-Ing. Moh'd Amro, Freiberg
Prof. Dr. Ingebret Fjelde, Stavanger
Dr. Foppe Visser, Braunatal

Date of the award: 30.01.2018

Declaration of Authorship

I, Christin Dieterichs, declare that this thesis and the work presented in it are my own and have been generated by me as the result of my own original research.

I confirm that I have acknowledged all main sources of help. Where I have consulted the published work of others, this is always clearly attributed. Where I have quoted from the work of others, the source is always given. With the exception of such quotations, this thesis is entirely my own work. Where the thesis is based on work done by myself jointly with others, I have made clear exactly what was done by others and what I have contributed myself.

Nobody received any financial payment from me for any work done for me. Neither this thesis nor parts of this work have previously been published in the same or a similar form in Germany or abroad.

Place, Date

Signature

Acknowledgement

This thesis was prepared within the framework of a joint research project headed by Wintershall Holding GmbH together with BASF and other university partners. It was financially supported by Wintershall Holding GmbH.

Including on behalf of the Institute of Drilling Engineering and Fluid Mining I want to express my deep thanks to Wintershall Holding GmbH for giving me the opportunity to work on an innovative and exciting research topic for the last years.

My sincere gratitude goes to Prof. M. Amro, my doctoral supervisor, for his professional guidance throughout the whole project. I appreciate all his contributions of time, ideas, and support.

In particular, I want to thank Dr. L. Siggel for the excellent professional support and the engagement to provide some new paths of research when another seems to reach an impasse.

I also want to acknowledge Dr. F. Visser, who always asked the right questions to promote my research and point out new challenges. He is a very inspiring person to me and encouraged me never to lose my curiosity and scrutinize everything.

There are many other persons, who were involved in the research project and all their work and results were incredibly valuable to me. I want to take this opportunity to sincerely thank all of them, especially Dr. M. Nowak, Dr. M. Hansch, Dr. A. Skauge and Dr. T. Skauge, S. Reimann, V. Boyko, and M. Radloff to mention only a few of these great researchers.

I was lucky to spend the last years at the Institute of Drilling Engineering and Fluid Mining in Freiberg and I want to thank all my former and current colleagues. I had such a great time with you. To produce good results you need a congenial work environment. This place was a source of friendship, collaboration, and knowledge to me. Most of all I want to thank Angelika, Heike, Ingo, Katja, Martin, Martina, Phillip, Romy, Sabine, Sven and Uwe for always having an answer when my head was full of question marks and making the impossible possible to keep the experiments going.

Of course, I have to thank my whole family: my sister, my grandparents, aunts, and uncles. I know you will always stand behind me and that is a very good and comforting feeling.

Special thanks go, of course, to my parents for always believing in me, supporting and encouraging me to go my way. Even if mom thought that a clean white doctor's coat would fit me better than oil stained workwear at first, and daddy sometimes wondered which part of my work could take so much time. I love you!

In the end, I have to thank Wusel and Mompel for being my private wingman and bringing so much sunshine into my life.

Abstract

Even in times of renewable energy revolution fossil fuels will play a major role in energy supply, transportation, and chemical industry. Therefore, increasing demand for crude oil will still have to be met in the next decades by developing new oil reserves. To cope with this challenge, companies and researchers are constantly seeking for new methods to increase the recovery factor of oil fields.

For that reason, many enhanced oil recovery (EOR) methods have been developed and applied in the field. EOR methods alter the physico-chemical conditions inside the reservoir. One possibility to achieve this is to inject an aqueous solution containing special chemicals into the oil-bearing zone. Polymers, for example, increase the viscosity of the injected water and hence improve the displacement of the oil to the production well. The injection of surfactant solutions results in reduced capillary forces, which retain the oil in the pores of the reservoir.

Some surfactants form viscoelastic solutions under certain conditions. The possibility to apply those solutions for enhanced oil recovery has been investigated by some authors in the last years in low salinity brines. Reservoir brines, however, often contain high salt concentrations, which have detrimental effects on the properties of many chemical solutions applied for EOR operations. The Triphenoxymethane derivatives, which were the subject of study in this thesis, form viscoelastic solutions even in highly saline brines. The aim of this thesis was to investigate the efficiency and the mode-of-action of this new class of chemical EOR molecules with respect to oil mobilization in porous media.

Abbreviations

AS	alkaline – surfactant (flooding)
ASP	alkaline – surfactant – polymer (flooding)
ASTM	American Society for Testing and Materials
CCP	Clean Power Plan
CF	core flood
CMC	critical micelle concentration
cum oil	cumulative oil production
dyn.	dynamic
EOR	enhanced oil recovery
FC	filtration core
HLB	hydrophilic-lipophilic balance
HPAM	hydrolyzed polyacrylamide
HT/HP	high temperature/high pressure
IFT	interfacial tension
LPG	liquefied petroleum gas
MC	main core
MW	molecular weight
OBT	oil breakthrough
OOIP	original oil in place, initial oil saturation
PAM	polyacrylamide
PV	pore volume
RF	resistance factor
RRF	residual resistance factor
SFT	surface tension

SP surfactant-polymer (flooding)

stat. static

TDS total dissolved solids

UV ultraviolet

WBT water breakthrough

Symbols**Latin**

Symbol	Description	Unit
A_0	surface area	m ²
a_0	specific surface area	m ² /g
a	cross-sectional area of "head" group of surfactant	m ²
c	concentration	ppm; mol/l
c_{surf}	surfactant concentration	wt. %
D_{cs}	cross section diameter of a worm-like micelle	m
De	<i>Deborah</i> number	-
$De_{crit.}$	critical <i>Deborah</i> number	-
E	Energy	J; Btu
E_D	microscopic displacement efficiency	-
$E_{vol.}$	macroscopic (volumetric) sweep efficiency	-
F	recovery factor	-
f_w	fractional flow	-
G	shear modulus	Pa
g	gravitational acceleration	m/s ²
G'	storage modulus	Pa
G''	loss modulus	Pa
k	absolute permeability of rock/reservoir	m ² ; D
k_o	phase permeability of oil phase	m ² ; D
k_{ro}	relative permeability of oil phase	-
$k_{ro}(S_w)$	relative permeability of oil phase as a function of water saturation	-
$k_{ro}(S_{wi})$	relative permeability of oil phase at irreducible water saturation	-

k_{rw}	relative permeability of aqueous phase	-
$k_{rw}(S_{or})$	relative permeability of aqueous phase at residual oil saturation	-
$k_{rw}(S_w)$	relative permeability of aqueous phase as a function of water saturation	-
k_w	phase permeability of aqueous phase	m ² ; D
L	contour length of a worm-like micelle	m
l	length of a core	m
L_c	maximum effective length of the "tail" group of a surfactant	D
l_p	persistence length	m
M	mobility ratio	-
n	porosity	-
N_1	first normal stress difference	Pa
N_B^{-1}	inverse <i>Bond</i> number	-
N_C	capillary number	-
N_p	ratio of cumulative produced oil	-
P	packing parameter	-
p	pressure	Pa
p_c	capillary pressure	Pa
p_{nw}	pressure in the nonwetting phase	Pa
p_w	pressure in the wetting phase	Pa
r	radial coordinate	m
r_p	pore radius	m
S_{oR}	remaining oil saturation	-
S_{or}	residual oil saturation	-
S_w	water saturation	-
$\overline{S_w}$	average water saturation of a reservoir	-
S_{wi}	irreducible water saturation	-

SG_{API}	API gravity	°API
t	time	s
t_0	starting time (of experiment)	s
t_c	characteristic time	s
t_r	relaxation time	s
$\tan\delta$	dissipation factor	-
V	volume	m ³
v	flow velocity	m/s
v_D	<i>Darcy</i> velocity	m/s
$\overline{v_{max}}$	average maximal flow velocity	m/s
v_p	pore velocity	m/s
We	<i>Weissenberg</i> number	-

Greek

Symbol	Description	Unit
γ	(shear) deformation amplitude	-
$\dot{\gamma}$	shear rate	1/s
η	dynamic viscosity	Pa·s
$ \eta^* $	complex viscosity	Pa·s
η_o	dynamic viscosity of the oil phase	Pa·s
η_w	dynamic viscosity of the aqueous phase	Pa·s
θ	contact angle	°
ϑ	temperature	°C
κ_o	<i>Corey</i> exponent for oil phase	-
κ_w	<i>Corey</i> exponent for aqueous phase	-
λ	wavelength	nm
ρ	density	kg/m ³
σ	interfacial tension	mN/m
τ	shear stress	Pa
τ_{xx}	normal stress in the direction of flow	Pa
τ_{yy}	normal stress perpendicular to the direction of flow	Pa
ω	angular frequency	1/s

Conversion factors

$$1 \text{ Pa} = 10^{-5} \text{ bar}$$

$$1 \text{ m/s} = 1440 \text{ m/d} = 4724.4 \text{ ft/d}$$

Table of Contents

Declaration of Authorship	I
Acknowledgement.....	II
Abstract	IV
Abbreviations	V
Symbols	VII
Conversion factors.....	XI
Table of Contents	XII
1. Introduction	1
1.1 Objectives of the Thesis	3
2. Enhanced Oil Recovery.....	4
2.1 Phases of Oil Production and Displacement Efficiency.....	4
2.2 EOR Methods	9
2.2.1 Chemical Enhanced Oil Recovery Methods	12
3. Viscoelastic Surfactant Solutions	17
3.1 Surfactant Structures in Aqueous Solution.....	17
3.2 Some Rheological Aspects of Viscoelasticity	21
3.3 Interaction of Viscoelastic Surfactants with Reservoir Fluids.....	28
3.3.1 Viscoelastic Surfactants and Saline Solutions	28
3.3.2 Viscoelastic Surfactants and Oil	30
4. Viscoelastic Flooding in Chemical Enhanced Oil Recovery	31
4.1 Viscoelastic Polymers	31
4.2 Viscoelastic Surfactants	34

5.	The Triphenoxymethane Derivatives	41
5.1	TriX-MB.....	42
5.2	TriX-TA.....	44
5.3	TriX-M.....	44
6.	Experimental Procedure and Data Analysis.....	46
6.1	Materials Used	46
6.1.1	Synthetic Reservoir Brine and Saline Solutions	47
6.1.2	Surfactant Solutions	48
6.1.3	Sand and Core Material	50
6.2	Critical Micelle Concentration of TriX-M and Triton-X-100 in Synthetic Reservoir Brine	51
6.3	Static Adsorption of TriX Derivatives and Triton-X-100 on Sand.....	52
6.4	Interfacial Tension and Interaction of Solutions of TriX Derivatives and Triton-X-100 with Crude Oil	53
6.4.1	Interfacial Tension Measurements	54
6.4.2	Changes in surfactant concentrations in aqueous solutions after oil contact.....	54
6.5	Spontaneous Imbibition Tests.....	54
6.6	Investigations on Salt Effects on TriX-MB Solutions	56
6.7	Core Flooding Experiments	57
6.7.1	Experimental Setup.....	57
6.7.2	Core Preparation	59
6.7.3	Injection Tests	60
6.7.4	Oil Displacement Tests.....	62

7.	Results and Discussion	64
7.1	Critical Micelle Concentration of TriX-M and Triton-X-100 in Synthetic Reservoir Brine	64
7.2	Static Adsorption of TriX Derivatives and Triton-X-100 on Sand	67
7.3	Interfacial Tension and Interaction of Solutions of TriX Derivatives and Triton-X-100 with Crude Oil	71
7.3.1	Interfacial Tension to Bockstedt Oil	71
7.3.2	Changes in surfactant concentrations in aqueous solutions after oil contact	73
7.4	Spontaneous Imbibition Tests.....	76
7.4.1	TriX Derivatives and Triton-X-100 in NDIIa brine.....	77
7.4.2	TriX-MB in NaCl brine.....	78
7.4.3	Summary: Spontaneous Imbibition Tests	79
7.5	Investigations on Salt Effects on TriX-MB Solutions	82
7.6	Injection Tests	87
7.6.1	Injectivity of 0.1 wt. % TriX-MB in NDIIa solution in high permeable cores (Bentheimer sandstone, $k_{brine} \approx 1.5$ D)	87
7.6.2	Injectivity of 0.1 wt. % TriX-MB in NaCl solution in high permeable cores (Bentheimer Sandstone, $k_{brine} \approx 1.5$ D).....	91
7.6.3	Injectivity of 0.1 wt. % TriX-MB in NaCl solution in lower permeable cores (Michigan sandstone, $k_{brine} \approx 0.6$ D)	93
7.6.4	Injectivity of 0.1 wt. % TriX-TA in NDIIa solution	96
7.6.5	Injectivity of 0.1 wt. % TriX-M in NDIIa solution	98
7.6.6	Retention of TriX derivatives in Michigan Sandstone.....	100
7.6.7	Summary: Injection tests and Retention of TriX derivatives	103

7.7	Oil Displacement Tests.....	106
7.7.1	Secondary oil recovery experiments using 0.1 wt.% TriX-MB in NaCl	106
7.7.2	Secondary oil recovery experiments using 0.1 wt. % TriX-TA in NDIIa.....	110
7.7.3	Tertiary oil recovery experiments using 0.1 wt. % TriX-MB in NaCl .	113
7.7.4	Tertiary oil recovery experiment using 0.1 wt. % TriX-TA in NDIIa...	118
7.7.5	Tertiary oil recovery experiment using 0.1 wt. % TriX-M in NDIIa ...	121
7.7.6	Summary: Oil Displacement Tests	123
8.	Summary	132
8.1	Bulk Studies on TriX Derivatives and Triton-X-100	132
8.2	Imbibition Tests.....	133
8.3	Injectivity and Retention	134
8.4	Oil displacement.....	135
9.	Outlook.....	137
	Bibliography.....	138
	List of Figures.....	149
	List of Tables	155
	Appendix.....	158
A1	The hydrophilic-lipophilic balance (HLB)	159
A2	Densities and viscosities of the used aqueous solutions.....	160
A3	Pore size distributions of Bentheimer and Michigan sandstone.....	163
A4	The Buckley-Leverett model and Corey relative permeability functions	164

1. Introduction

We are living in times of a renewable energy revolution, and experts expect the consumption of non-fossil fuels to grow faster than the consumption of fossil fuels. However, fossil fuels are predicted to still account for around 75 – 78 % of energy use in 2040 by both the International Energy Agency and U.S. Energy Information Administration. Liquid fuels, which are often petroleum based, will remain the largest source in the energy mix (Figure 1-1). Especially the emerging economies and rising populations in Asia, the Middle East, and Africa will increase the demand for petroleum based fuels. Ongoing globalization also contributes to an increasing need for liquid fuel for worldwide transportation services in the next years. [1–3]

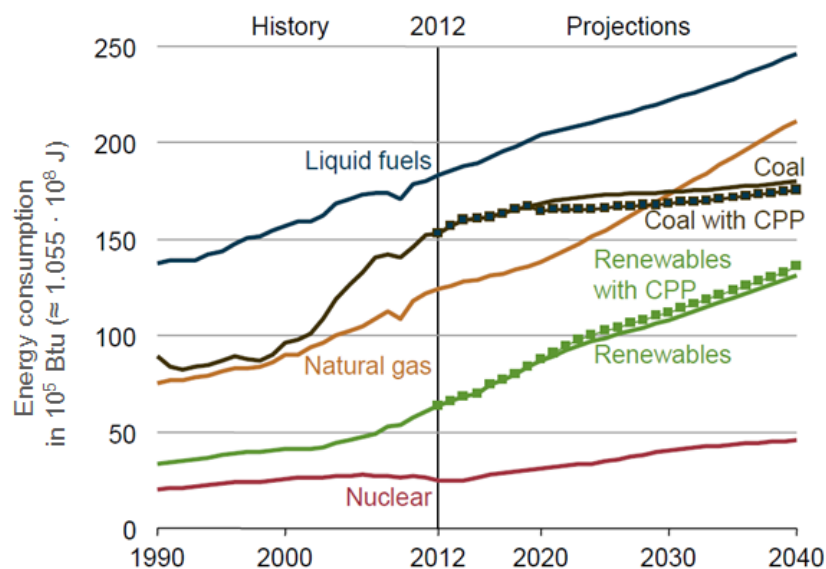


Figure 1-1: Total world energy consumption by energy source, 1990–2040, (CPP = Clean Power Plan) (after [1])

To meet these demands, new oil reserves have to be developed, either by the discovery of new oil fields or by increasing the recovery factor of mature fields. Since 2000 the latter reason primarily leads to the growth of proven reserves [1]. This requires technological advancement and innovation of so-called enhanced oil recovery (EOR) methods, which are characterized by altering the physico-chemical conditions in the reservoir.

During chemical EOR operations an aqueous solution containing special chemicals is injected into the oil-bearing zone. Polymers, for example, increase the viscosity of the injected water and hence improve the displacement of the oil to the production well. The injection of surfactant solutions results in reduced capillary forces, which retain the oil in the pores of the reservoir.

Some surfactants form viscoelastic solutions under certain conditions. This phenomenon has already been reported in 1976 [4]. In 1983 the Dow Chemical Company introduced this new class of thickeners in consumer products such as bleach, liquid dishwashing detergents and cosmetics [5]. These chemicals showed favorable rheological and lubrication properties. They effectively increased the viscosity of the aqueous solution and demonstrated shear thinning behavior without being sensitive to mechanical degradation. Due to their surface activity, the interfacial tension between phases was also reduced, and they could be used as emulsifiers. Viscoelastic surfactants have been broadly used in home and personal care products, as well as for industrial applications, for example as drag reducing agents in district heating and cooling fluid in Japan [6].

Since the late 1990s viscoelastic surfactant solutions have been successfully applied in oil field applications, such as selective matrix diversion, filter cake removal, and coiled tubing clean out. Because of their high particle transport capacity they are used as fracturing and gravel packing fluids. It is of particular interest for hydraulic stimulation operations that gelling of the viscoelastic surfactant solution is in some way controllable. For some systems, viscosity buildup can be initiated by adding special salt ions [7]. Then again the viscosity breaks down when the viscoelastic surfactant solution comes in contact with oil, which facilitates production from the reservoir [8].

Many of the mentioned characteristics of viscoelastic surfactant solutions are desirable for enhanced oil recovery chemicals. They seem to combine the advantages of polymers and surfactants. Researchers and companies are constantly seeking for new molecules and chemical structures to increase oil production. For these developments a thorough understanding of physical and chemical processes contributing to oil displacement and production under reservoir conditions is mandatory.

1.1 Objectives of the Thesis

In 2006 BASF started an R&D project to find new amphiphilic structures and patented the synthesis and usage of Triphenoxymethanes in 2011. In 2010 a joint research project was launched to understand the effects of this new class of viscoelastic surfactant structures in aqueous saline solution on oil displacement mechanisms in porous media. The Triphenoxymethanes have been tested for their applicability in enhanced oil recovery applications by a multidisciplinary team with expertise in synthesis, rheology, analytics, computational chemistry, and reservoir engineering [9]. During the project, other Triphenoxymethane derivatives with small variations in the chemical structure were steadily developed to improve the chemical properties with respect to oil mobilization, as well as to probe potential modes-of-action.

The objectives of this thesis were to investigate the behavior of some of the synthesized Triphenoxymethane analogs in porous media. This study should contribute to the assessment of the capability of Triphenoxymethanes to enhance oil recovery and to provide insight into the mode-of-action.

For this purpose, a comprehensive laboratory program was set up and implemented. The aims of the experiments were to understand the behavior of the Triphenoxymethanes in saline solutions and their interaction with the individual components of the oil reservoir (sandstone and oil) at first. Therefore, the critical micelle concentrations (CMC) were determined, static adsorption tests on sand were conducted, and interactions with reservoir oil were examined. Only after the interactions of the tested surfactant solutions with the reservoir components were separately analyzed and understood, experiments in porous media were carried out. Core flooding experiments were conducted under reservoir conditions to probe the injectivity of different Triphenoxymethane solutions, as well as to assess their potential regarding oil mobilization. Imbibition tests were also performed, as a quick and simple alternative to dynamic oil displacement in core floods, to better grade the results regarding oil recovery.

2. Enhanced Oil Recovery

In this chapter, the production phases of an oil field and factors influencing the efficiency of oil production are introduced. Furthermore, technological methods which are applied to increase the oil recovery are described.

2.1 Phases of Oil Production and Displacement Efficiency

Three production phases are usually distinguished during the development of an oil field. The primary production phase is often referred to as eruptive phase. After a well was drilled into an oil bearing formation, the higher energy (pressure) inside the reservoir forces the oil to surge to the surface.

When the natural energy within the reservoir decreases and becomes insufficient for oil production, the secondary production phase starts. It is characterized by means of pressure maintenance, such as gas injection into the gas cap of the reservoir or water flooding operations. The physico-chemical properties of the reservoir rock, oil and formation water are virtually unchanged. [10]

After the first and second production phase, only 20 – 40 % of the original oil in the reservoir are recovered on average [11]. The reason is that the oil is retained in the porous medium by several geological (e.g., reservoir heterogeneities) and physico-chemical reasons [12]. The remaining amount of oil is the target for enhanced oil recovery methods, which can be applied in the tertiary production phase. These processes are characterized by altering the interactions between reservoir rock, formation water, and the hydrocarbons to be produced. In most projects enhanced oil recovery methods are already applied before constant oil saturation was reached by secondary production.

Many EOR applications rely on the principle of water flooding. A fluid is injected into the reservoir to displace the hydrocarbons toward the production well. The displacement process is not piston-like, but oil and water flow simultaneously through the same pores [13]. Every phase is attributed with an own phase permeability; the oil phase permeability (k_o) or the water phase permeability (k_w). Usually, the relative

permeability, the ratio of phase permeability to absolute permeability (k), is used in reservoir engineering.

$$k_{ro} = \frac{k_o}{k} \tag{Eq. 2-1}$$

- k_{ro} – relative permeability of oil phase
- k_o – phase permeability of oil phase in m^2
- k – absolute permeability of reservoir in m^2

$$k_{rw} = \frac{k_w}{k} \tag{Eq. 2-2}$$

- k_{rw} – relative permeability of aqueous phase
- k_w – phase permeability of aqueous phase in m^2
- k – absolute permeability of reservoir in m^2

Relative permeabilities are highly dependent on reservoir saturation as shown in Figure 2-1.

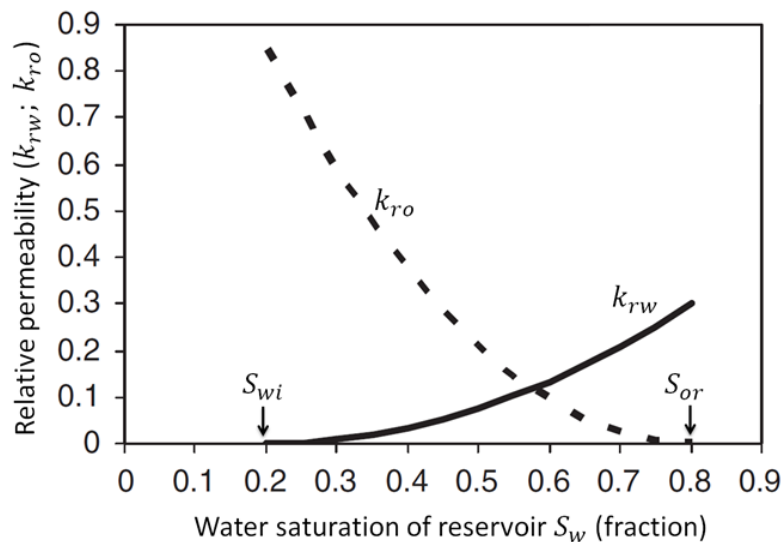


Figure 2-1: Relative permeability curves for water (k_{rw}) and oil (k_{ro}) as a function of the water saturation of the reservoir (S_w) [14]

The relative permeabilities of oil and water increase with increasing saturation of the reservoir with the respective fluid, which means that oil becomes less and less producible with the progress of water flooding. The intersections of the relative permeability curves with the x-axis specify the irreducible water saturation (S_{wi}), which is also known as connate water, and the residual oil saturation (S_{or}).

The aim of every enhanced oil recovery method is to maximize the recovery factor (F) of the reservoir. The recovery factor is defined by the ratio of cumulative produced oil (N_p) and the entirety of oil in the reservoir at the beginning of production (OOIP – original oil in place). The cumulative produced oil during a flooding operation is the difference between actual average water saturation of the reservoir ($\overline{S_w}$) and the irreducible water saturation (S_{wi}). The macroscopic (volumetric) sweep efficiency ($E_{vol.}$) and microscopic displacement efficiency (E_D) contribute to the recovery factor.

$$F = \frac{N_p}{OOIP} = \frac{\overline{S_w} - S_{wi}}{1 - S_{wi}} = E_{vol.} \cdot E_D \quad \text{Eq. 2-3}$$

F	–	recovery factor
N_p	–	cumulative produced oil
$OOIP$	–	original oil in place
$\overline{S_w}$	–	average water saturation of the reservoir
S_{wi}	–	irreducible water saturation
$E_{vol.}$	–	macroscopic (volumetric) sweep efficiency
E_D	–	microscopic displacement efficiency

The macroscopic sweep efficiency is a measure to state, how many parts of the reservoir have been penetrated by the displacing aqueous solution (Figure 2-2).

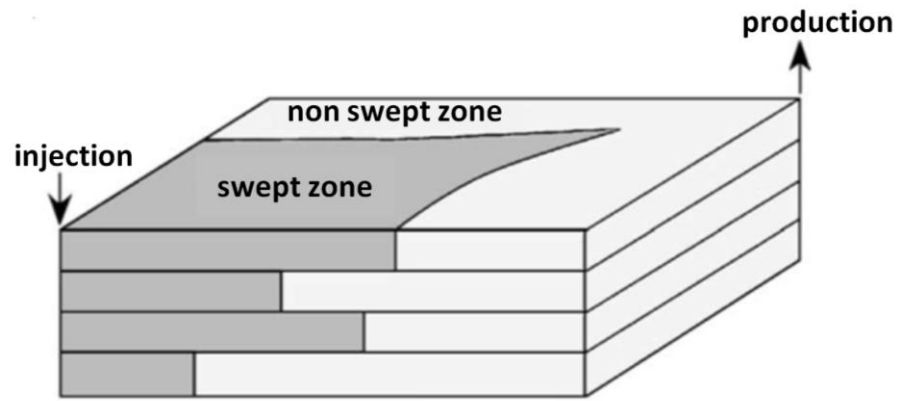


Figure 2-2: Schematic representation of macroscopic (volumetric) sweep efficiency (adapted from [15])

The mobility ratio (M) is the determining factor of the macroscopic sweep efficiency. It is specified by the relative permeabilities and the viscosities of aqueous and oil phase (Eq. 2-4). A low mobility ratio ($M \leq 1$) contributes to high oil recovery.

$$M = \frac{k_{rw} \cdot \eta_o}{k_{ro} \cdot \eta_w} \quad \text{Eq. 2-4}$$

- M – mobility ratio
- k_{rw} – relative permeability of aqueous phase
- η_o – viscosity of oil phase in Pa·s
- k_{ro} – relative permeability of oil phase
- η_w – viscosity of aqueous phase in Pa·s

A common method to decrease the mobility ratio is to increase the viscosity of the aqueous phase by adding viscosifiers (e.g., polymers) or to reduce the viscosity of the oil, for example by heating. Macroscopic sweep efficiency is also improved by selective plugging of high permeable parts of the reservoir. The displacing fluid is then forced to penetrate lower permeable areas with oil that has not been affected by the flooding operation up to that point.

The microscopic displacement efficiency characterizes the displacement of oil on pore level (from the pore walls, dead-end pores, etc.) in the swept zones of the reservoir. In this case the residual oil saturation (S_{or}), which can be reached by water flooding, is affected and might be reduced. The key parameters are the capillary pressure

and the capillary number. The capillary pressure (p_c) is defined as the pressure difference of the wetting and the non-wetting phase within a tube/pore with a defined radius.

$$p_c = p_{nw} - p_w = \frac{2 \cdot \sigma \cdot \cos\theta}{r_p} \quad \text{Eq. 2-5}$$

p_c	–	capillary pressure in Pa
p_{nw}	–	pressure in the nonwetting phase in Pa
p_w	–	pressure in the wetting phase in Pa
σ	–	interfacial tension wetting and nonwetting phase in N/m
θ	–	contact angle (measured in wetting phase) in °
r_p	–	pore radius in m

The capillary number (N_C) is the ratio of viscous and capillary forces (Eq. 2-5).

$$N_C = \frac{v \cdot \eta_w}{\sigma \cdot \cos\theta} \quad \text{Eq. 2-6}$$

N_C	–	capillary number
v	–	flow velocity of displacing fluid (aqueous phase) in m/s
η_w	–	viscosity of displacing fluid in Pa·s
σ	–	interfacial tension between aqueous and oil phase in N/m
θ	–	contact angle in °

As a rule of thumb, the residual oil saturation in the reservoir can be reduced significantly if the capillary number for water flooding is increased by factor 1000 or more. The interfacial tension (IFT) between water and oil can be reduced, for example, by surfactants. Another aspect affecting the microscopic displacement efficiency is the wettability of the reservoir. In oil-wet rocks, capillary forces, which retain oil, are higher than in water-wet reservoirs. Therefore water-wet conditions are more favorable for oil displacement. There are reservoirs of a wide variety of wettability, but greatest

part can be considered water- or intermediate-wet. Sandstone reservoirs remain water-wet over geologic time in most cases because of connate water [16].

Enhanced oil recovery methods are purposed to decrease the mobility ratio and/or to increase the capillary number. In the next chapter the different methods, as well as their modes-of-action will be described.

2.2 EOR Methods

At first, it has to be noted, that every enhanced oil recovery operation starts with an intensive screening phase. Sound knowledge of the reservoir conditions (pressure, temperature, depths, formation type, the composition of reservoir brine and crude oil, porosity, and permeability) is necessary because not every EOR method works in every reservoir.

Enhanced oil recovery methods can be categorized into miscible, microbial, thermal, chemical and other processes as shown in Figure 2-3. The description of the individual methods (except chemical) will be held very short in this thesis. For further information, the references [15, 17] can be recommended.

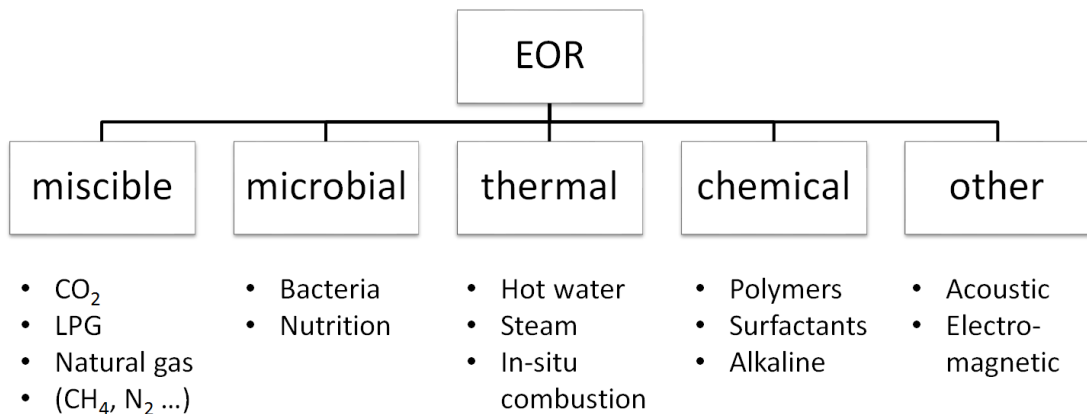


Figure 2-3: Categories of enhanced oil recovery methods

Oil recovery with miscible substances relies on displacement processes where the interfacial tension between the displacing fluid and the oil is almost decreased to zero. This leads to a very low capillary pressure between oil phase and displacing fluid in the reservoir pores, which has to be overcome during oil displacement.

Carbon dioxide is often used for miscible flooding because it affects the reservoir oil in multiple ways. Besides lowering the interfacial tension to the displacing fluid when dissolving into the oil, carbon dioxide also lowers the viscosity of the oil phase and causes the oil to swell. All the three effects contribute to improved oil displacement.

For successful miscible flooding operations, the knowledge of the phase behavior of the multicomponent system (injected fluid and reservoir oil) is essential. A critical parameter is the minimal miscible pressure, which can be determined by experimental measurements, empirical correlations or equation-of-state calculations. Hence, the consideration of the reservoir conditions (pressure, temperature, fluid properties) is highly relevant for planning a miscible flooding operation. A great challenge for these operations is to avoid gravity segregation and viscous fingering. Therefore, the application of miscible methods is recommended for oils with low density and viscosity in fairly homogeneous reservoirs. [18]

The intention of **microbial enhanced oil recovery** is to use the metabolic products of microorganisms in the reservoir. Therefore, a fluid containing either microbes or nutrition for microorganisms existing in-situ is injected into the reservoir. The metabolic products can be gases, biosurfactants, biopolymers or just biomass (dead microbes). By propagating with the fluid through the reservoir, the metabolic products can positively affect the viscous and capillary forces during oil displacement. The production of biomass might be used for selective plugging processes. Since there is such a great variety of microorganisms, which could be present in a reservoir and the fact that the microbes are very sensitive to any variation of their environmental conditions (pressure, temperature, salinity), these projects are very challenging and need intensive pre-screening.

Thermal enhanced oil recovery methods are the most applied and successful EOR methods by now. In those projects, parts of the reservoir are heated up by injection of steam or hot water, or by burning a small portion of the crude oil (in-situ combustion). Due to temperature increase, the viscosity of the oil is reduced, and it flows more easily through the pores. In cases of hot water or steam injection, the less viscous oil is produced by displacement by a water front using an injection and production well or by gravity drainage. The most limiting factor for hot water or steam injection projects is the depths of the reservoir because a high amount of thermal energy is lost in the

injection well. In in-situ combustion projects, an oxidant (i.e., air or oxygen) is injected into the oil reservoir and the hydrocarbons are ignited, generating a burning front. This burning front should be very small. It can be controlled by the injection rate of the oxidant. A considerable amount of heat is generated, which vaporizes connate water and light portions of the crude, as well as decreases the viscosity of the heavier oil portions in front of the burning front. By further injection of oxidant, the burning front propagates through the reservoir pushing the steam zone and the oil to the production well. Thereby, effects of steam-drive and miscible displacement are used to mobilize the oil [17]. Thermal methods are most effective for heavy crude oils with specific gravities of around 10 – 40 °API [10].

Electromagnetic and acoustic methods are widely used for wellbore stimulation. Their application as enhanced oil recovery methods is still subject of research [19]. Enhanced oil recovery by electromagnetic methods is based on thermal processes. The energy of electromagnetic waves heats up the reservoir. Hence, the oil viscosity is decreased, and a steam front is created by vaporizing the connate water. However, the heating radius is limited to a few meters [20]. This method is used in heavy oil reservoirs to remove precipitations of, for example, asphaltenes in the near-wellbore area of the producer. An interesting approach to increase the heating radius is the injection of ferric nanoparticles into the reservoir. By doing so, electromagnetic stimulation could possibly be developed to an EOR method [21]. Acoustic stimulation was certified as a new EOR process by the Texas Railroad Commission in 2007 [22]. However, the mechanisms, which promote oil production from a reservoir, are not entirely understood by now [23]. The acoustic waves emitted into the reservoir are assumed to change relative permeabilities, promote coalescence of oil droplets or emulsification if surfactants are present. Capillary forces might also be affected in a way contributing to oil mobilization [24].

Chemical enhanced oil recovery methods will be discussed in more detail in the next chapter since these are the baseline for the investigations that have been done in the scope of this thesis.

2.2.1 Chemical Enhanced Oil Recovery Methods

Chemical enhanced oil recovery is considered to provide the most promising technologies for tertiary oil production [25]. The efficiency of different chemical solutions for oil mobilization under various reservoir conditions can easily be investigated in laboratory studies to establish a good understanding of the interactions between chemicals, reservoir rock and fluids. This is the basis for successful field projects. In chemical enhanced oil recovery applications polymers, surfactants and/or alkaline are usually added to the injection water to decrease the mobility ratio and capillary forces.

Polymers build entangled networks in the aqueous phase resulting in high viscosities, when there is no stress applied. When the shear stress increases, the entanglements break up, and the molecules orientate in the flow direction. Hence, the viscosity of the solution decreases. This shear thinning behavior is very favorable for injection. At high flow velocities, e.g., near the injection well, a smaller pressure gradient is needed to pump the polymer solution into the reservoir. However, if the flow velocities and shear stresses become too high, the polymer molecules can be mechanically degraded. This degradation is not reversible and affects the rheological properties of the solution, often in a detrimental way. Within the reservoir the flow velocities become lower, causing the viscosity of the injected solution to increase. This contributes to a more uniform displacement front and the macroscopic sweep efficiency is increased as shown in Figure 2-4.

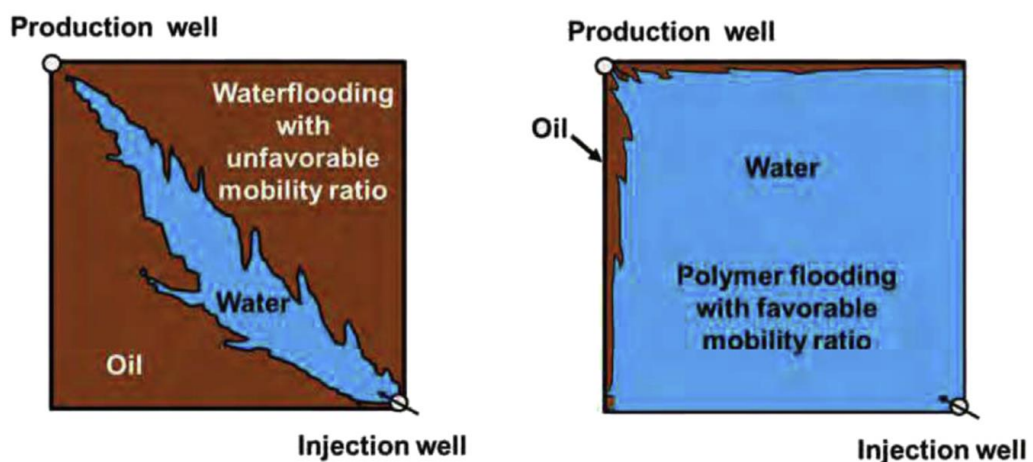


Figure 2-4: Water flooding with unfavorable mobility ratio, $M < 1$ (left) and polymer flooding with increased mobility ratio (right) [26]

Polymers can also be used for selective plugging of high permeable parts of the reservoir. The shear stress is very low in these locations. Hence, the fluid's viscosity increases and blocks the pore channels. Thereby, other lower permeable parts of the reservoir can be swept by the water front. For a long time, it was supposed, that polymer flooding can only enhance the mobility ratio but has no effect on residual oil saturation. Within the last years, the mechanism of polymer flooding was reconsidered, which will be referred to in chapter 4.1.

Surfactants are known to decrease the interfacial tension between polar and non-polar fluids. Hence, the capillary pressure between an aqueous phase and oil in the pores is reduced (see: Eq. 2-5), which contributes to oil production. In many surfactant flooding operations the aim is even to produce oil-in-water micro emulsions with low viscosities. The injection of surfactants is often followed by a polymer slug to enhance the sweep efficiency (SP-flooding). Some surfactants alter the wettability of the reservoir rock by adsorbing on it. A wettability change from oil- to water-wet conditions is favored. By using surfactants to generate foam in the reservoir, synergistic effects of chemical and miscible enhanced oil recovery can be used and, for example, gravity segregation can be retarded during carbon dioxide flooding.

Alkaline solutions are often injected in front of surfactants (AS-flooding). Due to their high pH-value, they promote water-wet conditions. Moreover, alkaline react with acidic components of the crude oil generating natural soaps, which can reduce the adsorption value of the following surfactant solution [27]. Alkaline and surfactants increase the microscopic displacement efficiency. A polymer slug that follows the AS-flooding assures a more uniform displacement front and forces the low viscous alkaline and surfactant solutions to propagate into more parts of the reservoir. Hence an ASP-flooding operation takes advantage of the synergistic effects of alkaline, surfactants, and polymers.

In recent research, some attention has been paid on the elastic properties of viscoelastic fluids for oil displacement. The literature on this topic is summarized in chapter 4. Another focus is on the viscoelastic properties of the liquid-liquid interface. The higher the elasticity of the interface between water and oil, the more snap-off of oil droplets is prevented. This leads to a more uniform water front and thus to better oil production [28, 29].

Most chemical enhanced oil recovery projects have been conducted in sandstone reservoirs because this formation has often moderate to high permeabilities, which is favorable for chemical flooding and even crucial for polymer injection (mechanical degradation). Furthermore, the adsorption of polymers and surfactants is moderate on sandstone compared to other formations (e.g., carbonates) [14]. Adsorption and mechanical trapping contribute to retention. Polymer retention in the field ranges from 4 to 75 $\mu\text{g}_{\text{polymer}}/\text{g}_{\text{rock}}$ with an average at around 20 $\mu\text{g}_{\text{polymer}}/\text{g}_{\text{rock}}$ [17]. For surfactants, the retention is higher because they more likely adsorb on pore walls. Adsorption values are often given in $\text{mg}_{\text{surfactant}}/\text{g}_{\text{rock}}$. Another challenge of mixtures of different molecules is chromatographic separation inside the reservoir. Therefore, a single component solution would be beneficial for chemical flooding.

Effect of temperature, pressure, and salinity on EOR chemicals

Enhanced oil recovery chemicals are expected to meet several demands. They must be stable at reservoir conditions, i.e., high temperatures (up to 100 °C and more) and pressures, as well as high salinity and hardness of the reservoir brines.

The temperature has a significant effect on the phase behavior of surfactant solutions in the reservoir. Therefore, it also affects interfacial tension and micellization. Temperature increase causes a higher solubility for most anionic surfactants, whereas the solubility of nonionic surfactants is decreased. High temperatures can cause breakdown of hydrogen-oxygen bonds leading to decreased solubility or even precipitation of surfactants containing those functional groups. The temperature, at which the surfactants precipitate and phase separation occurs causing the solution to become cloudy, is referred to as the cloud point. With respect to polymers, increasing temperatures first cause the viscosity of polymer solutions to decrease, but if it is too hot in the reservoir polymers can undergo hydrolysis (thermal degradation). Therefore, most biopolymers are only applied in reservoirs with temperatures below 60 °C [30].

The variation of reservoir pressure can also have an impact on the phase behavior of chemically treated injection water. The effect on the properties of the crude oil might be even more significant since the amount of gas dissolved in the reservoir oil depends on pressure.

Reservoir brines contain different salts; mostly sodium chloride, but often also significant amounts of calcium and magnesium salts, as well as small quantities of bromides and sulfates. Calcium and magnesium ions contribute to the hardness of the solution. If the salt concentration of the reservoir brine exceeds 200 g/l, the conditions are designated to be highly saline [31]. The salinity of the reservoir brine affects the properties of polymers and surfactants, especially if their functional groups are charged. Because of charged functional groups, which repulse each other, a polymer molecule has a relatively high hydrodynamic volume. By adding salt, the charges are neutralized, causing the molecule to curl. Hence, the hydrodynamic volume of a single molecule is reduced, and the viscosity of the solution decreases. The effect is higher for divalent cations (Ca^{2+} , Mg^{2+}) than for monovalent ions, such as Na^+ [30]. Salinity also has a great effect on the interfacial behavior and micellization, as well as on emulsification, especially of ionic surfactant solutions. At low brine salinity, an ionic surfactant solubilizes in water very well, and there are some micelles containing oil in the water phase. Hence, an oil-in-water emulsion is formed. By increasing the salt concentration, the solubility of the surfactants in water is decreased until the solubility of the molecules in oil is greater than in water. The conditions are reversed, and water-in-oil emulsions are formed, which show higher viscosities, which is unfavorable for production. Nonionic surfactants are less sensitive to salinity. Alkaline solutions react with calcium and magnesium ions in the reservoir brine, which results in precipitation of calcium and magnesium hydroxides. The removal of these ions from the brine is beneficial for the chemicals following the alkaline front. However, this process could be detrimental for further injection because of permeability reduction. [17]

Other factors, which affect the efficiency of chemicals, are oxidative and biological degradation. Especially polysaccharides are susceptible to bacterial attack and will lose their desired properties. To avoid oxidative and biological degradation antioxidants and bactericides are added to the injected water.

Since chemicals can – in principle – be synthesized and designed to match special requirements, there is great potential for chemical enhanced oil recovery. However, the challenge to find chemical formulations, which meet all demands, is still a great one. Extensive laboratory and simulation work is needed for every chemical enhanced

oil recovery project. Reliable data gained from laboratory experiments are the basis for numerical simulation and can be a decisive factor for or against the application of a chemical product in the field. Properly planned and accurately conducted laboratory investigations are therefore critical to a successful chemical EOR project, which results in increased oil production and financial gain.

3. Viscoelastic Surfactant Solutions

In this chapter, the principles of surfactant structures and micellization in aqueous solutions and the essential concepts of the rheology of viscoelastic fluids are addressed. It is not intended to be comprehensive. The intention is rather to establish a fundamental understanding of the processes, which lead to structural arrangements of surfactant molecules in solution and their effect on the rheological behavior. Furthermore, possible interactions of viscoelastic surfactant solutions with crude oil and different salts, which are present in reservoir brines, are discussed.

The whole chapter 3 refers to surfactants, which consist of a relatively small hydrophilic “head” and a long hydrophobic “tail” group since these systems are most widely used and reported in the literature. The Triphenoxymethane molecules, which are the research subjects of this thesis, have a different structure. Therefore, their behavior in solution is slightly different, which will be explained in detail in chapter 5. Nevertheless, many principles of micellization, viscoelastic behavior, and interaction with salts and oil apply to the Triphenoxymethane molecules, as well as to conventional surfactants. For that reason and for comparability purposes the next pages are included into the thesis.

3.1 Surfactant Structures in Aqueous Solution

Surfactant molecules consist of a hydrophilic and a hydrophobic part. In very dilute solutions (Figure 3-1, A) these molecules exist as single molecules or are oriented at the surface with the hydrophilic head towards the aqueous bulk phase. The hydrophobic group is removed from contact with water [32]. By increasing the surfactant concentration, more and more molecules will accumulate at the surface (Figure 3-1, B). When the surface is fully covered, the hydrophobic parts of the surfactants will attract each other in aqueous solution and assemble to micelles. This concentration is referred to as critical micelle concentration. Above CMC the surfactant molecules exist in equilibrium of single monomers and micellar associations (Figure 3-1, C).

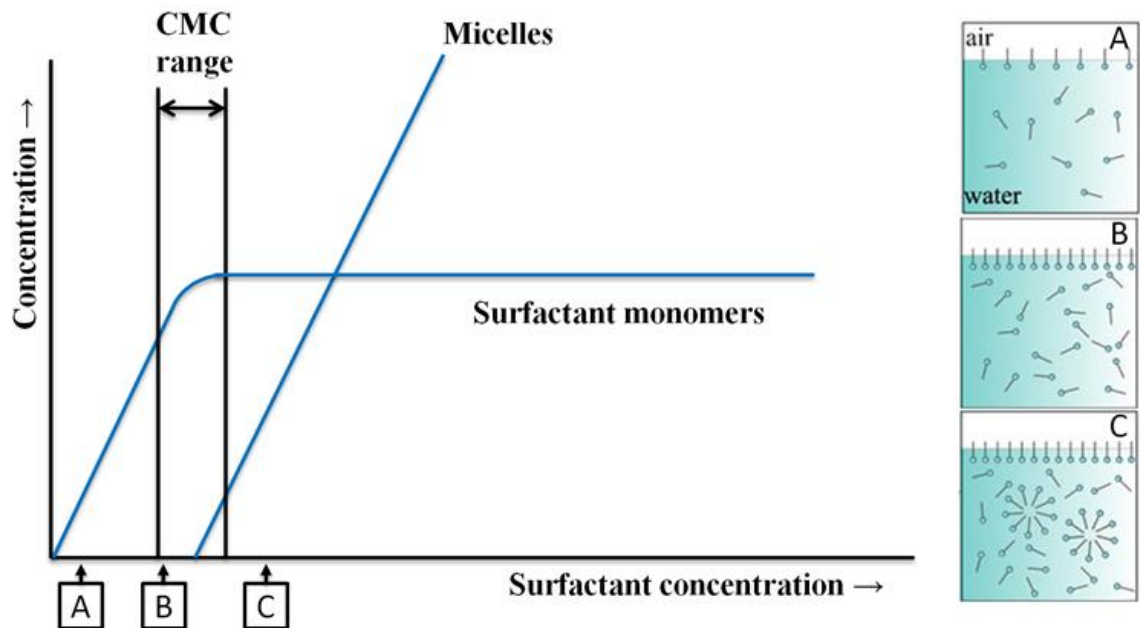


Figure 3-1: Critical micelle concentration (schematic) [33, 34]

The shape of the micelles depends on the geometrical structure of the surfactant molecules, as well as on the acting forces between single amphiphilic molecules and between the surfactants and the solvent.

The Tanford free energy model is an energetic approach to micellization. Its theory of the free energy change during micellization is discussed qualitatively here. There are basically three kinds of opposing forces (Figure 3-2) causing the single surfactant molecules to aggregate in solution in a specific way.

$$\begin{array}{c}
 \left[\begin{array}{c} \textit{free} \\ \textit{energy} \\ \textit{change} \end{array} \right] = \left[\begin{array}{c} \textit{hydrophobic parts} \\ \textit{are removed from} \\ \textit{water contact} \end{array} \right] + \left[\begin{array}{c} \textit{residual} \\ \textit{water contact of} \\ \textit{hydrophobic parts} \end{array} \right] + \left[\begin{array}{c} \textit{repulsive forces} \\ \textit{between} \\ \textit{hydrophilic groups} \end{array} \right] \\
 \left(\begin{array}{c} \textit{to be} \\ \textit{minimized} \end{array} \right) \quad \left(\begin{array}{c} \textit{negative} \\ \textit{contribution} \end{array} \right) \quad \left(\begin{array}{c} \textit{positive} \\ \textit{contribution} \end{array} \right) \quad \left(\begin{array}{c} \textit{positive} \\ \textit{contribution} \end{array} \right)
 \end{array}$$

Figure 3-2: Energetic contributions of different phenomena during micellization in a surfactant solution

The hydrophobic groups assemble in the core of the micelle, which is surrounded by the hydrophilic parts of the amphiphilic molecules. Hence, the hydrophobic core is removed from water contact, which results in a reduction of free energy of the system. The repulsive forces between the hydrophilic groups and the fact that the hydrophobic tails cannot be fully shielded from the aqueous solution and there is still residual water

contact contribute to an increase of free energy. To achieve a stable micellar solution (thermodynamic equilibrium) the free energy of a system should be minimal. [35]

The Tanford free energy model explains the formation and finite growth of the micelles. The strive to remove the hydrophobic parts of the surfactants from water contact gives a negative contribution to the free energy change of the system and therefore, is the driving force for aggregation. The effect of residual water contact increases the free energy, but the magnitude decreases with decreasing curvature of the surfactant layer, which is associated with micellar growth. The repulsive forces between the hydrophilic groups, however, positively contribute to the free energy of the system and the effect increases with the number of molecules forming a micelle. This is the limiting factor for micellar growth. [36]

The packing parameter (P) considers the effect of the geometrical form of the molecules on the shape of the built up micelles. It is defined by the proportions of the hydrophilic and hydrophobic groups of the surfactant [37].

$$P = \frac{V}{L_c \cdot a_0} \quad \text{Eq. 3-1}$$

- P – packing parameter
- V – volume of “tail” group in m^3
- L_c – maximum effective length of “tail” group in m
- a_0 – cross-sectional area of “head” group in m^2

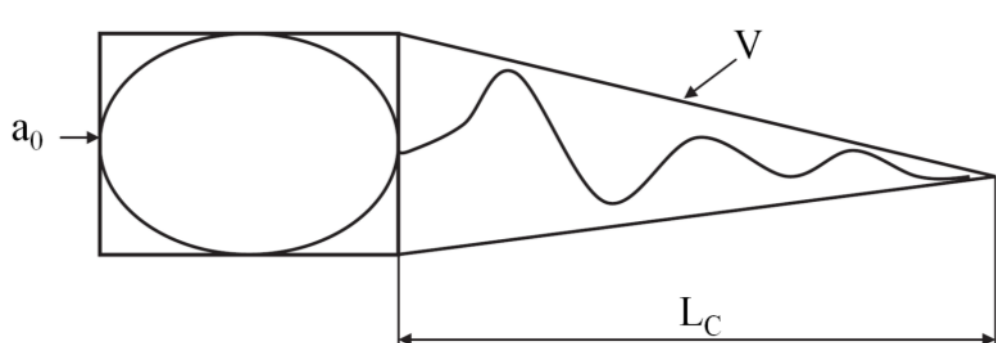


Figure 3-3: Parameters in Packing Factor [14]

Surfactant molecules with a packing parameter lower than $\frac{1}{3}$ will form spherical micelles. If the packing parameter is between $\frac{1}{3}$ and $\frac{1}{2}$, rod-like micelles will be found in solution. Under certain conditions, the micelles exhibit an enormous growth in one direction and form worm-like micelles. The packing parameter for this type of association is around $\frac{1}{2}$ [6]. For one specific surfactant, the packing parameter can be changed by variation of salinity or temperature [32]. Micellar growth, especially with ionic surfactants, is susceptible to the nature and amount of added salts [38]. For example, the one-dimensional micellar growth can be promoted in ionic surfactant solutions by adding counter ions, which results in reduced repulsive forces between the hydrophobic groups [39].

Worm-like micelles are characterized as long, cylindrically shaped associations of surfactants with relatively high flexibility. They can be considered to consist of many rigid sections with a persistence length (l_p). The persistence length depends on surfactant geometry, temperature and salinity [40]. It often ranges between 10 and 20 nm for micelles formed by nonionic surfactants and between 30 and 60 nm for systems of ionic surfactants [32]. Persistence lengths above 100 nm are very seldom. The cross section diameter of worm-like micelles (D_{cs}) is approximately 5 – 20 nm. The contour length of the whole worm-like micelle (L) can reach a few micrometers [6]. Figure 3-4 shows schematically the dimensions of a worm-like micelle.

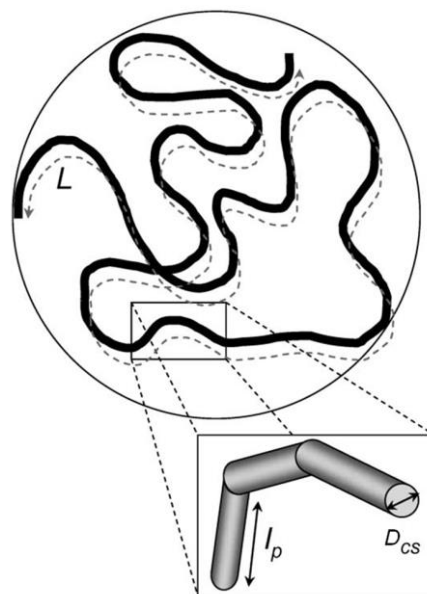


Figure 3-4: Schematic representation of contour length (L), persistence length (l_p) and cross section diameter (D_{cs}) of a worm-like micelle [41]

The relations between diameter, contour and persistence length of the micelle determine the grade of flexibility. Granted that the diameter of the micelle is small compared to persistence and contour length, the following relations apply [32].

- $l_p > L$: stiff and rod-like micelle
- $L \approx l_p$: semi flexible micelle
- $L \gg l_p$: flexible and worm-like micelle

If ambient conditions promote the growth of flexible worm-like micelles and the surfactant concentration is further increased, the micelles will eventually become larger than the intermicellar distance. At this point, which is referred to as overlap or crossover concentration, the micelles start to interpenetrate each other. A viscoelastic network is formed. From that point on, the viscosity of the solution increases sharply with surfactant concentration. The interpenetration is responsible for the buildup of elasticity [32, 37].

Formation of viscoelastic structures by worm-like micelles is reversible. On a microscopic scale, the micellar aggregates are always in equilibrium with single monomers [42]. The micelles break and reassemble all the time due to diffusion [37]. This process of steadily breaking and reformation differentiates micellar from polymeric systems. Therefore, these associations are often referred to as “living polymers” [6].

If viscoelastic surfactants are applied in chemical flooding, their efficiency will be closely related to their flow behavior in the reservoir. In order to establish a basic understanding, the next chapter will introduce the most important concepts of the rheology of viscoelastic fluids.

3.2 Some Rheological Aspects of Viscoelasticity

A viscoelastic system behaves partly like an elastic material and partly like a viscous fluid. A simple method to describe viscoelasticity is to combine the material laws for purely viscous and purely elastic behavior.

Purely viscous systems can be characterized by the properties of *Newtonian* fluids. The shear stress (τ), which is the tangential stress in the fluid opposed to its flow direc-

tion, is directly proportional to the shear rate ($\dot{\gamma}$), which correlates to the flow velocity. The factor of proportionality is the viscosity (η) of the respective fluid. Viscous flow is characterized by irreversible deformation.

$$\tau = \eta \cdot \dot{\gamma} \quad \text{Eq. 3-2}$$

τ	–	shear stress in Pa
η	–	dynamic viscosity in Pa·s
$\dot{\gamma}$	–	shear rate in 1/s

Purely elastic behavior can be characterized by *Hooke's law*, which states that the tensile stress (τ) developing in an elastic material is proportional to its deformation (γ). In this case the factor of proportionality is the shear modulus (G). The deformation of an elastic material is fully reversible.

$$\tau = G \cdot \gamma \quad \text{Eq. 3-3}$$

τ	–	shear stress in Pa
G	–	shear modulus in Pa
γ	–	(shear) deformation

In theoretical models, viscous and elastic behaviors are often illustrated by a (hydraulic) damper and a spring, respectively.

Viscoelastic fluids, including viscoelastic surfactant solutions [38], are typically described by connecting the “elements” of viscosity and elasticity in series (*Maxwell model*), as shown in Figure 3-5.

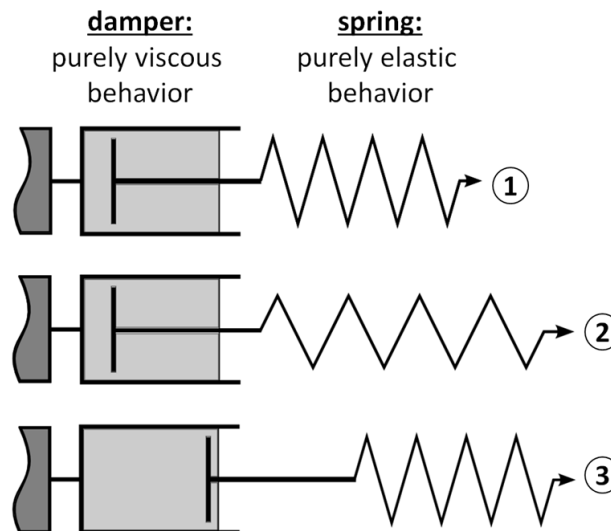


Figure 3-5: Viscoelastic deformation of a *Maxwell* fluid

The upper picture (1) in Figure 3-5 shows a linear damper/spring model in its initial equilibrium state. When the system is suddenly deformed (2), the spring immediately elongates and is subjected to tensile tension. This tension is transferred to the damper, causing the piston to move towards the spring. The spring recoils and the tension becomes smaller until an equilibrium state different from the initial one is reached (3). The velocity of the piston, and therefore, the time needed for the transition into equilibrium, depends on the viscosity of the damper fluid.

Viscoelasticity implies that one system behaves like a fluid and a solid simultaneously. In fact, this is depending on the time scales of observation. When a distinct amount of stress is slowly applied to a viscoelastic system over an extended period of time, the system will flow like a fluid, molecular rearrangements occur, and energy is dissipated. On the other hand, if the same amount of stress is applied all of a sudden (fast, a short period of time) a viscoelastic system will give a more elastic response, like a solid. [42]

A critical parameter to describe time-dependent rheological processes is the stress relaxation time (t_r). It is defined as the time a deformed system needs to relax into equilibrium. For linear viscoelastic fluids the relaxation time is described as the ratio of viscous and elastic behavior [43, 44].

$$t_r = \frac{\eta}{G} \quad \text{Eq. 3-4}$$

- t_r – relaxation time in s
 η – dynamic viscosity in Pa·s
 G – shear modulus in Pa

When a viscoelastic fluid flows through a porous medium, it steadily experiences different shear stresses due to the changing diameter of the pores. The fluid is accelerated and decelerated all the time, causing the molecules or worm-like micelles to stretch and recoil [45]. The induced normal stresses are, in contrast to *Newtonian* fluids, anisotropic. Figure 3-6 shows the stresses (τ_{xx}, τ_{yy}) acting on a *Newtonian* and a linear viscoelastic fluid under shear.

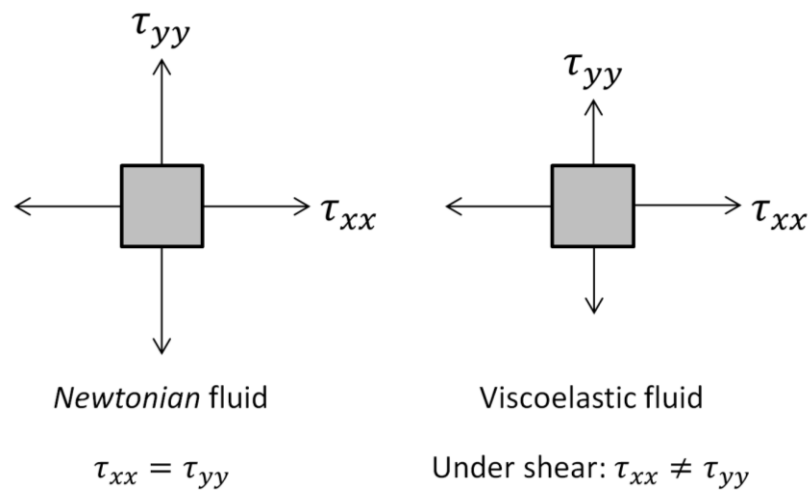


Figure 3-6: Normal stresses on a Newtonian and a viscoelastic fluid under shear [14]

The first normal stress difference is an important parameter for the description of viscoelasticity and is defined as follows.

$$N_1 = \tau_{xx} - \tau_{yy} \quad \text{Eq. 3-5}$$

- N_1 – first normal stress difference in Pa
 τ_{xx} – normal stress in direction of flow in Pa
 τ_{yy} – normal stress perpendicular to the direction of flow in Pa

Under shear, the first normal stress difference is positive, which can be explained by elongation of macromolecules or worm-like micelles in the direction of the streamline. In Figure 3-7 experimental data of first normal stress differences of polymer solutions as a function of shear rate and the molecular weight of hydrolyzed polyacrylamide (HPAM) are shown. The higher the molecular weight of these solutions, the more pronounced is their elasticity. The higher the shear rate (and therefore the shear stress) and the elasticity of the viscoelastic fluid, the higher the first normal stress difference.

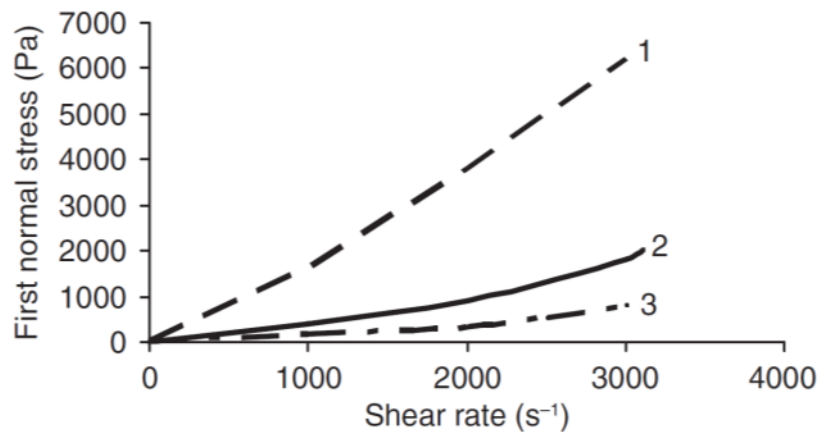


Figure 3-7: First normal stress differences of different HPAM solutions as a function of shear rate (1: $MW = 21 \cdot 10^6$, highest elasticity; 2: $MW = 12 \cdot 10^6$; 3: $MW = 7.5 \cdot 10^6$, lowest elasticity) [14]

By analysing such rheological measurements the relaxation time in viscoelastic flow can be defined. A common method is to combine the first normal stress difference and the shear rate [45].

$$t_r = \frac{N_1}{2 \cdot \eta \cdot \dot{\gamma}^2} \quad \text{Eq. 3-6}$$

t_r	–	relaxation time in s
N_1	–	first normal stress difference in Pa
η	–	dynamic viscosity in Pa·s
$\dot{\gamma}$	–	shear rate in 1/s

The relaxation time of viscoelastic surfactant systems can also be assessed from a frequency sweep as shown in Figure 3-8. It corresponds to the crossover of the storage

modulus (G'), which represents elasticity and the loss modulus (G'') representing viscous behavior. [46, 47]

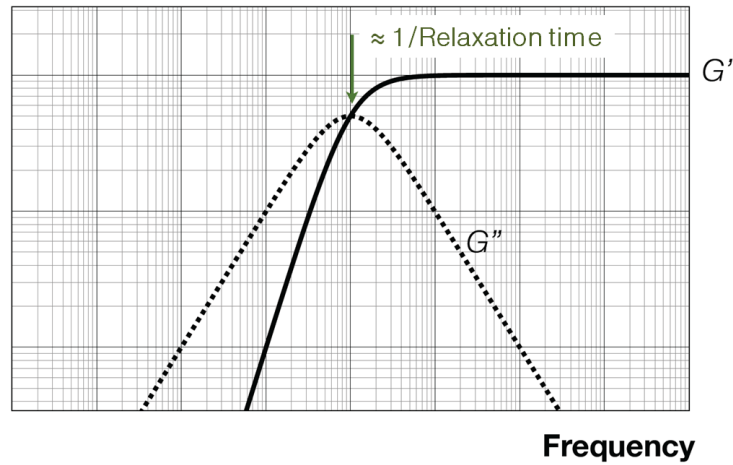


Figure 3-8: Principle using a frequency sweep to determine the relaxation time of a *Maxwell* Fluid [48]

To compare viscoelastic systems, dimensionless parameters are often used, like the dissipation factor, the *Weissenberg* number, and the *Deborah* number.

The ratio between the loss and the storage modulus is referred to as dissipation factor ($\tan\delta$).

$$\tan\delta = \frac{G''}{G'} \quad \text{Eq. 3-7}$$

A dissipation factor lower than 1 is typical for viscous (liquid-like) systems ($G'' > G'$). If the dissipation factor is higher than 1, the elastic (solid-like) behavior is more pronounced ($G' > G''$). Ideal viscoelastic behavior is characterized by a $\tan\delta = 1$, where the loss and the storage moduli are equal.

The *Weissenberg* number (We) is defined as the ratio of first normal stress difference to the applied shear stress.

$$We = \frac{N_1}{\tau} \quad \text{Eq. 3-8}$$

We	–	<i>Weissenberg</i> number
N_1	–	first normal stress difference in Pa
τ	–	shear stress in Pa

The higher the *Weissenberg* number, the more pronounced is the elasticity of a fluid in flowing processes [49, 50].

The *Deborah* number (De) is another common dimensionless parameter to characterize the viscoelasticity of a fluid. It is defined as the ratio of relaxation time of the fluid and the time scale of observation (t_c , characteristic time). [51]

$$De = \frac{t_r}{t_c} \quad \text{Eq. 3-9}$$

De	–	<i>Deborah</i> number
t_r	–	relaxation time in s
t_c	–	characteristic time in s

When the *Deborah* number is much smaller than 1, the system exhibits a pronounced viscous behavior. In cases where the *Deborah* number is much higher than 1, pronounced elastic behavior can be observed.

The flow behavior of viscoelastic surfactant solutions under reservoir conditions has been a subject of studies for the last ten years. [7, 52]

In dilute solutions, the surfactant molecules are present as single molecules or form spherical micelles. Such fluids often show *Newtonian* flow behavior and the viscosity is only slightly higher than that of pure water.

After the transition from spherical to worm-like micelles, the viscosity of the solution increases sharply with surfactant concentration [41]. By entanglement and interpenetration of micelles, elastic properties develop [53].

Viscoelastic surfactant solutions exhibit strong shear thinning behavior, similar to that of polymer solutions [54], which is very beneficial for the injection into porous media [12]. The significant advantage of viscoelastic surfactant solutions is their capability to withstand high shear stress, at which polymers underlie shear degradation. Due to the reassembly of the surfactant molecules into micelles, viscosity and elasticity are recovered in viscoelastic surfactant solutions after high shear stresses are removed [40]. The viscoelastic networks can be broken down to the very small structures of single surfactant molecules. This enables viscoelastic surfactant solutions to flow through tight pore necks into low permeable parts of the reservoir, which are inaccessible for high molecular weight polymer solutions.

3.3 Interaction of Viscoelastic Surfactants with Reservoir Fluids

The pores of oil reservoirs are filled with the hydrocarbons themselves and brines, which are often highly saline and contain polyvalent ions. The compatibility of the chemicals applied for enhanced oil recovery with the reservoir fluids even under harsh conditions (high pressure and temperature) is crucial for the success of a chemical EOR operation. In this chapter, possible interactions of viscoelastic surfactants with salt and oil are described.

3.3.1 Viscoelastic Surfactants and Saline Solutions

In chapter 2.2.1 the influence of salinity on surfactants as single molecules in the reservoir has already been discussed. This chapter intends to explain the effects of salt ions on the macrostructures in viscoelastic surfactant solutions.

The effect of different ions depends on their valence and their capability to promote either the hydrophobic or the hydrophilic properties of a macromolecule or giant micelle in aqueous solution. Intensified hydrophilic properties lead to better solubilization of a macromolecule, whereas intensified hydrophobicity results in aggregation, structure buildup and in extreme cases precipitation. These phenomena were first observed by *F. Hofmeister* in 1888 [55]. He investigated the influence of different salts

on precipitation of globulin from chicken egg white and established a sequence of salt ions in order of their protein denaturing potential, which is shown in Figure 3-9.

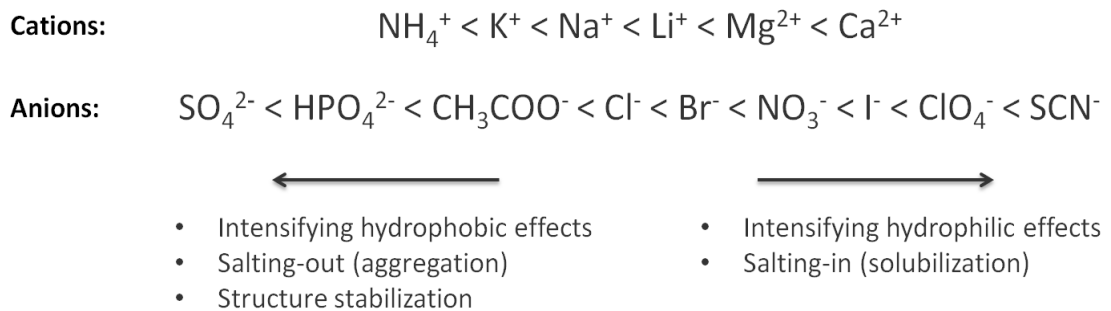


Figure 3-9: Hofmeister series of cat- and anions and effects in aqueous solution [53, 56]

The effects are more pronounced for anions than for cations. The exact physical and chemical mechanisms behind the *Hofmeister* series are not entirely understood yet. However, other researchers have studied the influence of salts on different phenomena and found that the *Hofmeister* series applies in many cases, e.g., silk proteins, surface and interfacial tensions of saline solutions to nonpolar fluids, microemulsion microstructure, and colloid stability [56–58]. Reservoir formation water contains such inorganic anions, sometimes in concentrations up to saturation limit.

Worm-like micelles can be formed by ionic and nonionic surfactants. Most widely studied are the effects of different anions on the growth of micelles composed of long-chain cationic surfactants. There are contrasting views on the validity of *Hofmeister* series for viscoelastic solutions of cationic surfactants. Some researchers observed, that the transition from spherical to elongated micelles and micellar flexibility is influenced by non-aromatic counterions in a way that applies to the *Hofmeister* series [59, 60]. Others found only poor conformity or even contradiction of their experimental results to the ionic sequence [61, 62]. In general inorganic ions only have little effect on the micellar structure of cationic surfactant solutions. Aromatic counterions, such as salicylate or tosylate, are much more efficient in stimulating micellar growth [54, 63, 64]. Furthermore, the blending of cationic viscoelastic surfactant solutions with anionic viscoelastic surfactants was found to effectively stimulate the growth of worm-like micelles.

For nonionic surfactants, it was found, that anions decrease (salting-out) or increase (salting-in) the cloud point in accordance with the *Hofmeister* series [57]. A viscousifying effect of sodium sulfate on a nonionic viscoelastic solution was also reported [65, 66].

In solutions of anionic surfactants, one-dimensional micellar growth was observed in the presence of mono-, bi- and trivalent counterions, but viscoelasticity could only be observed with bi- and trivalent ions [37]. The effect of cations on micelle formation and structure buildup in anionic viscoelastic solutions due to their valence is much higher than due to their salting-in/out potential. Until now there have been no publications regarding effects of different anions on anionic viscoelastic surfactant solutions.

3.3.2 Viscoelastic Surfactants and Oil

The addition of oil to aqueous micellar surfactant solutions results in changes of the shape of the micelles. Nonpolar hydrocarbons solubilize inside the core of the micelles. Hence the mean curvature tends to increase. In the end, the elongated micelles transform to spheres, which causes a sharp decrease in the viscosity of the solution and loss of elastic properties. [5, 37, 67]

The interfacial tension between an aqueous solution and oil is lowered by viscoelastic surfactants since there are always single surfactant molecules, which are not integrated into a micelle and can orientate to the oil/water interface.

An effect on the viscosity of the oil/water interface has also been observed and reported. The interfacial viscosity is increased in the presence of viscoelastic surfactants. Thereby, the formation of a stable micro emulsion is impeded [12]. On the one hand, this might be a negative effect because the creation of micro emulsions is a desired process in chemical flooding. On the other hand, such a highly viscous oil/water interface could probably contribute to a better mobility ratio while propagating through the reservoir pores during a flooding process.

4. Viscoelastic Flooding in Chemical Enhanced Oil Recovery

In this chapter, the literature dealing with oil displacement by viscoelastic solutions is summarized. The influence of elastic effects on oil mobilization was predominantly investigated by application of viscoelastic polymer solutions in oil displacement tests. These results are presented in the first part of this chapter. The second part deals with the reported results regarding the effect of viscoelastic surfactant solutions on oil production.

4.1 Viscoelastic Polymers

For a long time, the consensus about polymer flooding was that the macroscopic sweep efficiency could be improved, but residual oil saturation is not affected. In 2000 *Wang et al.* reported an additional oil production of more than 12 % of OOIP during injection of highly concentrated polyacrylamide solutions in the Daqing oil field. The authors concluded that this significant amount of incremental oil recovery must be accompanied by a reduction of the residual oil saturation [68]. Based on these observations viscoelastic polymer flooding was intensively studied by several research groups by analysis of lab and field results, as well as mathematical simulation.

Several researchers conducted comparative core flooding experiments with polymer solutions, which exhibited similar viscosity and interfacial tension to oil, but showed different elastic behavior. The higher the elasticity of the driving fluid, the lower was the residual oil saturation. This could be observed under water-wet, oil-wet and mixed-wet conditions in secondary (no previous brine flooding) and tertiary (after brine flooding) mode [69, 70]. A delayed water breakthrough (WBT) was also observed for viscoelastic flooding [71].

In tertiary mode, the residual oil starts to mobilize at lower capillary numbers when the displacing fluid has viscoelastic properties. The elastic properties of a driving fluid could increase oil recovery without increasing the pressure gradient over the core. The application of viscoelastic fluids was found to be as efficient as ultra-low interfacial tension chemical flooding [69].

Residual oil can occur as oil films on the pore walls, trapped oil in dead end pores or as column or droplet type retained by capillary forces. According to the authors viscoelastic flooding could mobilize every type of residual oil [72]. The authors surmised that due to the entanglement of large and long molecules in viscoelastic flow, not only the fluid front was pushed, but also other (entangled) structures beside or behind it were dragged with it. This resulted in pulling and stripping effects, which also affected hydrocarbon molecules [14]. Furthermore, the velocity at pore walls increased with more pronounced elastic behavior, represented by increasing *Deborah* number in Figure 4-1.

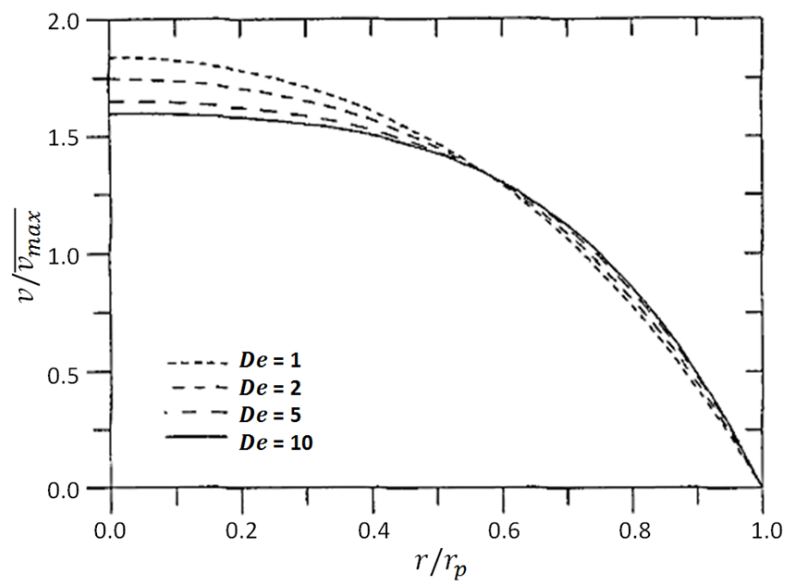


Figure 4-1: Velocity profiles in tube flow for varying *Deborah* numbers [73]

The changes in the velocity profile resulted in forces on oil droplets different from that caused by water or other *Newtonian* driving fluids. According to the authors, the higher velocity led to higher mass flow rate and therefore, higher kinetic energy near the pore wall. This resulted in better displacement of the residual oil film [70].

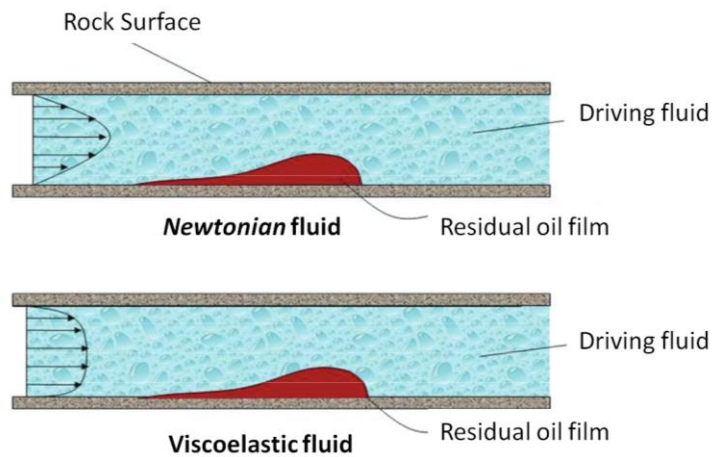


Figure 4-2: Velocity profile of different fluids and on residual oil film on oil wet pore wall [70]

Wang *et al.* [70] presented a series of photos of an oil film displacement process in a visualization core (Figure 4-3) over time. Photo 1 shows the initial state of the experiment.

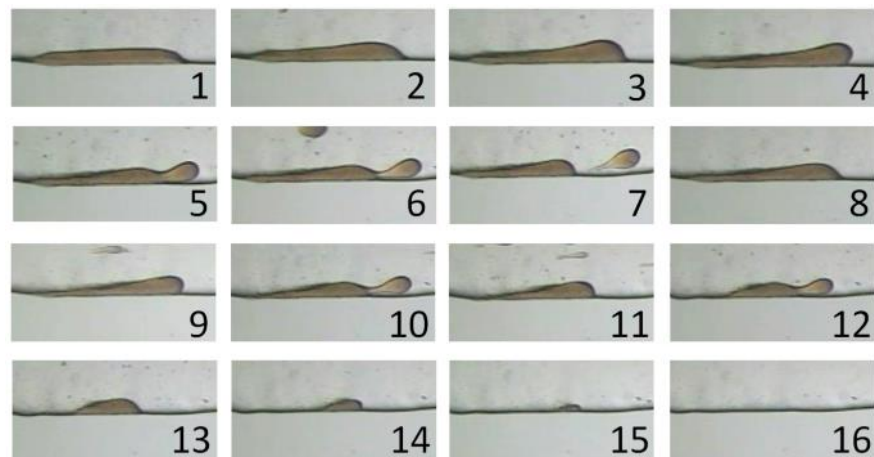


Figure 4-3: Mobilization of oil film [70]

While purely viscous fluids would just flush over the residual oil films in laminar flow, the viscoelastic fluid caused the oil to accumulate at the end of the film forming an elevation (picture 1 – 4 in Figure 4-3). Due to further pushing by the viscoelastic fluid a necking occurred in the film (picture 5). Eventually a single oil drop was formed (picture 7), which could be carried away by the driving fluid. This process repeated itself until the whole oil film was mobilized.

In high concentrated viscoelastic solutions the polymers orientate to the flow lines in small diameter pore necks and recoil in large diameter pores [71]. For that reason,

the fluids intrude deeper into recesses causing additional oil production out of dead-end pores, which was observed by *Wang et al.* (Figure 4-4).

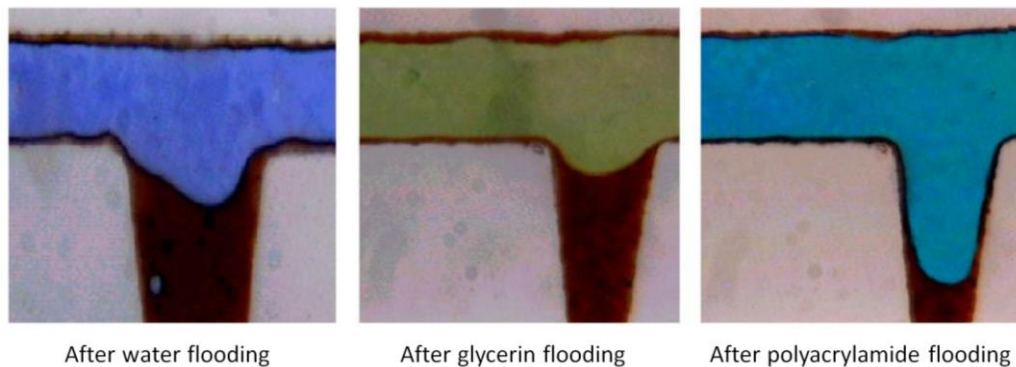


Figure 4-4: Recovery of residual oil from dead-end pores by water, viscous glycerin and viscoelastic polyacrylamide [74]

Mathematical simulations confirmed the experimental observations and showed that the flow lines of a viscoelastic driving fluid differ from purely viscous fluids [50]. Moreover, it was found, that the effect of elasticity on oil recovery is much more pronounced than that of viscosity increase [75].

In the Daqing oil field, viscoelastic polymer flooding was successfully applied. The incremental oil recovery valued 20 – 21 %_{OIP}, which is twice as high as incremental oil recovery reached with conventional polymer flooding, and the same like ASP flooding [75].

4.2 Viscoelastic Surfactants

In the literature, there are many reports on viscoelastic surfactant based fluids applied in hydraulic or acid stimulation of wells taking advantage of the favorable rheological properties for proppant transport and better acid distribution in the well [76–79]. However, the applicability of viscoelastic surfactant solutions for oil mobilization has been studied by only some researchers within the last ten years. Noteworthy papers are discussed in this paragraph.

Lakatos et al. [12] compared a conventional mixture of surfactants (alkyl-aryl-sulfonate and nonionic co-surfactant) to a viscoelastic surfactant solution with respect to their IFT reducing potential, bulk and interfacial rheology, and oil mobilization efficiency. As the solvent, synthetic reservoir brine with total dissolved solids (TDS) of around 5 g/l and a concentration of calcium chloride of only 0.05 g/l was used. The critical micelle concentration of the viscoelastic surfactant in the synthetic reservoir brine was found to be at only 0.005 g/l at 25 °C. This was an astonishing low value for the authors and indicates, that the formation of micelles was energetically very favorable for this type of surfactant. The CMC of the conventional surfactant mixture amounted around 1 g/l. The interfacial tension of the viscoelastic surfactant solution to crude oil was ca. 0.2 mN/m and thus, not sufficiently lowered to mobilize oil by the mechanism of IFT reduction alone. The IFT of the other surfactant mixture showed values less than 0.1 mN/m at and slightly above CMC. Neither of the surfactants induced spontaneous emulsification with crude oil. However, by adding alkaline to the conventional surfactant solution, strong emulsification of oil in water was observed. The viscoelastic surfactant increased the viscosity of the solution remarkably at concentrations higher than 1 g/l. The interfacial viscosity was also significantly increased from ca. 2 mPa·s ($c_{VES} = 0$) to nearly 150 mPa·s at low shear rates. Both the bulk and the interfacial viscosity decreased sharply at higher shear rates. The viscoelastic surfactant solution was not stable in the presence of higher concentrations of multivalent ions. The worm-like micelles were deteriorated, which resulted in the breakdown of any rheological effects. The efficiency of the different surfactant solutions with respect to mobilizing residual oil after brine flooding was tested by dynamic displacement tests in sandstone cores. The additional oil recoveries are summarized in Table 4-1.

Table 4-1: additional oil production in core floods conducted by *Lakatos et al.* [12]

chemicals used	additional oil recovery in %
conventional surfactant solution	4 %
conventional surfactant solution + alkaline	12 %
viscoelastic surfactant solution	10 %
conventional surfactant solution + alkaline followed by viscoelastic surfactant	15 – 17 %

According to the authors, the higher oil production of the viscoelastic surfactant solution compared to the conventional one was due to its higher viscosity and therefore, the better mobility ratio. In the case of the conventional system with added alkaline, the authors assumed that emulsification processes led to better oil production than in the core flood with the conventional surfactant alone. In the last oil displacement test, the viscoelastic solution acted again as mobility control agent. Therefore, it increased the volumetric sweep efficiency, while the conventional system improved microscopic oil displacement.

In 2009 *Morvan et al.* [80] reported the results of rheological measurements and oil displacement tests with a viscoelastic surfactant system. By conducting micro-rheological measurements it was found, that viscoelastic properties of the surfactant solution start to develop at concentrations higher than 0.5 wt. % in deionized water. At a surfactant concentration of 1 wt. % the solution showed ideal viscoelastic behavior ($G' = G''$). Three different brines were used to investigate the effect of salinity on the rheological properties of the solution. Brine 1 contained 20 g/l sodium chloride and was buffered to pH = 12. Brine 2 was synthetic sea water with TDS of 39 g/l. Brine 3 corresponded to double concentrated sea water. The amount of magnesium and calcium salts in brine 2 and brine 3 was 13.4 g/l and 26.8 g/l, respectively. The viscosity of the surfactant solution increased with surfactant concentration in all brines as a result of micellar growth and more entanglements. However, the viscosity increase in brine 3 was not as high as in the lower concentrated brines indicating that the surfactant system might be susceptible to high-salinity conditions. The researchers conducted an oil displacement test in a sandstone core at residual oil concentration at 80 °C. Surfactant solutions with a concentration of 0.1, 0.2, and 0.3 % in brine 1 were prepared and injected one after another into the core according to an elaborate procedure starting with the lowest concentration. The surfactant adsorption in the oily core was stated to amount to 50 µg/g, which is an acceptable level for an EOR surfactant according to the authors. During injection of the 0.1 % surfactant solution, the mobility was reduced by factor 1.5 (0.2 % surfactant solution – factor 18; 0.3 % surfactant solution – factor 25). The permeability reduction was negligible. In the end, the surfactant solutions could

mobilize 29 % of incremental oil. The authors assumed that this is a result of combined viscoelastic effects and IFT reduction.

In 2011 *Degré et al.* [25] published a paper on laboratory investigations on a viscoelastic surfactant solution followed by a field simulation study. In the laboratory, viscosity measurements, thermal stability tests, and core floods were conducted. The viscosities of two different surfactant systems (A and B) in four different brines (TDS: 0 – 194 g/l) were determined at four different temperatures and at a shear rate of 4 1/s. According to the authors both surfactant systems benefit from increasing salinity, since the viscosities increase up to salt concentrations of 97 g/l. Thermal stability tests have been conducted under anaerobic conditions with both surfactant systems in different brines (TDS: 6 – 97 g/l). The experiments were performed at 51 °C and 90 °C and lasted more than three months. No significant viscosity decrease could be observed after aging. Therefore, the surfactants were considered to be stable at these temperatures. The surfactant adsorption was determined by analyzing the breakthrough delay of the surfactant molecules in a single phase core flood and amounted to 2.4 – 2.9 mg/g on sandstone. The oil displacement experiments were conducted at 51 °C using a sandstone core at residual oil saturation after brine flooding. The brine had a salinity of 6.3 g/l TDS. By injecting the surfactant solution ($c_{surf} = 0.3$ wt. %) an incremental oil recovery of 12 – 15 % could be achieved.

In 2012 two other papers were published on the application of viscoelastic surfactants for chemical EOR by *Morvan et al.* [49, 81]. The authors analyzed rheological properties and oil displacement efficiency. The bulk flow behavior of a highly concentrated viscoelastic surfactant solution (1 wt. %) was investigated in comparison to a hydrolyzed polyacrylamide (polymer) solution (0.3 wt. %) in deionized water. Measurements on viscosity and first normal stress difference were conducted at a range of shear rates corresponding to typical flow velocities in the reservoir using a stress controlled rheometer. Both solutions showed shear thinning behavior. The shear dependent viscosity of the viscoelastic surfactant solution was always lower than that of the polymer solution, even though the surfactant solution was much higher concentrated. The first normal stress differences of the solutions are very similar in the tested range

of shear rates. Due to its lower viscosity, the shear stress on the viscoelastic surfactant solution is lower at the tested shear rates. According to Eq. 3-8, this results in a higher *Weissenberg* number for the surfactant solution compared to the polymer solution and therefore, more pronounced elastic properties. The adsorption was investigated by performing an injection test similar to that of *Degré et al.* [25]. As a result, an adsorption value of 350 $\mu\text{g/g}$ on sandstone was determined. The oil displacement test was performed in a sandstone core, again at residual oil saturation after a brine flood. The salinity of the used reservoir brine amounted to 6.3 g/l TDS, which had no significant influence on the bulk viscosity of the polymer and surfactant solution. At first, the polymer solution with a concentration of 0.1 % was injected at residual oil saturation, which led to an additional oil production of 26.6 % of the oil originally existing in the core. After that, the surfactant/polymer blend was injected, and again residual oil was mobilized. The cumulative oil production was increased by 13.2 %_{OIP}, which was proof to the authors for the efficiency of the surfactant.

Zhu et al. [82] tested a zwitterionic betaine surfactant with long carbon chains for its applicability in a chemical flooding operation in a sandstone reservoir with high water cut. The synthetic reservoir brine used had a salinity of 5.1 g/l TDS, and the concentration of divalent cations was 0.4 g/l. The viscosifying properties of the betaine surfactant in synthetic reservoir brine were investigated in a rotational viscometer. The viscosity of the solution increased with betaine concentration from 12 mPa·s at 0.1 wt. % to 99 mPa·s at 0.5 wt. % at 35 °C. At different concentrations and temperatures, the viscoelastic surfactant solutions showed shear thinning behavior. In oscillatory rheological tests (frequency sweeps) the storage and loss moduli of the betaine solutions followed similar trends, indicating a high grade of viscoelasticity over a concentration range of 0.3 – 0.5 wt. % and temperatures between 35 °C and 65 °C. The results of interfacial tension measurements between reservoir oil and viscoelastic surfactant solutions were also reported and showed promising values. For example, the interfacial tension between 0.1 wt. % betaine solution and oil amounted to $6.2 \cdot 10^{-3}$ mN/m at 35 °C and could be further decreased by one order of magnitude by addition of co-surfactants and alkali. Oil displacement tests were conducted in sandstone cores. When the water cut of brine flooding in the oil displacement test reached 98 %, a

chemical slug with a surfactant concentration of 0.3 wt. % was injected. All of the tested chemical slugs contained co-surfactants and/or 0.8 wt. % alkali. The injection of the (alkali-) surfactant solutions resulted in an additional oil recovery of 13 – 17 % of the original oil in place. Chemical slugs containing alkali were most effective.

Summary

All the papers mentioned above contain promising aspects for chemical flooding with viscoelastic surfactant solutions. Viscosifying properties, shear thinning behavior, thermal stability and the potential to reduce the interfacial tension to oil were reported, and the efficiency of the used surfactants to mobilize additional oil after brine flooding was confirmed in every publication. The incremental oil production amounted to 12 – 17 %_{OOIP} [25, 49, 81, 82]. The reported adsorption values varied between 0.35 and 2.9 mg/g on sandstone and 50 µg/g in the presence of oil in a sandstone core. Measurements, which are used to identify viscoelastic behavior, and the obtained data are only included into the publications of *Morvan et al.* and *Zhu et al.*

All the reported tests were conducted with low saline brines. In the tests of *Lakatos et al.* [12] no worm-like micelles are formed in the presence of polyvalent cations, and *Morvan et al.* [80] reported a sharp decrease in viscosity at a salinity of 78 g/l TDS. However, *Degré et al.* [25] showed that salinity could also have a beneficial effect on the structure and the rheological properties of a viscoelastic solution to a certain extent.

The interpretation of the published core flooding data is quite complicated for an external party. The reason for that is that the conditions (temperature, salinity, the concentration of surfactants) of the core flooding tests were not comparable to the conditions, where the bulk properties were determined in some papers [49, 81]. In the other publications the chemical solutions contained co-surfactant and alkali in addition to the surfactant, which was supposed to form a viscoelastic network [12, 80, 82]. Therefore, the potential of the viscoelastic surfactants alone regarding oil mobilization could not be rated. If there were any viscoelastic effects contributing to oil production is not clear, either. *Lakatos et al.* concluded that mobility control is the primary mechanism for oil recovery of viscoelastic solutions.

In chapter 3.3.2 the influence of oil on the shape of the micelles and hence, on the rheological properties of the viscoelastic surfactant solutions is discussed. The micelles transform from worm-like to spherical in the presence of hydrocarbons. Therefore, such solutions lose their viscoelastic properties. This effect was not considered in any of the publications presented in this paragraph.

5. The Triphenoxymethane Derivatives

Triphenoxymethanes are known and have been synthesized since 1973 [83]. They have broadly been used as complexing agents for ions of tin and alkali metals [84, 85]. About ten years ago BASF Se was looking for new amphiphilic structures and patented the synthesis of Triphenoxymethane derivatives and the usage thereof, especially as surfactants and thickeners, in 2011 [9].

The generic structure of a Triphenoxymethane is given in Figure 5-1.

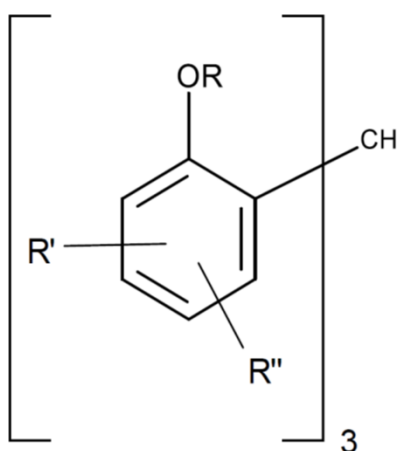


Figure 5-1: Generic chemical structure of a Triphenoxymethane [86]

R represents a long chain hydrophilic group, whereas R' and R'' symbolize compact hydrophobic groups. Triphenoxymethanes are amphiphilic molecules with surfactant properties. The structure is different from conventional viscoelastic surfactant molecules, which typically consist of a compact hydrophilic head and a long hydrophobic tail group. As a result, the formation of micelles with novel morphology was expected, characterizing a new class of viscoelastic surfactant solutions. Indeed it could be shown by molecular modeling, that, when associating to micelles, the hydrophobic heads assemble towards each other, forming a compact core. The long hydrophilic tails protrude into the water phase and enable interactions between different micelles, forming a network [86]. Viscoelastic solutions of conventional surfactants with long hydrophobic chains lose their viscosity and elastic properties in contact with oil since the micelles become spherical [52, 87]. By designing the hydrophobic core of Triphenoxymethane micelles as compact as possible, it was thought that the accumulation of oil

inside a micelle could be prevented. Known viscoelastic surfactants are often cationic, exhibit high levels of adsorption and are environmentally hazardous. The Triphenoxymethane derivatives, which were synthesized for possible application in enhanced oil recovery, are anionic and their non-toxicity in seawater was verified [88, 89].

In the following sections the three Triphenoxymethane derivatives, which were investigated in the scope of this thesis are described in more detail. Henceforward, Triphenoxymethane will be abbreviated with TriX.

5.1 TriX-MB

TriX-MB was the primary subject of the study. The main characteristic of this molecule is the formation of viscoelastic solutions in highly saline brines at moderate temperatures. TriX-MB forms very stiff, rod-like micelles with very high persistence lengths of several hundreds of nanometers in synthetic reservoir brine (NDIIa, TDS = 186 g/l, composition described in chapter 6.1.1) and in a sodium chloride solution with the same ionic strength as NDIIa. Henceforth, these are referred to as secondary aggregates. The micellization occurs at very low concentrations (≈ 50 ppm) [90]. The formation of rod-like micelles is energetically very favorable for the TriX-MB molecules, and takes place even before the surface of the solution is fully covered (cf. chapter 3.1). Therefore, the CMC cannot be determined by surface tension measurements. The aggregation to rod-like micelles is thermodynamically stable to the extent that these aggregates can be considered to be more robust to break-up than other worm-like micelles [90].

At low shear, the secondary aggregates interact with one another and form a viscoelastic network (tertiary aggregation). The network mesh size can be greater than 1 μm . In this network, the rod-like micelles are linked by salt bridges. The viscoelastic properties become more pronounced with increasing salinity and are not negatively affected by the presence of divalent cations. The cross-linking is even more stable with divalent than with monovalent cations. This results in a stronger and more rigid network and therefore, higher viscosity in NDIIa brine compared to NaCl solution. It was found that calcium cations have a particularly beneficial effect on the interactions be-

tween TriX-MB molecules, which is unique for EOR chemicals. In deionized water, TriX-MB induces no viscosity increase and no development of viscoelasticity. A detailed rheological characterization of the complex structures formed by TriX-MB molecules was compiled by experienced and skilled scientists of BASF and was not part of the thesis. The rheological measurements were extensively carried out in NDIIa at 55 °C, which corresponds to the reservoir temperature of a possible field test and is the test temperature of most experiments conducted in the scope of this thesis. Figure 5-2 shows a frequency sweep of TriX-MB in NDIIa at a constant deformation amplitude of $\gamma = 100\%$ and a test temperature of $\vartheta = 55\text{ °C}$ [86, 88].

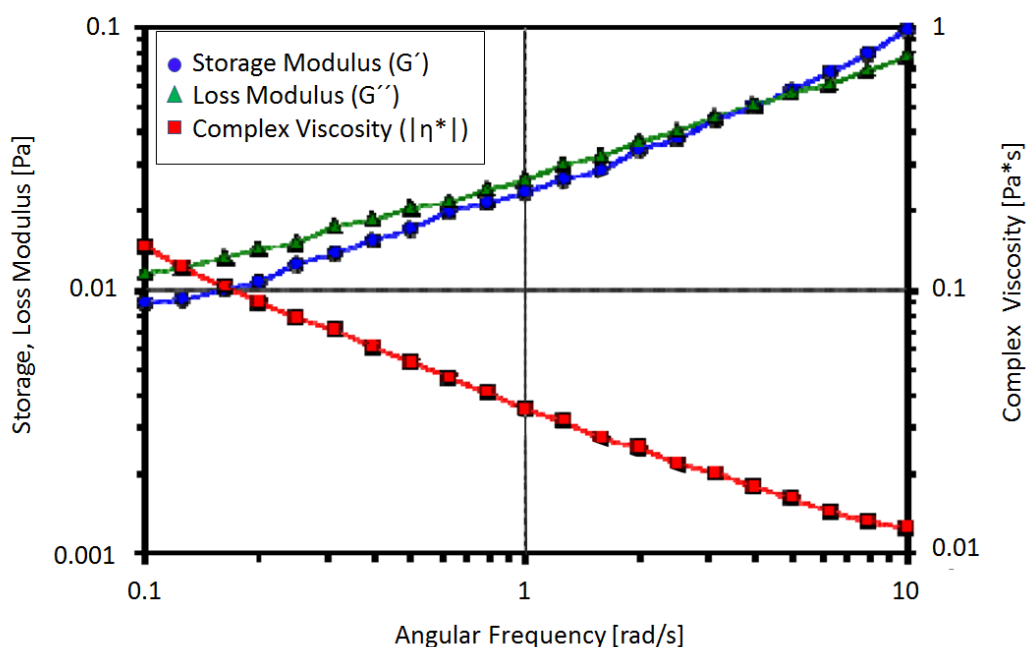


Figure 5-2: Results of a frequency sweep of TriX-MB in NDIIa at 55 °C with constant deformation of 100 % [86]

At low frequencies, the viscous behavior is slightly more dominant than the elastic behavior. This turns at higher frequencies. The crossover ($G' = G''$) is at around 4 rad/s. Within the whole range of frequencies the storage and the loss modulus are very close to each other, which means that the dissipation factor ($\tan\delta$) is close to 1. The solution is highly viscoelastic. In sodium chloride solution TriX-MB also develops good viscoelastic behavior with a dissipation factor close to 1. However, the magnitude

of the storage and loss modulus, as well as the viscosity, are lower. TriX-MB obtains shear thinning behavior in saline solution.

The cloud point of TriX-MB in NDIIa is at around 90 °C and over 100 °C in diluted NDIIa with TDS = 10 %. The molecular weight of TriX-MB is around 2250 g/mol. The HLB (hydrophilic-lipophilic-balance) value is ca. 16. The HLB concept is described in Appendix A1.

Preliminary porous media tests have been reported [86]. The injection of 0.25 wt. % TriX-MB in synthetic reservoir brine (NDIIa) into a sandstone core with a permeability of ca. 2 D was quite difficult at 55 °C. It resulted in a pressure increase by a factor of around 200 compared to brine. In oil displacement tests TriX-MB solutions mobilized significantly more oil than brine alone.

The great advantages of TriX-MB over other reported viscoelastic surfactants are that it shows viscoelastic behavior in saline solutions at surfactant concentrations below 0.5 wt. %.

5.2 TriX-TA

TriX-TA is closely related to TriX-MB, with a chemical variation in the “head” of the molecule. TriX-TA forms spherical micelles as secondary aggregates under the same conditions like TriX-MB. The aggregation to micelles is energetically also very favorable, and the CMC is not predictable by surface tension measurements. The micelles are 9 – 15 nm in size [91] and do not cross-link to a network (tertiary aggregation). TriX-TA was shown not to develop any viscoelasticity in solution in experiments at BASF [91]. Therefore, it was intended as a control for the mechanistic probing of the mode-of-action of TriX contributing to oil mobilization.

The molecular weight is around 2340 g/mol, and the HLB value is 16.

5.3 TriX-M

TriX-M is much smaller in size (molecular weight \approx 750 g/mol) than TriX-MB and TriX-TA and has the structure of a typical anionic surfactant, apart from the fact that the “head” group is hydrophobic and the “tail” hydrophilic. TriX-M does not associate

to any aggregations or networks. It has the simplest chemical structure of the Triphenoxymethane derivatives. Therefore, it should give an even deeper insight into the mechanisms of the molecular structure (“inverted surfactant”) contributing to oil production. The HLB value is very similar to the other derivatives (HLB \approx 16).

6. Experimental Procedure and Data Analysis

The objectives of this thesis were to assess the applicability of the TriX derivatives, which were presented in the last chapter, in chemical enhanced oil recovery operations and to investigate which mode-of-action contributes to oil mobilization. The focus of the laboratory investigations was on TriX behavior in porous media.

An experimental procedure was conceived in order to examine the bulk properties and the interaction of the TriX solutions with single components of an oil reservoir (rock, brine, oil) at first. Initially, the surface tensions of differently concentrated TriX solutions and the CMC of TriX-M in reservoir brine were determined. Furthermore, static adsorption on sand, the interaction with crude oil, and the properties of TriX solutions containing different salt ions were investigated. These tests were necessary for the interpretation of the behavior of TriX in porous media. Single phase core flooding experiments were carried out to probe the injectivity of various TriX solutions into reservoir rock.

Only when the behavior of the TriX molecules in contact with sand, oil and different saline solutions was understood, and the injectivity into reservoir rock was proven, oil displacement tests were conducted. Static imbibition tests should give a first impression about the effectivity of TriX derivatives with respect to oil mobilization. Extensive oil displacement experiments in a core flooding unit were the main part of the analysis.

In this chapter, the materials used are introduced at first. After that, the experimental procedures and approaches to analyze the results are explained.

6.1 Materials Used

The aqueous solutions used in the experiments first passed quality assurance by determining density and viscosity at 20 °C and 55 °C.

Density was measured with a density meter (DMA 4500, Anton Paar). The viscosities, with the exception of TriX-MB solutions, were determined with a rolling ball viscometer (Lovis 2000 ME, Anton Paar).

Viscosity measurements of TriX-MB solutions were done with the Modular Compact Rheometer (MCR 302, Anton Paar) with concentric cylinder geometry at 55 °C. The

viscosity was measured in oscillation at an angular frequency of $\omega = 10$ rad/s and deformation of $\gamma = 100$ %. The density and viscosity values of the solutions used are given in Appendix A2.

6.1.1 Synthetic Reservoir Brine and Saline Solutions

As a basis for all aqueous solutions, either the synthetic reservoir brine NDIIa with 18.6 wt. % TDS, or saline solutions of different chlorides, all with the same ionic strength as NDIIa, were prepared. The composition of NDIIa is given in Table 6-1.

Table 6-1: Composition of NDIIa

Salt	molecular formula	salt concentration in g/l
Sodium chloride	NaCl	132
Calcium chloride dihydrate	CaCl ₂ · 2 H ₂ O	56.429
Magnesium chloride hexahydrate	MgCl ₂ · 6 H ₂ O	22.42
Sodium sulfate	Na ₂ SO ₄	0.27
Sodium (meta) borate tetrahydrate	NaBO ₂ · 4 H ₂ O	0.38

The ionic strength of NDIIa is 3.75. In Table 6-2 the names and compositions of the other saline solutions used, having the same ionic strength as NDIIa, are given.

Table 6-2: Designation and compositions of saline solutions

designation	salt	molecular formula	salt concentration in g/l
NaCl	Sodium chloride	NaCl	219.13
0.5 NaCl			109.57
Na ₂ SO ₄	Sodium Sulfate	Na ₂ SO ₄	177.53
0.5 Na ₂ SO ₄			88.77
NaSCN	Sodium thiocyanate	NaSCN	303.98
0.5 NaSCN			151.55

For simplification and better legibility of the chapters dealing with experimental investigations, the saline solutions will be mentioned by their designation. Salt concentration will not be described again.

The pH value of all brines was adjusted to 5.5 – 6.0 with hydrochloric acid.

6.1.2 Surfactant Solutions

TriX-MB Solutions

The stock solution was provided by BASF and contained 17.4 wt. % TriX-MB in deionized water. This was diluted to concentrations of 0.1 wt. % or 0.25 wt. % in the different brines.

The preparation of 0.1 wt. % TriX-MB solution in NDIIa, NaCl or 0.5 NaCl brines was conducted in the following steps:

1. Solution of 5.747 g of TriX-MB stock solution in 1000 g brine
2. Stirring for at least 24 hours at room temperature
3. Heating to 70 °C for at least 2 hours
4. Storage of the solution at 55 °C until use (maximum 14 days)

Preconditioning of TriX-MB solutions was necessary to ensure uniform rheological properties. The formation of the secondary aggregates takes a long time at ambient conditions but is accelerated by heating to 70 °C. After heating the sample overnight, the very long and thermodynamically stable rod-like micelles were formed. These secondary aggregates are the basis for the association to form the viscoelastic network (tertiary aggregation), which exhibits the desired rheological properties. Hence proper and defined formation is essential [92].

To prepare 0.25 wt. % TriX-MB solution, the mass of TriX-MB stock solution, which was dissolved in the different brines, was adjusted accordingly (14.37 g/1000 g), otherwise steps 2 – 4 are identical.

TriX-MB solutions in sodium sulfate and sodium thiocyanate were prepared just as the solutions in NDIIa and NaCl brines, except the temperature in step 3 was different. Solutions in Na₂SO₄ and 0.5 Na₂SO₄ had to be heated to 55 °C; solutions in NaSCN and 0.5 NaSCN were heated up to 105 °C.

TriX-TA Solutions

The stock solution was provided by BASF and contained 18.3 wt. % TriX-TA in deionized water. 0.1 wt. % and 0.25 wt. % TriX-TA in NDIIa solutions were prepared by dissolving 5.464 g and 13.66 g stock solution in NDIIa brine, respectively. Further preconditioning of the solutions was carried out as described for TriX-MB solutions to accelerate the formation of secondary aggregates.

TriX-M Solutions

The stock solution was provided by BASF and contained 88 % pure TriX-M (+ ca. 9 % NaCl and 3 % other components). To prepare TriX-M solutions, the surfactant was dissolved in NDIIa brine to the target concentrations.

Triton-X-100 Solutions

Triton-X-100 is a nonionic surfactant commonly used in oilfield applications [93] and structurally very similar to TriX-M. Because of that, comparative studies were done on these two molecules. Since there are several publications about this surfactant, it was also the subject of choice for comparative investigations with TriX-MB and TriX-TA. The molecular weight of Triton-X-100 is 625 g/mol, and the HLB value amounts to 13.5 [94].

The surfactant was dissolved in NDIIa to the target concentrations of 0.1 wt. % and 0.25 wt. %.

Crude Oil

Bockstedt oil, provided by Wintershall Holding GmbH, was used as the oil phase. Water had already been separated by centrifugation. The densities and viscosities at room temperature and 55 °C are given in Table 6-3.

Table 6-3: Density and Viscosity of Bockstedt oil

	ρ in g/cm ³	η in mPa·s
$\vartheta = 25\text{ }^{\circ}\text{C}$	0.90	200
$\vartheta = 55\text{ }^{\circ}\text{C}$	0.88	32.1

Only in one core flooding experiment (CF #8), a charge of Bockstedt oil with a viscosity of 280 mPa·s at 25 °C and 56.5 mPa·s at 55 °C was used.

6.1.3 Sand and Core Material

In static adsorption tests, burned out natural sand with grain sizes between 400 and 500 μm was used. The specific surface area was determined by taking an adsorption isotherm with nitrogen and BET analysis. It was found to be 0.962 m²/g.

Two types of sandstone (Bentheimer and Michigan) were used for the imbibition and core flooding experiments. Thin sections of sandstone probes were produced and analyzed [95]. The pore size distribution and the specific surface area of the core material were determined by mercury porosimetry. The pore size distributions of both sandstones are given in the Appendix A3.

The Bentheimer sandstone was a well-sorted rock material consisting of 94 % quartz, around 4 % feldspar and around 2 % other phases. It could be considered to be almost free of clay (< 2 %). The median pore diameter of the Bentheimer sandstone was at 42.1 μm , and the specific surface area amounted to 0.234 m²/g. More than 90 % of the pore volume is characterized by pore diameters between 10 and 100 μm . Less than 1 % of the pore volume is occupied by pore with less than 30 nm in diameter.

The Michigan sandstone showed a moderately sorted texture and contained 93 % quartz, ca. 4 % feldspar, less than 1 % muscovite and 2 % other phases. Thus, the clay content was also very low (< 3 %). The Michigan sandstone had a median pore diameter of 24.3 μm and a specific surface area of 0.69 m²/g. The pore size distribution of the Michigan sandstone is wider than for Bentheimer. More than 80 % of the pore volume belongs to pores with a diameter between 1 and 100 μm . Again less than 1 % is characterized by a pore diameter below 30 nm.

6.2 Critical Micelle Concentration of TriX-M and Triton-X-100 in Synthetic Reservoir Brine

The critical micelle concentration was determined since this is a crucial parameter to adjust the target concentrations of testing solutions for other experiments (e.g., static adsorption and imbibition tests). The surface tensions (SFT) of differently concentrated surfactant solutions were used to determine the CMC. Since the critical micelle concentration of a surfactant depends on experimental conditions (temperature, type of solvent, salinity, the surface area of the solution), it is not a characteristic value of the system of surfactant and solvent or even a material characteristic of the surfactant.

The TriX derivatives and Triton-X-100 were subjects of investigation. TriX-MB and TriX-TA do not have a classical CMC (cf. chapters 5.1 and 5.2). However, they were included in this study for reasons of comparability and the sake of completeness. Comparative studies of TriX-M and Triton-X-100 were of particular interest since these molecules are classical surfactants and structurally very similar.

Dilution series of TriX-M, Triton-X-100, TriX-TA, and TriX-MB in NDIIa brine were prepared for surface tension measurements. Every solution was stirred for at least 24 hours at room temperature. TriX-M and Triton-X-100 solutions were then stored at 20 °C until usage. For preconditioning, TriX-TA and TriX-MB solutions were stored at 70 °C in a compartment dryer overnight and at 55 °C for at least one more day. Before usage TriX-TA and TriX-MB solutions were tempered to 20 °C.

Surface tension measurements were carried out with a ring tensiometer (K11, Krüss) using the Du Noüy ring method. By using the same vessel and adjusting the same filling height for every measurement, the outer surface area of the solutions was held almost constant.

6.3 Static Adsorption of TriX Derivatives and Triton-X-100 on Sand

To investigate the static adsorption of TriX-MB, TriX-TA, TriX-M, and Triton-X-100, solutions of all surfactants in NDIIa brine were prepared and mixed with sand. Since most of the core flooding experiments were carried out with NaCl as brine, solutions of TriX-MB in NaCl were also prepared and included in the studies.

Before usage in adsorption tests the sand was washed over a 315 μm sieve, to avoid the supernatant surfactant solution becoming turbid because of fine suspended particles. The washed sand was then dried at 180 $^{\circ}\text{C}$ for at least 16 hours. After that, the sand cooled down to room temperature in a desiccator.

The surfactant solutions were used at a concentration of 0.1 wt. %, which exceeds the CMC of the classical surfactants TriX-M and Triton-X-100 by a factor of more than 20 at room temperature (see chapter 7.1). In Table 6-4 the concentration of the surfactant solutions is given in $\text{mmol}/\text{kg}_{\text{solution}}$.

Table 6-4: Concentration of used surfactants

Surfactant	TriX-MB	TriX-TA	TriX-M	Triton-X-100
c in $\text{mmol}/\text{kg}_{\text{solution}}$	0.44	0.43	1.33	1.55

The surfactant solutions were mixed with sand in equal weight quantities in closed glass flasks. The samples were stored in a compartment dryer at 55 $^{\circ}\text{C}$ for 14 days, which corresponds to the duration of the static oil displacement tests. During this time the samples were shaken at least every three days.

Adsorption was evaluated by determining the loss of surfactant molecules out of bulk solution after storage with sand for 14 days at 55 $^{\circ}\text{C}$. Therefore, the concentrations of the solutions were determined before and after storage.

As a measure of the concentration of the surfactant solutions the extinction of the clear fluids was measured with a UV spectrophotometer (DR 6000, Hach). In a wavelength scan a suitable peak, which correlates with the concentration of the corresponding surfactant solution, was characterized. For the TriX derivatives, the strongest peak should be around 190 – 200 nm. Since this is at the end of the measuring spectrum of the device and could, therefore, be imprecise, it was decided to analyze the $n-\pi^*$ -transition peak at ca. 270 – 280 nm (detection of aromatics) [96].

The wavelengths (λ) used for the extinction measurements of the four surfactants are given in Table 6-5.

Table 6-5: Wavelength for extinction measurements

Surfactant	TriX-MB	TriX-TA	TriX-M	Triton-X-100
λ in nm	272	272	274	278

A calibration curve of the extinction as a function of concentration was taken for every TriX derivative and Triton-X-100, and later used to determine the unknown concentration of a surfactant solution.

The exact concentrations of the surfactant solutions at the beginning of the experiments were identified and used as the baseline for the static adsorption tests. After 14 days in contact with sand, samples for extinction measurements were taken from the supernatant solutions.

6.4 Interfacial Tension and Interaction of Solutions of TriX Derivatives and Triton-X-100 with Crude Oil

Knowing how TriX derivatives and oil interact with each other is essential for planning and assessment of enhanced oil recovery processes.

There are different modes of interaction between a surfactant and oil:

- a) adsorption onto the interphase between aqueous solution and oil
- b) dispersion and dissolution of surfactant molecules from the aqueous into the oil phase
- c) dispersion and dissolution of oil components in the aqueous phase by means of a surfactant
- d) reactions of surfactant molecules with oil components, changing their structure and surfactant efficiency

All these processes may modify the properties of the water and oil bulk phases as well as the contact area (interface) between them.

6.4.1 Interfacial Tension Measurements

The reduction of interfacial tension and therefore capillary forces, which retain oil in the pores of the reservoir, is an important mechanism to mobilize more oil.

Interfacial tension measurements were conducted on all surfactant solutions that were used to determine CMC of the TriX derivatives, as well as Triton-X-100 in NDIIa brine. Bockstedt oil was used as the oil phase.

The measurements were carried out with the ring tensiometer (K11, Kruess) at 20 °C with lamella tear-off method (ASTM D971-99a). Again the same vessel was used for every measurement, and the filling height was held constant.

6.4.2 Changes in surfactant concentrations in aqueous solutions after oil contact

These tests were intended to investigate if dispersion and solution of surfactant molecules from the aqueous into the oil phase (or vice versa) take place. Emulsification could also be rated by visual examination.

0.1 wt. % surfactant solutions were mixed with Bockstedt oil in glass vessels in equal weight quantities. For every surfactant two samples were prepared in NDIIa, and for TriX-MB two additional samples were prepared in NaCl. The samples were stored for 14 days at 55 °C and shaken every three days. Following storage, the samples were cooled down to room temperature, and probes from the clear aqueous phases were taken to determine the surfactant concentrations by UV extinction measurements as described in chapter 6.3.

6.5 Spontaneous Imbibition Tests

The ability of TriX-MB, TriX-TA, and TriX-M in NDIIa to improve spontaneous imbibition into oil saturated sandstone was studied and compared to Triton-X-100. Imbibition tests with TriX-MB were also conducted in NaCl since this combination of surfactant and brine was used in core flooding experiments.

Displacement of a fluid from a porous medium by another fluid phase is always an interplay of gravity, capillary, and viscous forces. To determine which of these mechanisms is dominant the inverse *Bond* number can be used. The inverse *Bond* number N_B^{-1} is defined as ratio of capillary to gravity forces [97].

$$N_B^{-1} = c \cdot \frac{\sigma \cdot \sqrt{\frac{n}{k}}}{\Delta\rho \cdot g \cdot l} \quad \text{Eq. 6-1}$$

N_B^{-1}	–	inverse <i>Bond</i> number
c	–	constant ($c = 0.4$)
σ	–	interfacial tension in N/m
n	–	porosity
k	–	absolute permeability in m^2
$\Delta\rho$	–	density difference of aqueous phase and oil in kg/m^3
g	–	gravitational acceleration in m/s^2
l	–	length of the core in m

An inverse *Bond* number less than 1 is an indicator for gravitational dominated imbibition process, while higher than 1 means that the imbibition is mainly caused by capillary forces. Imbibition processes also depend on initial water saturation. The higher the initial water saturation in sandstone cores, the more uniform is the spreading of the water front from all open faces of the core (less fingering) [98].

Imbibition Tests were carried out with Bentheimer sandstone cores, with the following characteristics:

- length: ca. 6 cm
- diameter: ca. 3.8 cm
- pore volume (PV): ca. 15 cm^3
- brine permeability: ca. 1500 mD

As aqueous phases different brines (NDIIa and NaCl) and solutions of TriX derivatives and Triton-X-100 at concentrations of 0.1 wt. % and 0.25 wt. % were tested. The surfactant solutions were conditioned as described in chapter 6.1.2. As oil phase Bockstedt oil was used.

Bentheimer sandstone cores were first saturated with brine; afterward, ca. 7 pore volumes of Bockstedt oil were injected to set original oil in place. The cores were then aged in Bockstedt oil for two weeks. After that, the cores were put into an Amott cell (Figure 6-1) and surrounded by the aqueous solution to be tested. Aging of the cores and imbibition tests were conducted at 55 °C.

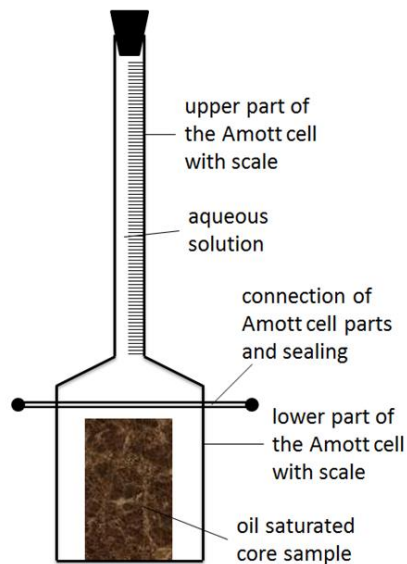


Figure 6-1: Amott cell

The aqueous solutions imbibed into the pores of the sandstone, while oil was mobilized and produced from the core, accumulating in the throat on top of the Amott cell. The produced oil volume could be measured by reading the scale, providing a straightforward comparison of the effectiveness of the different additives.

6.6 Investigations on Salt Effects on TriX-MB Solutions

In saline solutions, TriX-MB forms very stiff rod-like structures. The network structure of TriX-MB in aqueous solutions was found to be depending on the valence of cations that are present in the brine. With monovalent ions (Na^+) the cross-linking between the rods in the network is much weaker than with divalent ions (especially Ca^{2+}).

The experiments intended to investigate if different anions also influence the bulk properties and performance of TriX-MB solutions in porous media and if these effects

correlate with the *Hofmeister* series, which has been introduced in chapter 3.3.1. The *Hofmeister* series arranges anions by their capability to promote either the hydrophobic or the hydrophilic properties of a macromolecule in aqueous solution.

For the investigations, TriX-MB was diluted in sodium sulfate (intensifying hydrophobic effects), sodium chloride (neutral) and sodium thiocyanate (intensifying hydrophilic effects) solutions. The salinity of the brines corresponded to 100 % and to 50 % of the ionic strength of NDIIa. Pure brine, as well as solutions with TriX-MB concentrations of 0.1 wt. % and 0.25 wt. % were investigated concerning bulk viscosity and interfacial tension to Bockstedt oil.

Viscosity measurements were conducted with the Modular Compact Rheometer (MCR 302, Anton Paar) in oscillatory mode at constant deformation amplitudes of 100 % and angular frequencies of 10 rad/s.

Measurements of interfacial tension were carried out with the ring tensiometer (K11, Kruess), using the lamella tear-off method (ASTM D-971-99a) at 55 °C.

Moreover, spontaneous imbibition tests were conducted to investigate the influence of the different ions (sulfate and thiocyanate) on the oil displacement performance of TriX-MB. Core preparation and experimental procedure of the imbibition tests have been described in chapter 6.5.

6.7 Core Flooding Experiments

In the core flooding experiments, visually homogeneous cores were used. The focus of the investigation was on the capability of TriX to alter the physico-chemical properties of fluids and rock, as well as their interaction, to maximize oil recovery.

6.7.1 Experimental Setup

Figure 6-2 shows the scheme, and Figure 6-3 a photo of the core flooding unit. A dosing pump (double piston pump) delivers water as a driving fluid for the piston accumulator. Using the dosing pump and a piston accumulator, the test fluid (brine with or without additives, oil) can be injected into the cores, which are installed in two Core Holders (Hassler cells). The cores can be flooded in series or independently. Pressure

sensors are installed at the inlet and outlet of both cores. The piston accumulator, the core holders with pressure sensors and all the pipes are in a heating chamber (experimental temperature: 55 °C). The main material of all parts of the core flooding unit is stainless steel.

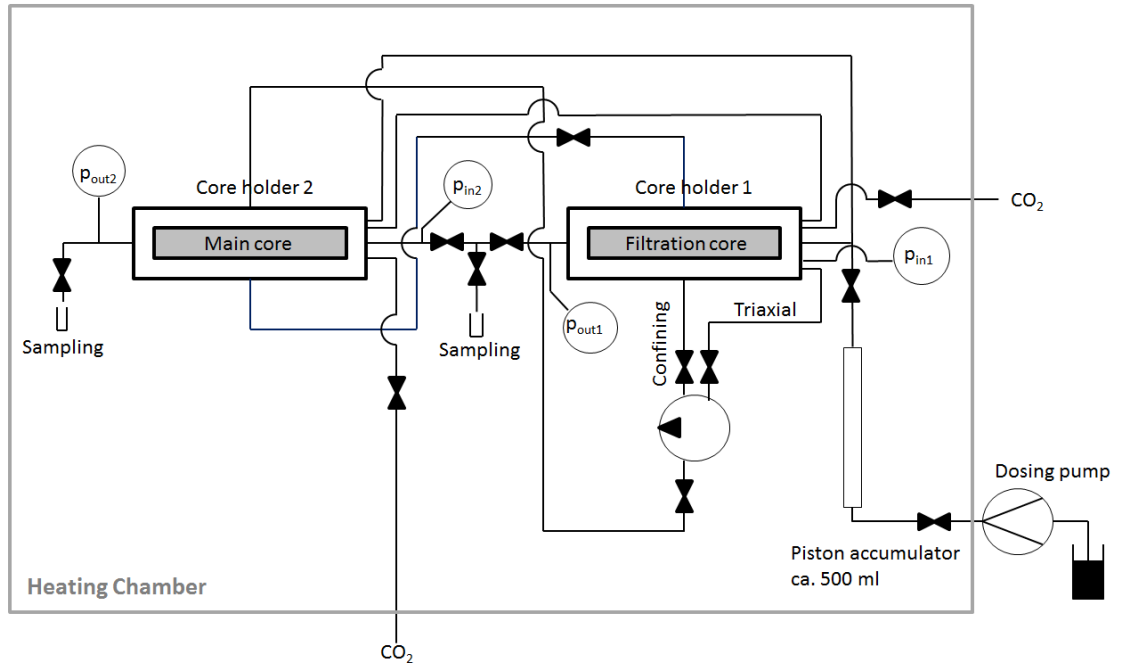


Figure 6-2: Scheme of the core flooding unit

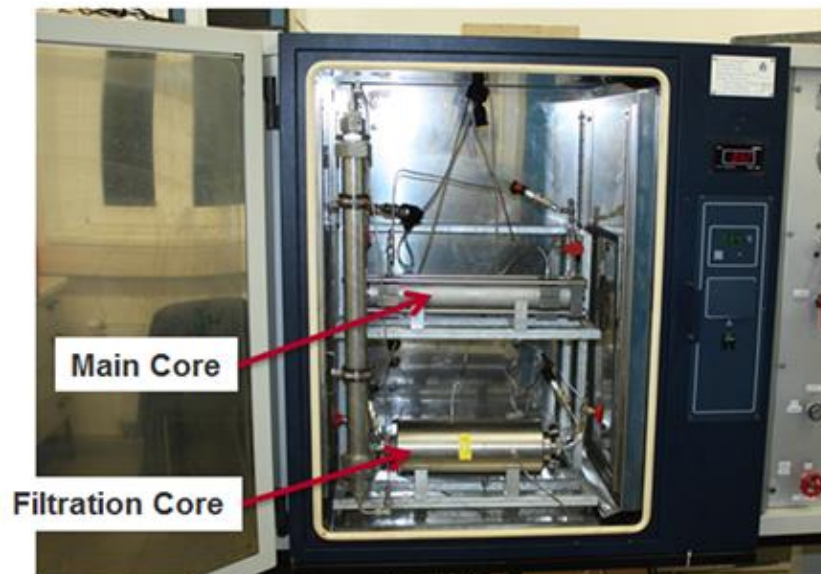


Figure 6-3: Photo of the core flooding unit

For core flooding experiments the following aqueous solutions were applied.

- NDIIa brine
- NaCl brine
- 0.1 wt. % TriX-MB in NDIIa brine
- 0.1 wt. % TriX-MB in NaCl brine
- 0.1 wt. % TriX-TA in NDIIa brine
- 0.1 wt. % TriX-M in NDIIa brine

Bockstedt oil was used as the oil phase.

The core flooding experiments were carried out with two different types of sandstone. Injection of TriX-MB in NDIIa solution and the first injection tests with TriX-MB in NaCl were conducted using Bentheimer sandstone. For the other tests, lower permeable Michigan sandstone was applied.

Every core flooding test (except CF #8) was conducted using a filtration core (FC) (ca. 6 cm in length) and a main core (MC). For the first tests the main core also had a length of ca. 6 cm, but for most experiments, a core of ca. 30 cm in length was used. The filtration core should simulate the near-wellbore area, where filtration of very rigid and large TriX structures is expected. The main core represented the reservoir.

6.7.2 Core Preparation

For the experiments the cores were prepared as follows:

1. Cutting to desired dimensions
2. Drying in an oven for ca. 16 hours at 120 °C
3. Installation into core holders (Hassler cells)
4. Setting confining pressure
5. 1st evacuation of the core sample
6. Saturating the core with CO₂
7. 2nd evacuation of the core
8. Saturating the core with brine
→ steps 5 to 8 were conducted on both cores separately
9. Tempering the core flooding unit to 55 °C
10. Determining brine permeability of each core

Brine permeability was generally determined at ten different flow rates, unless noted otherwise. The ramp of flow rates was run from high to low to high rates.

6.7.3 Injection Tests

An injection test was composed of two parts: 1st – Injection of TriX solution; and 2nd – Brine injection to flush TriX solution out of the core.

After core preparation as described in the previous section, the appropriate TriX solution was injected into the cores at a flow rate of 0.24 ml/min, which corresponded to a Darcy velocity of $v_D = 1$ ft/d. During injection the cores were connected, hence the solution first passed the filtration core and after that the main core. The increase of the pressure drop over the cores was recorded and evaluated. When the pressure drop reached a constant level, or after injection of a sufficient volume of solution (in case there was no steady state achieved), the cores were separated again to determine the resistance factor (RF). Therefore, the same ramp of flow rates as during the determination of brine permeability was run. The pressure drops over the cores at each flow rate during determining brine permeability were compared to the pressure drops occurring while TriX injection.

$$RF = \frac{dp_{TriX}}{dp_{brine\ before\ TriX}} \quad \text{Eq. 6-2}$$

RF	–	resistance factor
dp_{TriX}	–	pressure loss during TriX injection in Pa
$dp_{brine\ before\ TriX}$	–	pressure loss during brine injection before TriX was in contact with the core in Pa

The resistance factor yields information about the injectivity of the TriX solution. A resistance factor of 10 means that a pressure gradient ten times higher than for brine injection is needed to reach the same injection rate with TriX solution. It contains increasing pressure drop due to the higher viscosity of TriX solution and permeability reduction due to adsorption or plugging. In the literature several authors report RF values up to ten [14, 99], occasionally resistance factors up to 30 can be found [100]. A

low resistance factor between 1 and 10 would be a favorable result in an injection test with TriX. However, it had to be expected, that the *RF* value, especially for TriX-MB in the filtration core, would be much higher since the formation of a rigid network would lead to a high degree of filtration.

In the second step of an injection test, only brine was injected to flush out any remaining mobile TriX. When the pressure drop across the core reached a constant value, the ramp of different flow rates was rerun. The pressure drops at the single flow rates were also compared to the pressure drops, which were observed during the determination of brine permeability. Hence, the residual resistance factor (*RRF*) could be calculated.

$$RRF = \frac{dp_{brine\ after\ TriX}}{dp_{brine\ before\ TriX}} \quad \text{Eq. 6-3}$$

<i>RRF</i>	–	residual resistance factor
$dp_{brine\ after\ TriX}$	–	pressure loss during brine injection after TriX injection in Pa
$dp_{brine\ before\ TriX}$	–	pressure loss during brine injection before TriX was in contact with the core in Pa

The residual resistance factor gives information about any permeability alteration caused by injection of TriX solution; hence it is often determined for the main core only. Filtration effects in the near wellbore area were not considered and further evaluated by *RRF* studies. The value should be lower than the *RF* value (between 1 and approx. 5), since the effect of higher viscosity is not present anymore. Furthermore, some loosely bound TriX molecules, which had been stuck on the pore walls and contributed to permeability reduction, might be flushed out [14, 100].

During some injection tests, the concentration of the injected TriX solution was determined by UV extinction measurements, as well as the concentration of TriX in the effluent of the cores. Thereby, retention of TriX in the cores could be investigated.

6.7.4 Oil Displacement Tests

Investigation of the capability of TriX to mobilize oil was a main part of the project. For the experiments, a filtration and a main core were used, though only the main core was saturated with oil. It might be possible that the TriX solution is altered on its way through the core material. Therefore, it was decided to use a filtration core to assess the oil recovery potential of the altered TriX solution and to approach reservoir conditions. The filtration core should simulate the near wellbore area of the injector, which is considered to be almost oil depleted.

For the tests, Michigan sandstone cores ($k_{brine} \approx 0.5 D$) were used and prepared as described in chapter 6.7.2. To set original oil saturation in the main core, several pore volumes of Bockstedt oil were injected into the core at a flow rate corresponding to a Darcy velocity of $v_D = 1$ ft/d. Then the core was shut in at 55 °C for one week to give some time for possible wettability alterations.

Oil displacement tests were conducted in secondary and tertiary mode, i.e., without and with an initial water flood.

In secondary mode core flooding experiments, the TriX solution was injected directly at original oil saturation. This procedure corresponds to field projects, where the typical secondary production phase is skipped. The focus of these experiments was on the residual oil saturation, which could be reached by injection of the TriX solution $S_{or,TriX}$, compared to after brine injection $S_{or,brine}$. For secondary oil displacement tests, relative permeability and fractional flow curves were also analyzed. The basis for these investigations were the *Buckley-Leverett* model and the *Corey* relative permeability functions, which are described in detail in Appendix A4.

In tertiary mode core flooding experiments, the oil saturated core was first flooded with brine until no more oil was produced. This was followed by TriX solution. This approach simulates the tertiary production phase (EOR phase) of a field operation. Of particular interest was the capability of the TriX solution to decrease the remaining or residual oil saturation ($S_{OR,brine}$ or $S_{or,brine}$), which was achieved by the previous brine injection.

By comparison and analysis of this and other experimental data, such as water breakthrough, pressure drops over the cores and fractional flow during oil displace-

ment, the efficiencies of different flooding modes (secondary and tertiary) and TriX solutions to mobilize oil were evaluated.

7. Results and Discussion

7.1 Critical Micelle Concentration of TriX-M and Triton-X-100 in Synthetic Reservoir Brine

The measurement values of the surface tension of the differently concentrated surfactant solutions (in NDIIa) at 20 °C are presented in Table 7-1, as well as in the Figures 7-1 and 7-2. For better assessment of the CMC, the intersection of the regression lines of the almost linear dependent regions below and above CMC was used.

Table 7-1: Surface tension measurements of TriX derivatives and Triton-X-100 dilution series

TriX-M	c in	ppm	5.0	7.0	10.0	15.0	20.0	24.9	49.9	99.9	999.7
		μmol/l	7.6	10.6	15.1	22.6	30.1	37.6	75.2	150.6	1506
	SFT in	mN/m	45.7	43.4	41.7	39.4	37.8	36.7	33.6	33.3	32.8
Triton-X-100	c in	ppm	5.0	7.0	9.9	15.0	20.0	25.0	50.0	100.0	1000
		μmol/l	8.8	12.3	17.3	26.3	35.0	43.8	87.6	175.2	1752
	SFT in	mN/m	37.6	36.3	33.5	31.6	30.8	30.6	30.7	29.8	30.7
TriX-TA	c in	ppm	20.0	50.0	99.9	149.5	199.8	499.9			999.1
		μmol/l	9.7	24.1	48.2	72.2	96.5	241.4			482.5
	SFT in	mN/m	60.4	58.2	56.1	54.6	52.4	45.8			46.7
TriX-MB	c in	ppm	100.1	200.1	300.2	400.2	500.2				1001
		μmol/l	50.2	100.5	150.8	201.0	251.2				502.5
	SFT in	mN/m	50.6	43.9	40.1	39.9	37.8				37.8

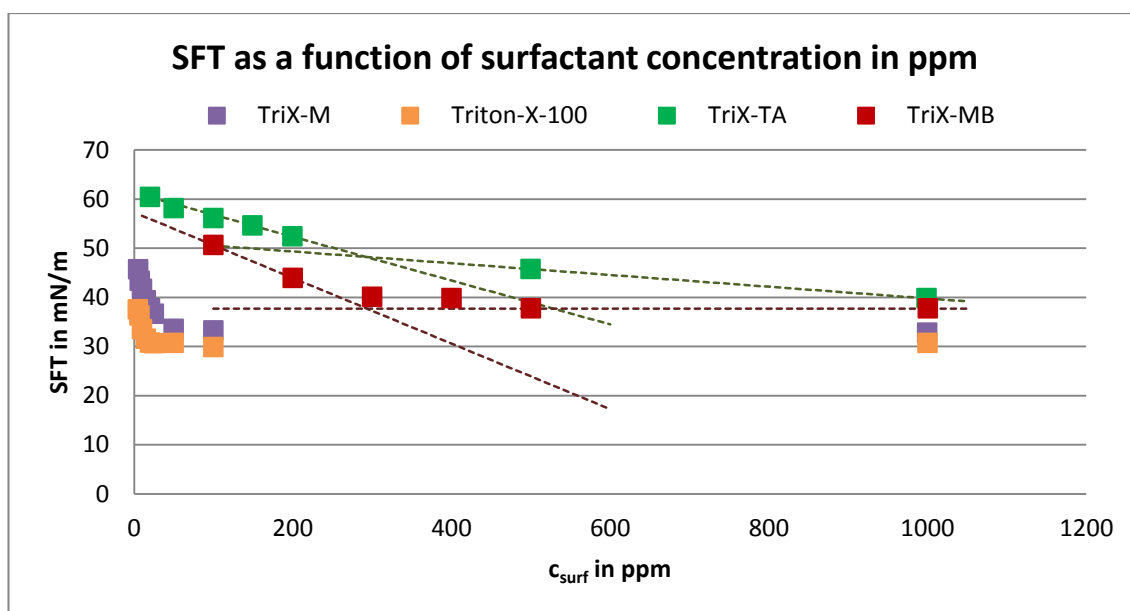


Figure 7-1: Surface tensions of TriX derivatives and Triton-X-100, concentration in ppm

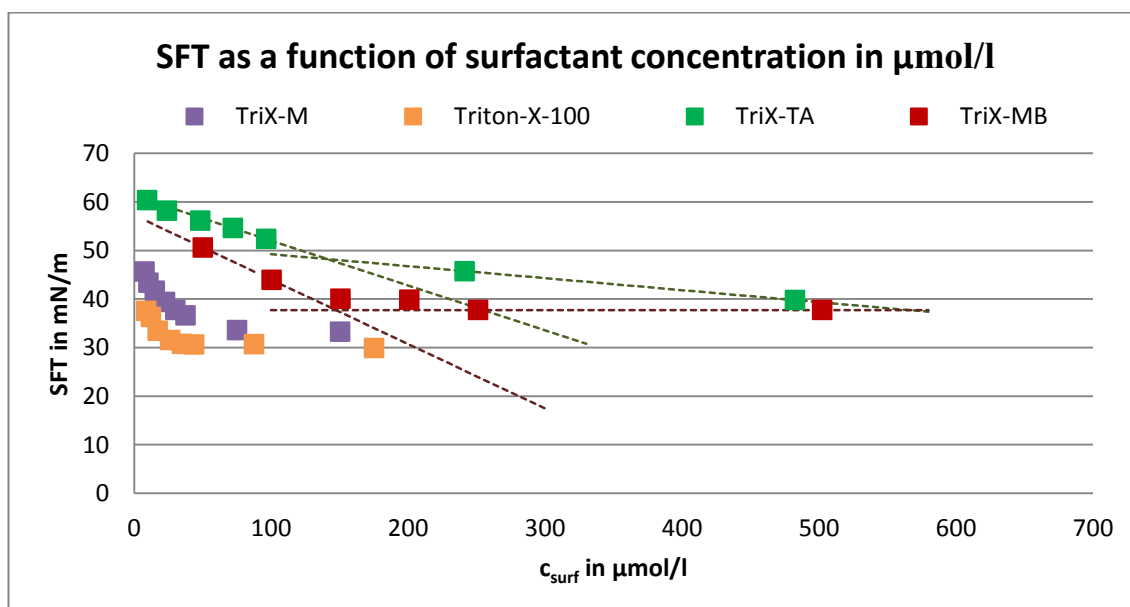


Figure 7-2: Surface tensions of TriX derivatives and Triton-X-100, concentration in mmol/l

Triton-X-100 and TriX-M had the lowest surface tension, especially at low concentrations, which has been expected because of their typically surfactant-like structure.

It was already mentioned in chapter 5.1 and 5.2 that it is more favorable for TriX-MB and TriX-TA to form micelles than to orientate on the surface of the solution. Therefore, it is not sensible to interpret surface tension measurements with respect to critical micelle concentration for these molecules. However, the saturation of the surface by TriX-MB and TriX-TA molecules could be deduced from the measurements. At a

concentration of around 290 ppm (146 $\mu\text{mol/l}$) the surface became saturated by TriX-MB at 20 °C. For TriX-TA this happened in a range 200 – 500 ppm (96 – 241 $\mu\text{mol/l}$).

Taking a closer look at TriX-M and Triton-X-100 (Figure 7-3), the CMC of TriX-M was at around 20 ppm (30 $\mu\text{mol/l}$) and the CMC of Triton-X-100 at around 15 ppm (26 $\mu\text{mol/l}$). The values are quite similar, which is due to the structural similarity of both molecules and comparable molecular weight. These factors indicate comparable molecular size. The constant outer surface area of the solutions could be covered by a distinct number of similarly sized molecules.

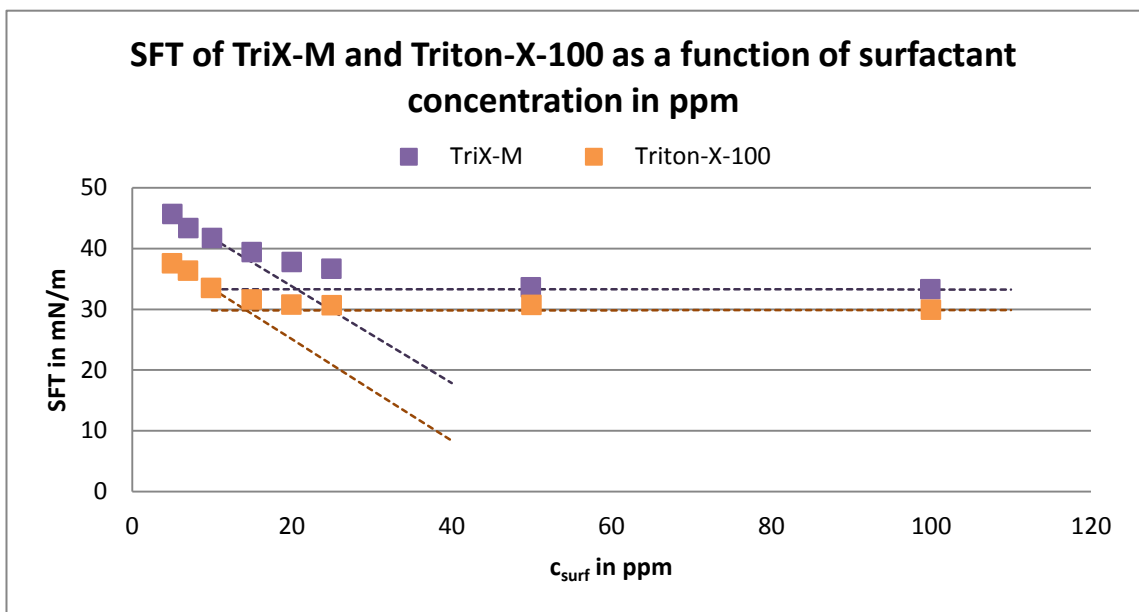


Figure 7-3: Surface tensions of TriX-M and Triton-X-100 as a function of concentration in ppm

For Triton-X-100, the values obtained were in line with the literature. The product data sheet and *Ruiz, et al.* report a CMC of Triton-X-100 in deionized water of around 144 ppm [94, 101]. *Alam et al.* have shown that the CMC of Triton-X-100 is decreasing with increasing salt concentration [102]. According to their publication, a concentration of sodium chloride of $c_{NaCl} = 5.8 \text{ g/l}$ led to a CMC of Triton-X-100 of around 62 ppm. Since the salt concentration in NDIIa brine was much higher, the CMC was likely to be significantly lower than the reported 62 ppm.

The following experiments were conducted at surfactant concentrations of 1000 ppm or higher. This was far above CMC or the concentration, at which the surface became saturated, for all molecules used. This was important to ensure, that there is a sufficient amount of molecules in solution to interact with sand and oil.

7.2 Static Adsorption of TriX Derivatives and Triton-X-100 on Sand

In Table 7-2 and Figure 7-4 the concentrations of the surfactant solutions at the beginning of the experiment (t_0) and of the supernatant solution after 14 days in contact with sand are presented.

Table 7-2: Changes in surfactant concentration after sand contact

solvent (brine)	NDIIa				NaCl
surfactant	TriX-MB	TriX-TA	TriX-M	Triton-X-100	TriX-MB
$c_{surf}(t_0)$ in wt. %	0.1025	0.1006	0.1000	0.0993	0.1015
Std. deviation	0.0008	0.0005	0.0000	1.7E-17	0.0000
$c_{surf}(14\text{ d})$ in wt. %	0.1002	0.0989	0.0532	0.0210	0.1006
Std. deviation	0.0022	0.0027	0.0010	0.0043	0.0010

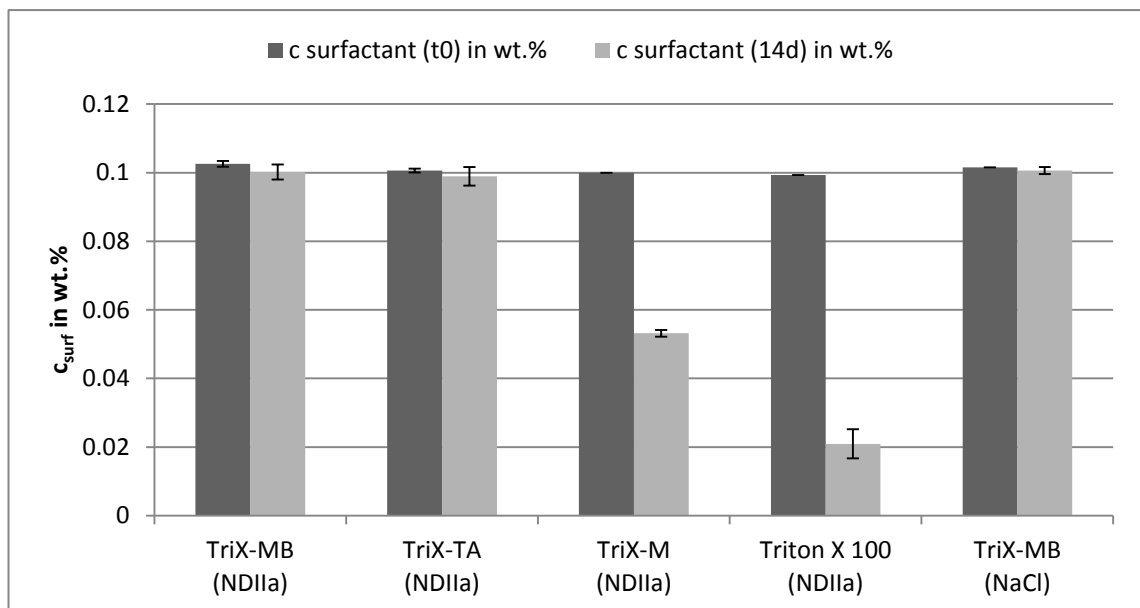
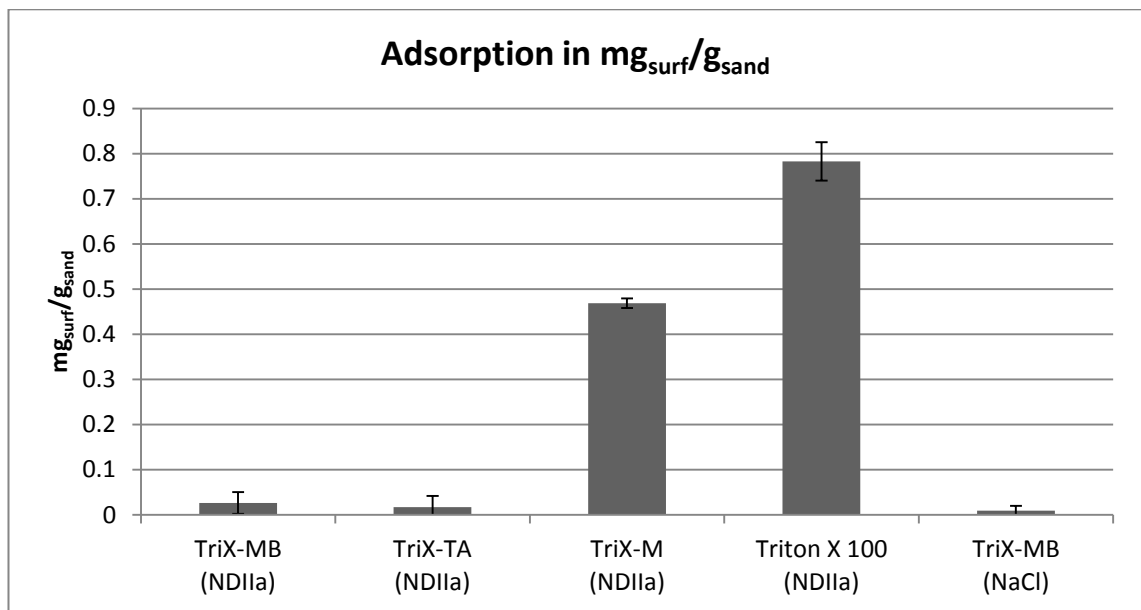


Figure 7-4: Changes in surfactant concentration after sand contact

Based on the assumption, that all the molecules, which were not dispersed in the surfactant solution, were adsorbed on the sand grains, the adsorption of the TriX derivatives and Triton-X-100 could be calculated in $\text{mg}_{\text{surf}}/\text{g}_{\text{sand}}$ and $\mu\text{mol}_{\text{surf}}/\text{g}_{\text{sand}}$. The results are presented in Table 7-3, as well as in Figure 7-5 and Figure 7-6.

Table 7-3: Static adsorption of surfactants on sand

solvent (brine)	NDIIa				NaCl
surfactant	TriX-MB	TriX-TA	TriX-M	Triton-X-100	TriX-MB
adsorption in $\text{mg}_{\text{surf}}/\text{g}_{\text{sand}}$	0.026	0.017	0.469	0.783	0.009
Std. deviation	0.024	0.024	0.010	0.042	0.010
adsorption in $\mu\text{mol}_{\text{surf}}/\text{g}_{\text{sand}}$	0.012	0.007	0.625	1.214	0.004
Std. deviation	0.011	0.010	0.014	0.066	0.005

Figure 7-5: Static adsorption of surfactants on sand in $\text{mg}_{\text{surf}}/\text{g}_{\text{sand}}$

TriX-MB (in both brines) and TriX-TA showed low adsorption values compared to TriX-M and Triton-X-100, which might be explained by the higher molecular weight of TriX-MB and TriX-TA compared to TriX-M and Triton-X-100 (adsorption decreases with increasing molecular weight [103]). Regarding the amount of substance in moles, the difference in adsorption becomes even more drastic. (Figure 7-6; note: logarithmic scale).

The loss of TriX-M molecules in solution was significantly lower than of Triton-X-100, which was a promising result for further work with TriX-M.

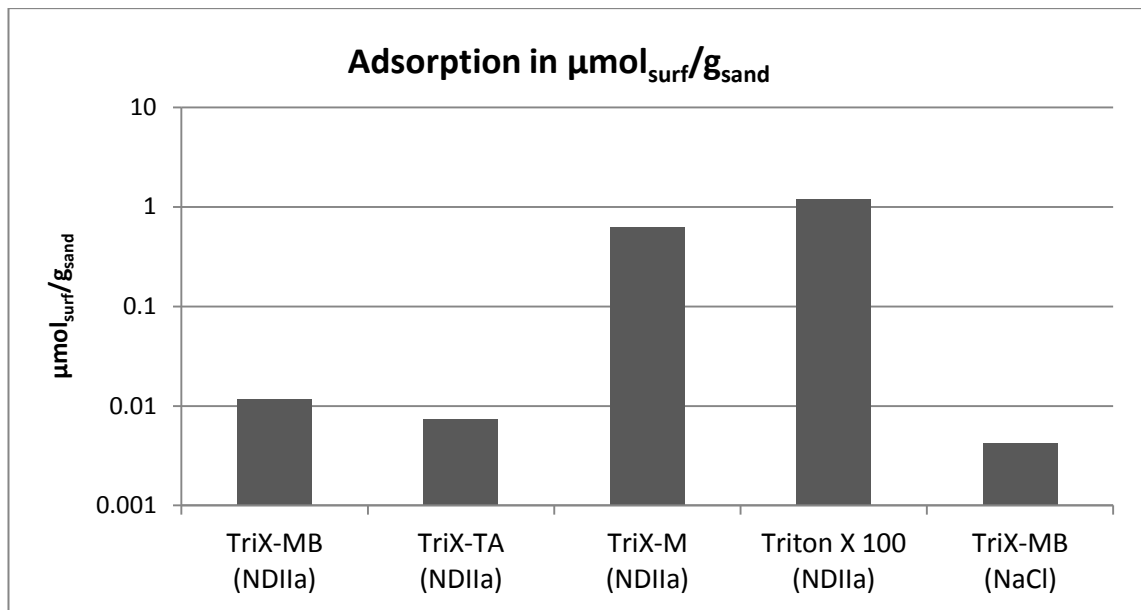


Figure 7-6: Static adsorption of TriX derivatives and Triton-X-100 on sand in $\mu\text{mol}_{\text{surf}}/\text{g}_{\text{sand}}$

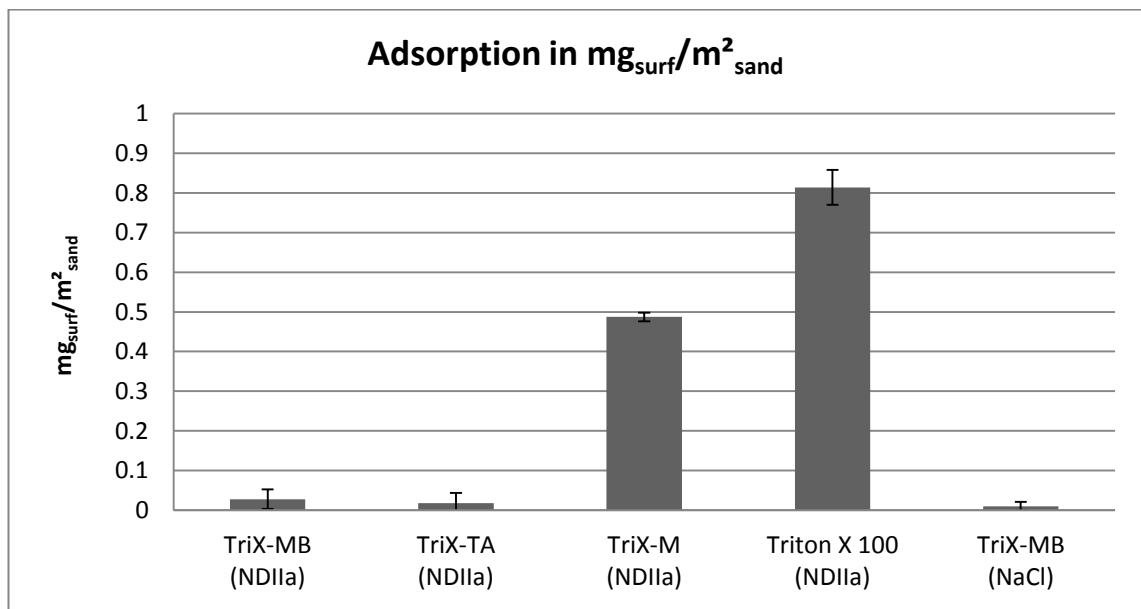
TriX-MB in NDIIa brine exhibited higher adsorption values than TriX-MB in NaCl. The tertiary network with divalent ions was more rigid and stronger than in NaCl solution. If one part of the network built up with Ca^{2+} and Mg^{2+} was adsorbed on the rock, more adjacent TriX-MB molecules were likely to be fixed by that network, compared to the weaker cross-links in NaCl solution. *Sheng* published various adsorption data for HPAM and biopolymers and stated, that 70% of the data for HPAM are below $0.03 \text{ mg}_{\text{polymer}}/\text{g}_{\text{rock}}$. Adsorption values for biopolymers would be slightly higher [14]. The adsorption values of the viscoelastic surfactants reported by other researchers (cf. chapter 4.2) were between 0.35 and 2.9 mg/g on sandstone. Compared to these values, TriX-MB and TriX-TA showed good results in static adsorption tests. The adsorption of Triton-X-100 on sand seemed to be nearly twice as high as the adsorption of TriX-M when expressed in $\mu\text{mol}/\text{g}$. This could be explained by Triton-X-100 being a nonionic surfactant in contrast to anionic TriX-M. The adsorption of nonionics is higher than of anionics [27, 104]. The amount of Triton-X-100 adsorbed on sand (0.8 mg/g) exactly corresponded to static adsorption value published in another publication by *Ramirez et al.* [105].

Adsorption is related to surface. In order to compare adsorption values gained from static experiments with results from dynamic tests (core flooding experiments), it was necessary to specify the values related to surface area, rather than mass. The following

amounts of adsorbed material per unit of surface area of sand could be calculated (Table 7-4, Figure 7-7 and Figure 7-8).

Table 7-4: Static adsorption related to surface area

solvent (brine)	NDIIa				NaCl
surfactant	TriX-MB	TriX-TA	TriX-M	Triton-X-100	TriX-MB
adsorption in $\text{mg}_{\text{surf}}/\text{m}^2_{\text{sand}}$	0.027	0.018	0.487	0.814	0.010
Std. deviation	0.025	0.025	0.011	0.044	0.011
adsorption in $\mu\text{mol}_{\text{surf}}/\text{m}^2_{\text{sand}}$	0.012	0.008	0.650	1.262	0.004
Std. deviation	0.011	0.011	0.014	0.068	0.005

Figure 7-7: Adsorption of TriX derivatives and Triton-X-100 in $\text{mg}_{\text{surf}}/\text{m}^2_{\text{sand}}$

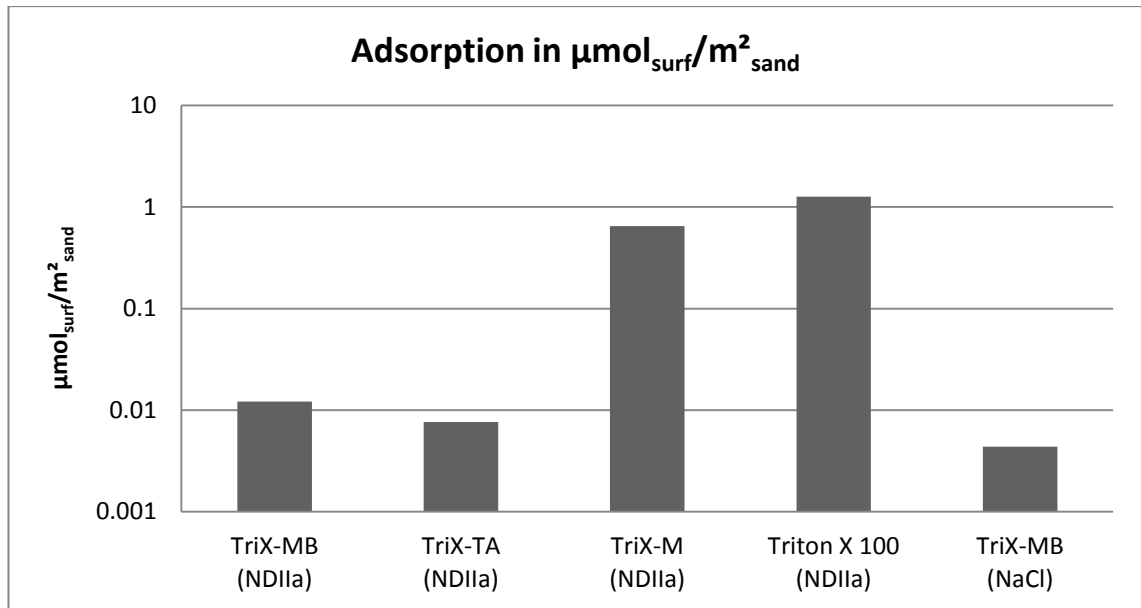


Figure 7-8: Adsorption of TriX derivatives and Triton-X-100 in $\mu\text{mol}_{\text{surf}}/\text{m}^2_{\text{sand}}$

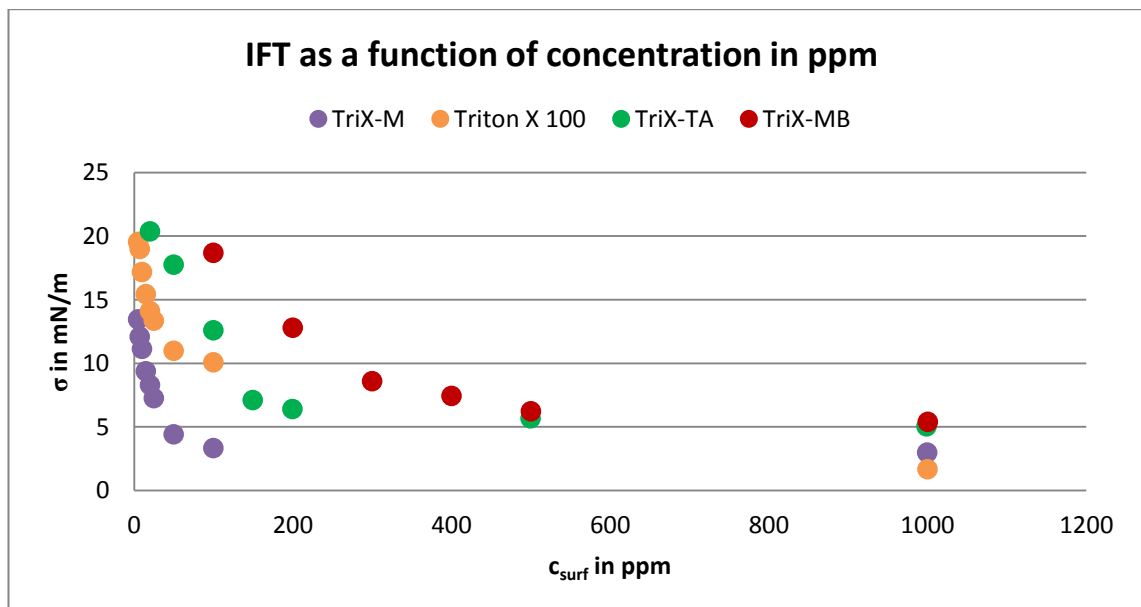
7.3 Interfacial Tension and Interaction of Solutions of TriX Derivatives and Triton-X-100 with Crude Oil

7.3.1 Interfacial Tension to Bockstedt Oil

Table 7-5 and the following Figures 7-9 and 7-10 show the interfacial tension (σ) values for the dilution series of the different TriX derivatives and Triton-X-100 in synthetic reservoir brine (NDIIa).

Table 7-5: Interfacial tension measurements of TriX derivatives and Triton-X-100 dilution series to Bockstedt oil

TriX-M	c in	ppm	5.0	7.0	10.0	15.0	20.0	24.9	49.9	99.9	999.7
		$\mu\text{mol/l}$	7.6	10.6	15.1	22.6	30.1	37.6	75.2	150.6	1506
	σ in	mN/m	13.4	12.1	11.1	9.4	8.3	7.3	4.4	3.3	3.0
Triton-X-100	c in	ppm	5.0	7.0	9.9	15.0	20.0	25.0	50.0	100.0	1000
		$\mu\text{mol/l}$	8.8	12.3	17.3	26.3	35.0	43.8	87.6	175.2	1752
	σ in	mN/m	19.6	19.0	17.2	15.4	14.1	13.4	11.0	10.1	1.7
TriX-TA	c in	ppm	20.0	50.0	99.9	149.5	199.8	499.9			999.1
		$\mu\text{mol/l}$	9.7	24.1	48.2	72.2	96.5	241.4			482.5
	σ in	mN/m	20.4	17.8	12.6	7.1	6.4	5.7			5.0
TriX-MB	c in	ppm	100.1	200.1	300.2	400.2	500.2				1001
		$\mu\text{mol/l}$	50.2	100.5	150.8	201.0	251.2				502.5
	σ in	mN/m	18.7	12.8	8.6	7.5	6.22				5.4

Figure 7-9: Interfacial tensions of TriX derivatives and Triton-X-100 to Bockstedt oil (c in ppm)

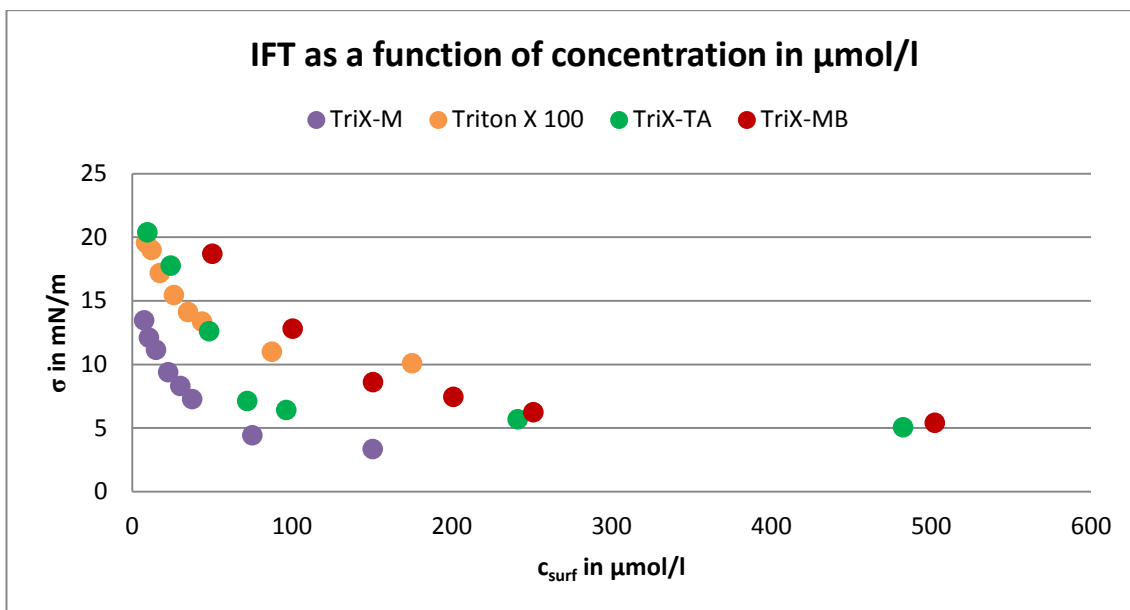


Figure 7-10: Interfacial tensions of TriX derivatives and Triton-X-100 to Bockstedt oil (c in $\mu\text{mol/l}$)

All tested surfactants reduced the interfacial tension to Bockstedt oil. Expressed in molar units, the IFT to Bockstedt oil of all TriX derivatives was lower than that of Triton-X-100 at concentrations around 200 $\mu\text{mol/l}$. The interfacial tension of TriX-M to Bockstedt oil was lower than that of Triton-X-100 at all concentrations.

The values of interfacial tension at high concentrations (≈ 1000 ppm) did not differ very much between the four molecules.

The reduction of interfacial tension was not sufficient to increase the capillary number significantly. The tested molecules would not be able to mobilize additional residual oil by that mechanism alone; however, lowering the interfacial tension between water and oil is a positive effect in any case.

7.3.2 Changes in surfactant concentrations in aqueous solutions after oil contact

The surfactant concentrations before and after being in contact with oil for 14 days are given in Table 7-6, as well as in the Figures 7-11 and 7-12. In the glass vessels containing TriX-MB in NDIIa and Bockstedt oil, a turbid solution was forming after shaking by hand. The macro emulsion was stable until the end of the experiment, and also when the samples were cooled down from 55 $^{\circ}\text{C}$ to room temperature. The emulsion

could be separated into a clear aqueous phase and oil phase by filtration (2.5 μm syringe filter). In the other samples, no emulsification could be seen.

Table 7-6: Apparent changes of concentration in bulk solutions of TriX derivatives and Triton-X-100 after oil contact

solvent	NDIIa				NaCl
surfactant	TriX-MB	TriX-TA	TriX-M	Triton-X-100	TriX-MB
$c_{surf}(t_0)$ in wt. %	0.1013	0.1002	0.1000	0.0993	0.1008
Std. deviation	0.0000	0.0000	0.0000	0.0000	0.0000
$c_{surf}(14\text{ d})$ in wt. %	0.1082	0.1362	0.1063	0.0032	0.1107
Std. deviation	0.0005	0.0018	0.0033	0.0001	0.0008
$c_{surf}(t_0)$ in mmol/kg	0.4504	0.4280	1.3333	1.5390	0.4482
Std. deviation	0.0000	0.0000	0.0000	0.0000	0.0000
$c_{surf}(14\text{ d})$ in mmol/kg	0.4810	0.5820	1.4178	0.0503	0.4920
Std. deviation	0.0020	0.0076	0.0435	0.0013	0.0036

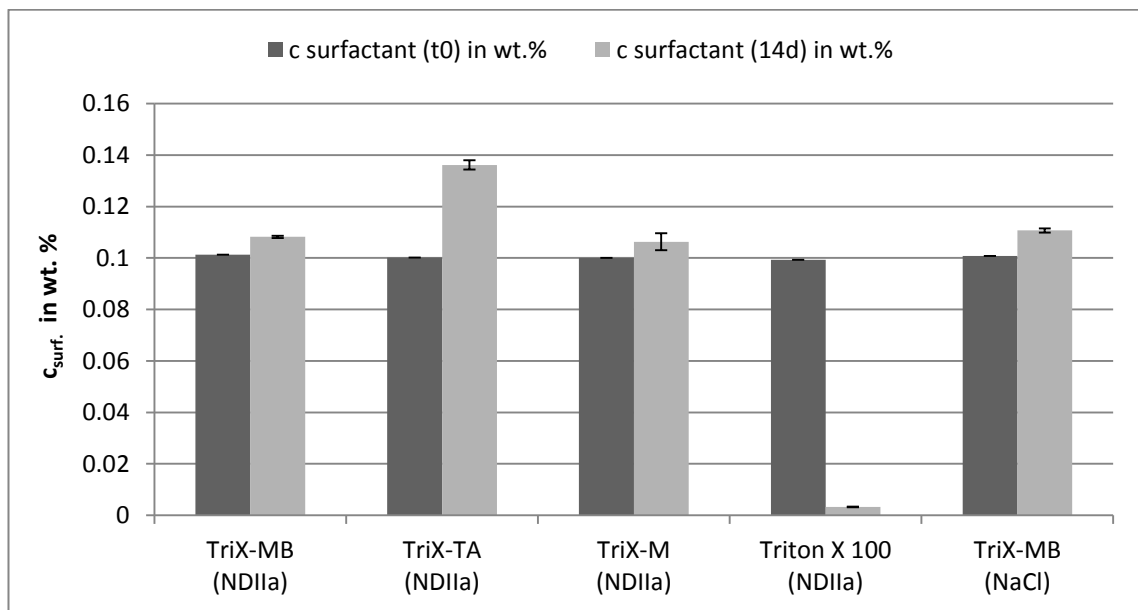


Figure 7-11: Apparent changes in concentration in wt. % of bulk solutions after oil contact

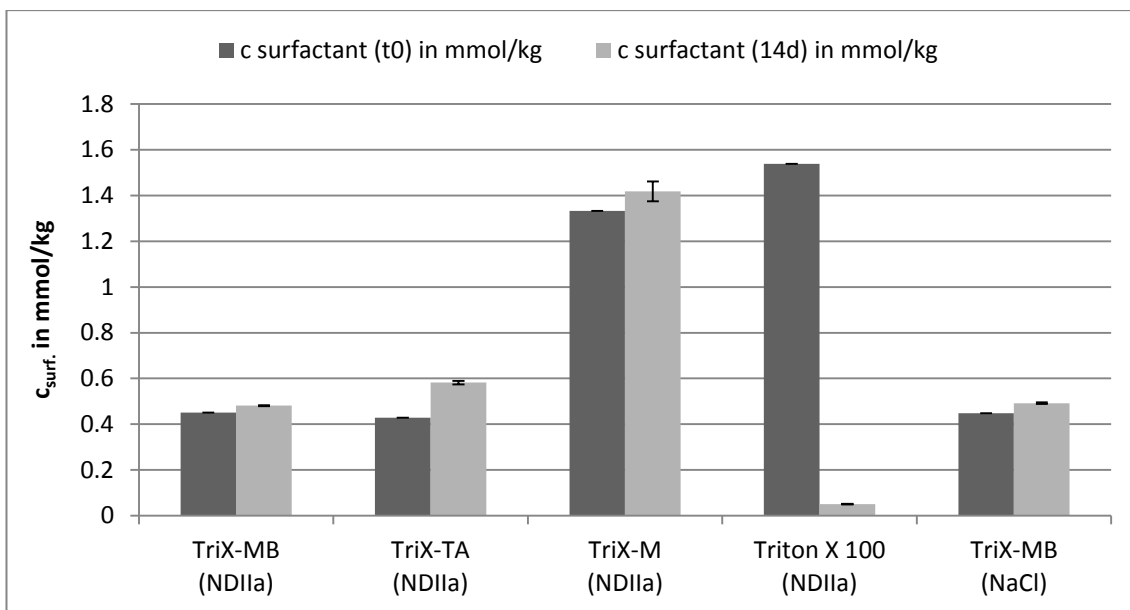


Figure 7-12: Apparent changes in concentration in mmol/l of bulk solutions after oil contact

For all three TriX derivatives, the concentration in aqueous solution appeared to increase after oil contact. The concentration of Triton-X-100 decreased drastically under the same conditions. Ca. 97 % of the initial Triton-X-100 was lost from the aqueous phase.

The apparent increases in the concentrations of all three TriX derivatives indicated an interaction with oil. Because of an HLB value of the TriX molecules of around 16, an oil-in-water-emulsion was promoted. It could be surmised that among others, aromatic parts of the crude oil were dissolved in the water phase by TriX, giving an extra signal in extinction measurements. Since the solution of TriX molecules in model oil was excluded by preliminary testing [106], it could be assumed that no TriX diffused into the oil phase. Mixing of NaCl brine with oil led to no signal in extinction measurements. Hence, dissolving of components of Bockstedt oil in the aqueous phase was only possible in the presence of surfactants.

The HLB value of Triton-X-100 is 13.5, which also indicates that oil-in-water-emulsions are formed. However, the results of UV extinction measurements have shown that there were only very little aromatics in aqueous solution after contact of 0.1 wt. % Triton-X-100 in NDIIa solution with Bockstedt oil. Therefore, the Triton-X-100 molecules, lacking in the aqueous bulk phase, had to be located at the interface between surfactant solution and oil, as well as dispersed in the oil phase (excluding chemical reactions, which altered Triton-X-100, so that it could not be detected in ex-

tingtion measurements anymore). Those molecules would be fixed and could not affect other parts of the reservoir in practical field applications. Taking into account that Triton-X-100 also strongly adsorbs on sand, the effective concentration in the water front for oil mobilization processes would sharply decrease.

A significant problem for EOR with viscoelastic surfactants is that the solutions lose their viscoelastic properties in contact with oil, because of the transformation from worm-like to spherical micelles. As already explained in chapter 5, the TriX molecules were expected to form a very compact micelle core by design. This should have prevented the dissolution of oil inside the worm-like TriX micelles, causing the aggregates to become spherical. However, dynamic light scattering tests at BASF showed that TriX-MB micelles change their shape in the presence of oil, just like the micelles of other surfactants [106]. Therefore, TriX-MB solutions also lose their viscoelasticity in contact with oil.

7.4 Spontaneous Imbibition Tests

In Table 7-7 the inverse *Bond* numbers for the imbibition tests are given.

Table 7-7: Inverse *Bond* numbers of imbibition tests

brine	additive	N_B^{-1}
NDIIa	no additive	42.9
	0.1 wt. % TriX-MB	3.9
	0.25 wt. % TriX-MB	4.5
	0.1 wt. % TriX-TA	3.1
	0.25 wt. % TriX-TA	4.1
	0.1 wt. % TriX-M	2.1
	0.25 wt. % TriX-M	2.5
	0.1 wt. % Triton-X-100	1.6
	0.25 wt. % Triton-X-100	1.7
	NaCl	no additive
0.1 wt. % TriX-MB		3.9
0.25 wt. % TriX-MB		3.4

The initial water saturation was at around 0.19, indicating water wet pore surfaces. This fact and inverse *Bond* numbers higher than one are typical for counter-current imbibition with dominant capillary drive [97, 98].

7.4.1 TriX Derivatives and Triton-X-100 in NDIIa brine

In Figure 7-13 the imbibition curves for solutions of all TriX derivatives and Triton-X-100 in NDIIa brine at concentrations of 0.1 wt. % and 0.25 wt. % are shown. After 14 days no additional oil was displaced in any of the experiments

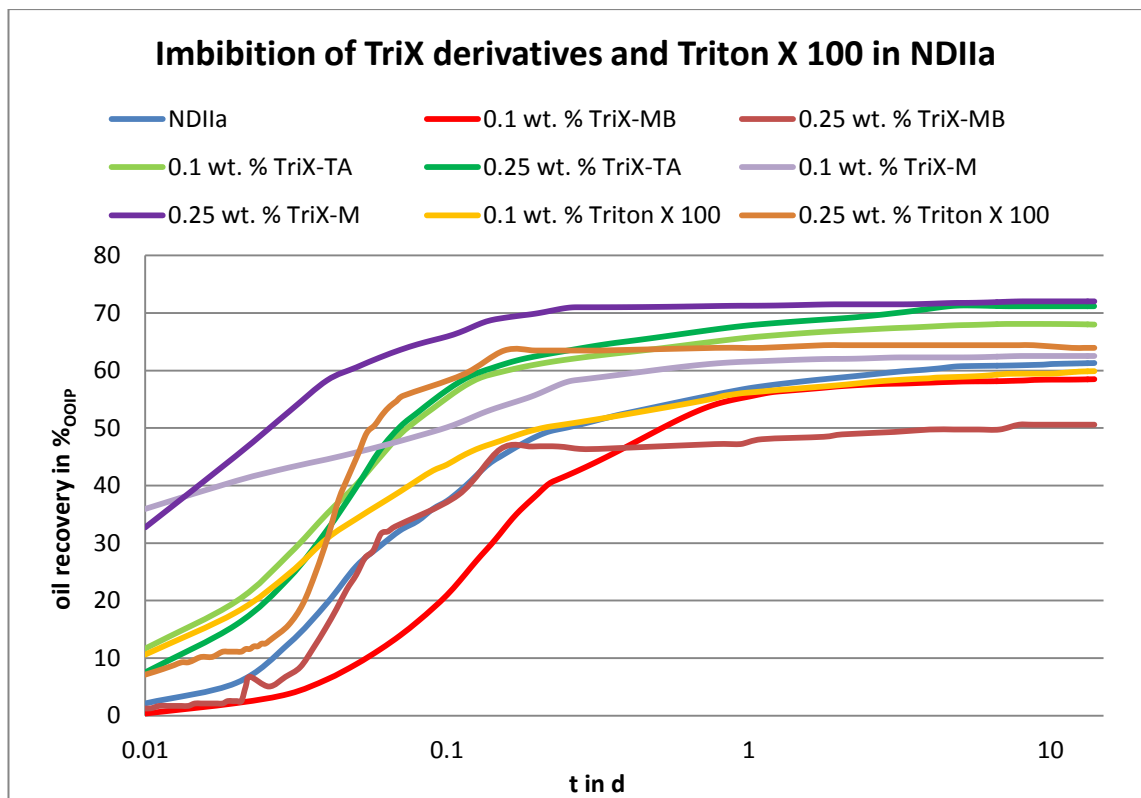


Figure 7-13: Imbibition curves of TriX derivatives and Triton-X-100 in NDIIa brine

The blue line in Figure 7-13 represents spontaneous imbibition of NDIIa solution without any additives. Significant oil mobilization by imbibition of the brine started between 0.01 and 0.1 days (between 15 minutes and 2.5 hours), and the ultimate recovery was ca. 61 %_{OOIP}.

The red lines are the imbibition curves for TriX-MB in NDIIa brine (0.1 wt. %: light, 0.25 wt. %: dark). Oil mobilization with 0.1 wt. % TriX-MB solution started later and

resulted in a slightly lower ultimate oil recovery than NDIIa brine only. 0.25 wt. % TriX-MB in NDIIa brine resulted in an even lower ultimate recovery of around 50 %_{OOIP}.

The light and dark green curves show oil recovery by imbibition of TriX-TA at concentrations of 0.1 wt. % and 0.25 wt. % in NDIIa solution, respectively. Both solutions showed high imbibition rates at the beginning of spontaneous imbibition. Ca. 10 %_{OOIP} were already produced during the first 15 minutes of the test. 0.1 wt. % TriX-TA in NDIIa solution led to an ultimate oil recovery of 68 %_{OOIP}, which was 7 %_{OOIP} higher than with NDIIa brine only. By applying 0.25 wt. % TriX-TA solution the ultimate oil recovery even increased further to 71 %_{OOIP}.

TriX-M is represented by the dark (0.25 wt. %) and light (0.1 wt. %) violet curves. In the first minutes, these solutions exhibited the highest imbibition rate in this series of experiments. However, after 1 hour the efficiency of TriX-M was overcome by 0.25 wt. % Triton-X-100 and both TriX-TA solutions. The ultimate recovery of 0.1 wt. % TriX-M in NDIIa brine was only 1.3 %_{OOIP} higher than that of brine only. In the case of 0.25 wt. % TriX-M the imbibition rate stayed high. The maximum oil recovery was almost reached after only 6 hours. Ultimate oil recovery also exceeded the recovery of all the other tested surfactants.

The imbibition curves of Triton-X-100 solutions are represented by the yellow (0.1 wt. %) and orange (0.25 wt. %) lines. 0.1 wt. % Triton-X-100 showed a high imbibition rate at the beginning; within the first 15 minutes, already 10 % of the original oil in the core were produced. However, after 14 days no more oil than with pure NDIIa solution had been recovered. A particularly high imbibition rate could be observed for 0.25 wt. % Triton-X-100 in NDIIa between 40 and 90 minutes after starting the experiment. It took only 1.5 hours to produce more than 50 % of the original oil in the core. The ultimate recovery after 14 days was around 64 %_{OOIP}.

7.4.2 TriX-MB in NaCl brine

To compare oil displacement by spontaneous imbibition with forced displacement studied in core flooding experiments, imbibition tests with NaCl as brine were conducted.

In Figure 7-14, the solid blue line represents the oil recovery as a function of time for NaCl brine without additives. It was conspicuous that oil displacement with NaCl started much later than with NDIIa brine (dashed blue line). However, ultimate oil recovery after 14 days was around 66 %_{OOIP}, which was higher than with NDIIa brine.

Spontaneous imbibition with 0.1 wt. % TriX-MB in NaCl is represented by the light red line in Figure 7-14. The imbibition rate was very high at the beginning of the experiment; 50 %_{OOIP} were already produced after 1.5 hours. With 0.25 wt. % TriX-MB in NaCl, production of 50 %_{OOIP} took more than 2 hours. Ultimate recovery was slightly higher than with 0.1 wt. % TriX-MB in NaCl (70.5 %_{OOIP} compared to 67.0 %_{OOIP}). Imbibition rate of TriX-MB in NaCl solutions exceeded the rates of TriX-MB in NDIIa brine, as well as ultimate oil recoveries.

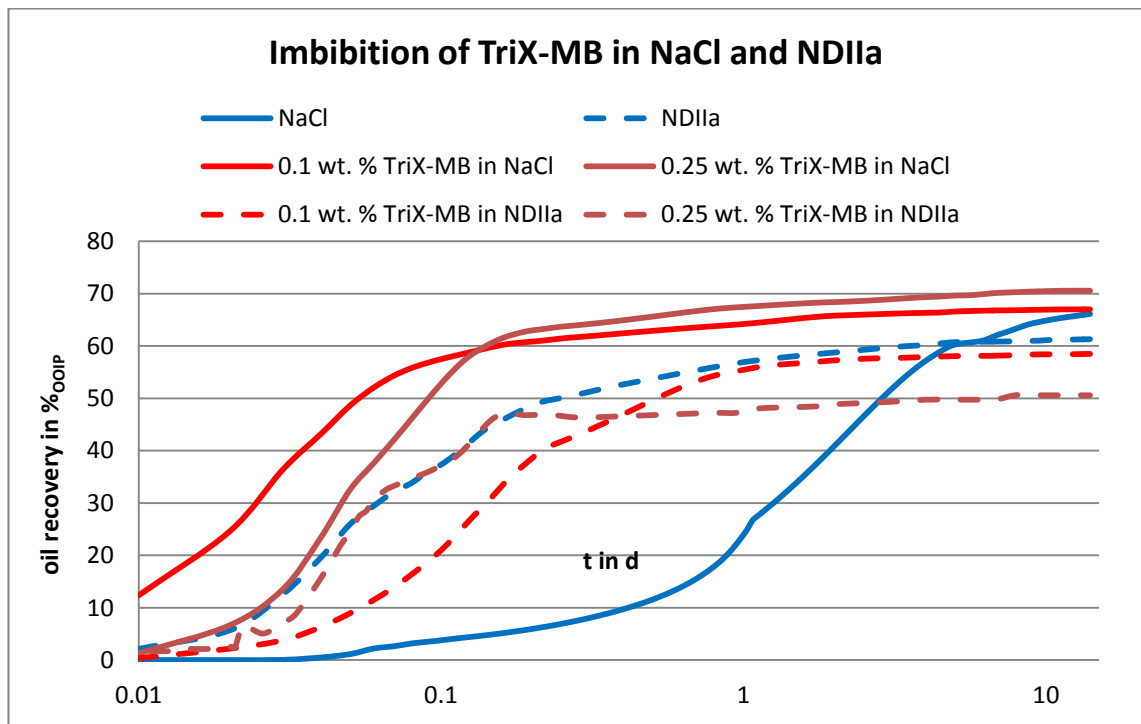


Figure 7-14: Imbibition curves of TriX-MB and Triton-X-100 in NaCl

7.4.3 Summary: Spontaneous Imbibition Tests

In Figure 7-15 the ultimate oil recoveries of the different combinations of brines and surfactants are presented.

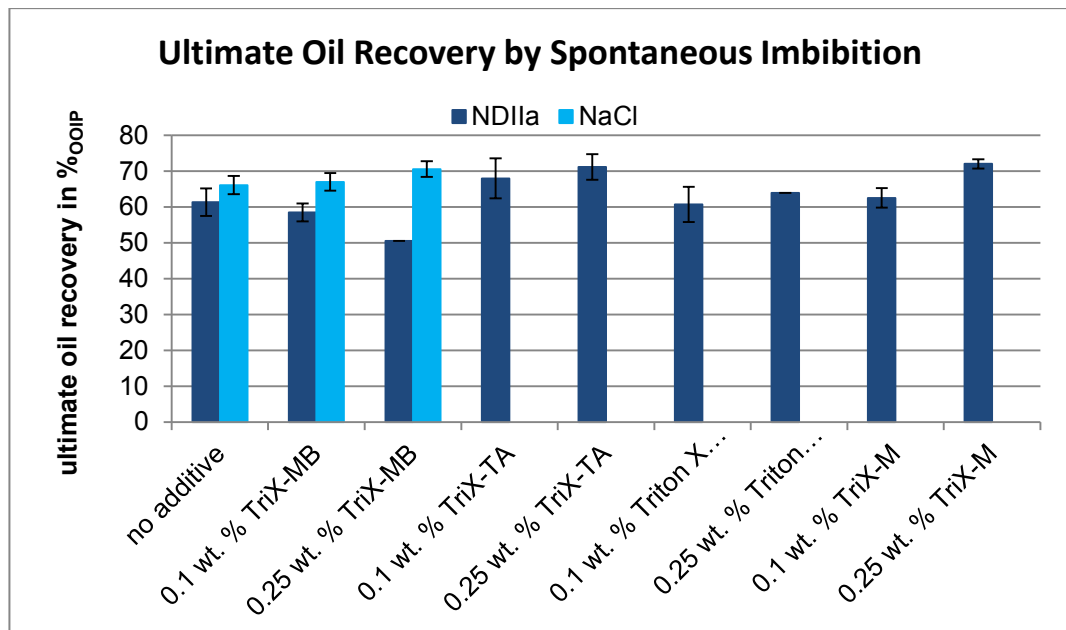


Figure 7-15: Ultimate recoveries of imbibition tests

Without any additives, NaCl led to a higher oil recovery than NDIIa brine.

Adding TriX-MB to NDIIa resulted in less recovery than with brine only. With 0.1 wt. % TriX-MB in NDIIa solution the imbibition rate is decreased, as well. The reason might be the stiff and large tertiary aggregates of TriX-MB in NDIIa brine. This rigid network resulted in an increase of viscosity and hindered the aqueous solution to be soaked into the pores by capillary forces before it even came into contact with oil. It is also possible that the solution could not penetrate through narrow pores, and therefore, did not reach every part of the core, because of high viscosity and filtration of parts of the network. Oil displacement from lower permeable parts of the cores would be impeded. This effect on ultimate recovery was greater at higher concentration (0.25 wt. %). TriX-MB in NDIIa solutions could reach only poor sweep efficiency during static oil displacement tests.

0.1 wt. % TriX-MB in NaCl did not lead to a higher oil recovery than NaCl only. By adding higher concentrations (0.25 wt. %) of TriX-MB to NaCl, oil recovery could be increased by 4 %_{OOIP}. The recovery rate of 0.25 wt. % TriX-MB in NaCl was not as high like the lower concentrated solution in NaCl at the beginning, which is a result of the higher viscosity. Recoveries of TriX-MB in NaCl were greater than in NDIIa brine. The solutions in NaCl could penetrate better into the core, due to the weaker and less rigid network built up with monovalent ions only.

TriX-TA showed good results in the imbibition tests. It led to a high recovery rate at the beginning of the experiments and to high ultimate oil recovery. The effect increased by increasing concentration. TriX-TA forms only small spherical micelles, which could easily penetrate into the pores. Due to low adsorption on sandstone, the effective concentration of TriX-TA was high in every part of the core, which was contacted by an aqueous solution.

By adding TriX-M to NDIIa, the highest imbibition rate at the beginning was obtained with both tested concentrations. However, with 0.1 wt. % TriX-M the recovery rate quickly decreased because of a high level of adsorption of TriX-M molecules onto the pore walls. Thereby, the concentration of the TriX-M solution was steadily decreased on the way to the inner parts of the core. The imbibition rate of the higher concentrated TriX-M solution stayed high and maximum ultimate recovery of all imbibition tests was reached. The effective concentration seemed to be sufficient in all parts of the core to contribute to oil mobilization, despite adsorption.

Adding TriX-TA or TriX-M to NDIIa did not result in a viscosity increase. Therefore, viscous effects were not responsible for higher oil recovery by these molecules. The reduction of interfacial tension was not sufficient enough to contribute to additional oil production, either. However, the increase in oil recovery was remarkable, especially for TriX-TA. It might be possible that the TriX structures promoted water-wet conditions, which contributed to enhanced oil mobilization.

Triton-X-100 was only effective at concentrations higher than 0.1 wt. %. This was because this molecule to a great extent adsorbed on sandstone and dissolved in crude oil. Therefore, the effective concentration in aqueous solution decreased sharply. The ultimate recovery of the 0.25 wt. % Triton-X-100 solution was only 3 %_{OIP} higher than the recovery with brine.

7.5 Investigations on Salt Effects on TriX-MB Solutions

In Figure 7-16 the complex viscosities of TriX-MB solutions in different brines are given as a function of TriX-MB concentration.

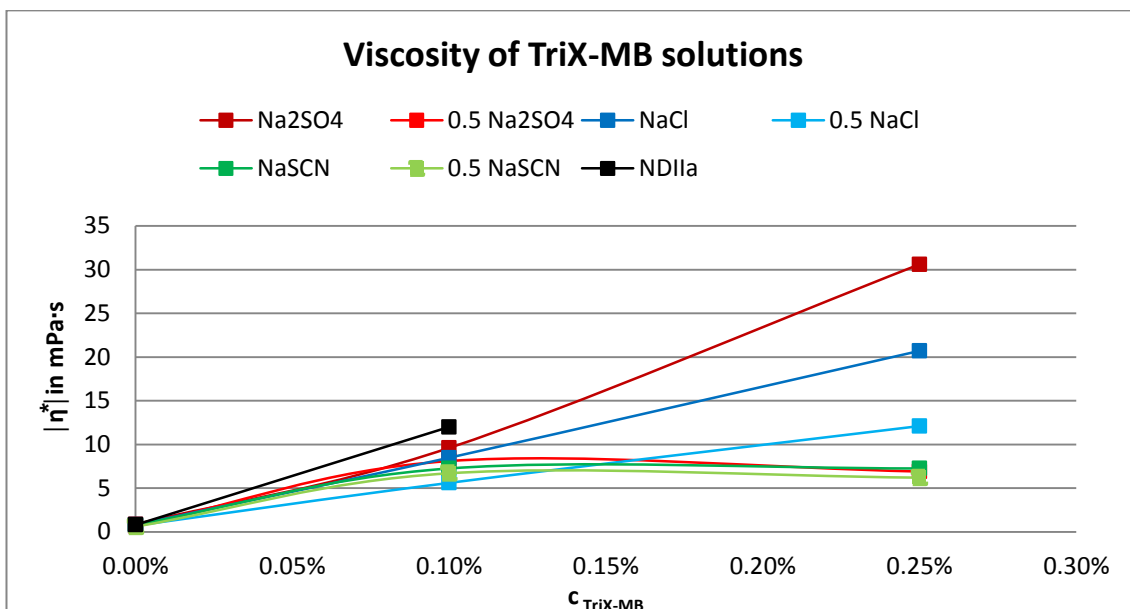


Figure 7-16: Viscosity of TriX-MB solutions in different brines

There was no significant viscosity buildup when using TriX-MB in brines with only half ionic strength of NDIIa brine. This proved that the tertiary structures of TriX_MB are build and strengthened by salt ions. The effect of the different anions on the viscosity of the TriX-MB solution showed a good correlation to the *Hofmeister* series. The highest viscosity (strongest aggregation) was observed with Na₂SO₄ (salting-out). By adding sulfate, the rod-like micelles became more rigid and therefore reinforced the strength of the network. In NaSCN (salting-in) there was no significant viscosity buildup even at high TriX-MB concentrations at 55 °C. Intensification of the hydrophilic effects led to an increased interaction of the long hydrophilic chains with each other and with the solvent. This resulted in higher flexibility of the micelles. It could be stated, that the *Hofmeister* effects apply for the aggregates formed by TriX-MB in aqueous solution.

The interfacial tensions between the TriX-MB solutions and Bockstedt oil were not significantly reduced by increasing TriX-MB concentrations from 0.1 wt. % to 0.25 wt. %, as can be seen in Figure 7-17.

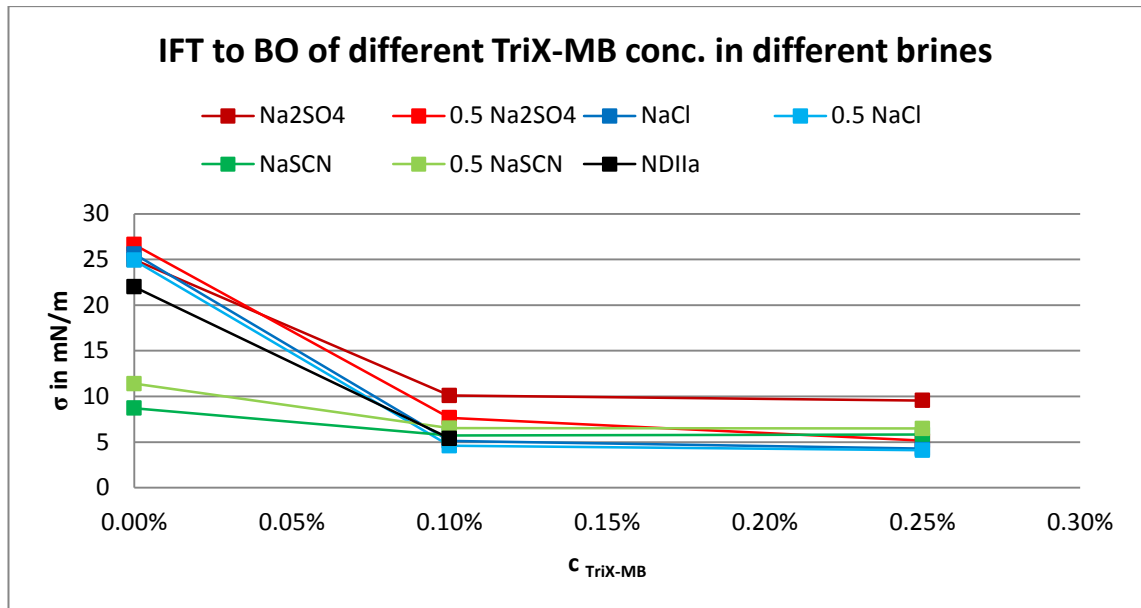


Figure 7-17: Interfacial tension to Bockstedt oil of TriX-MB solutions in different brines

The reason is that both concentrations were above the concentration, at which the surface was saturated with TriX-MB. The interfacial tension measurements of pure salt solution (without TriX) contributed to the theory of *Hofmeister* series, which predicts lower surface and interfacial tensions for ions, which intensify hydrophilic effects (SCN^-), than for ions, which intensify hydrophobic effects (SO_4^{2-}) [107, 108]. A significant effect of different anions on TriX-MB in contact with oil could not be observed in this study.

The imbibition curves for the different brines without TriX-MB are presented in Figure 7-18. They show the impact of the salt ions alone on imbibition behavior and are considered to be a baseline for the imbibition tests with TriX-MB in the different brines. Thus, the effect of the various anions on the capability of TriX-MB to mobilize oil in porous media should be probed.

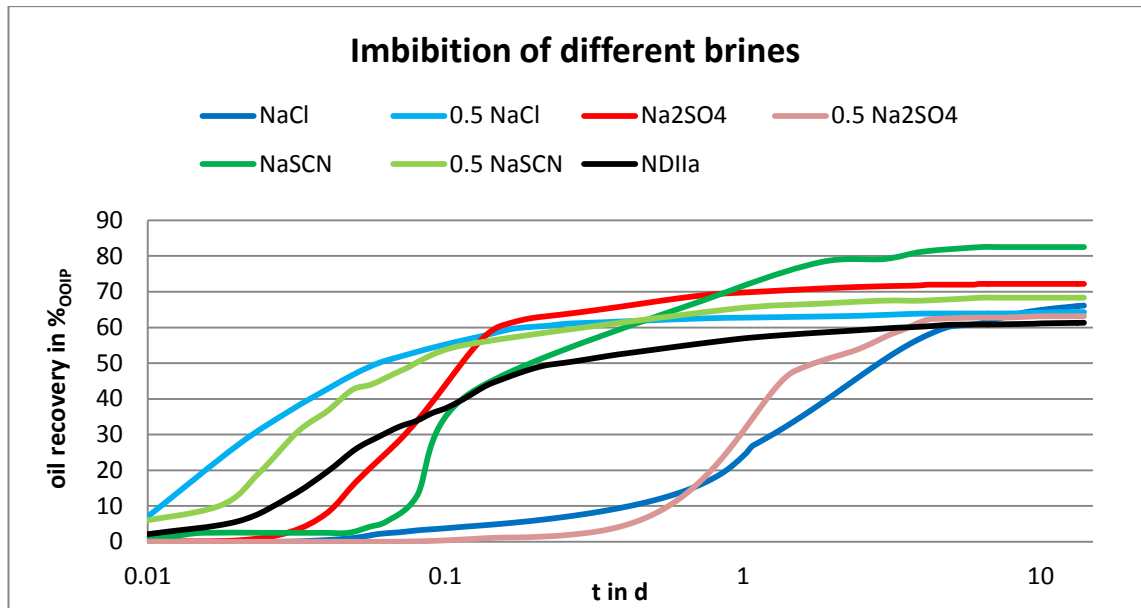


Figure 7-18: Imbibition curves of different brines

The trend was that brines with lower salinity show a higher recovery rate at the beginning. The ultimate recovery was always higher for higher concentrated solutions. Thiocyanate led to highest ultimate recoveries. The thiocyanate ion promoted hydrophilic conditions in the core. This might have resulted in changing the system to more water-wet conditions and additionally decreased the interfacial tension between water and oil phase. Both effects contribute to higher oil recovery. NaCl and 0.5 Na₂SO₄ showed a very low recovery rate at the beginning of the experiments, which is hard to explain. There were no conspicuous features in the raw data. The recoveries after 14 days are very similar for sulfate and chloride solutions.

In the Figures 7-19 and 7-20, the imbibition curves for the brines with 0.1 wt. % and 0.25 wt. % TriX are presented to show, how different types of salt ions might have an impact on the imbibition efficiency of TriX-MB.

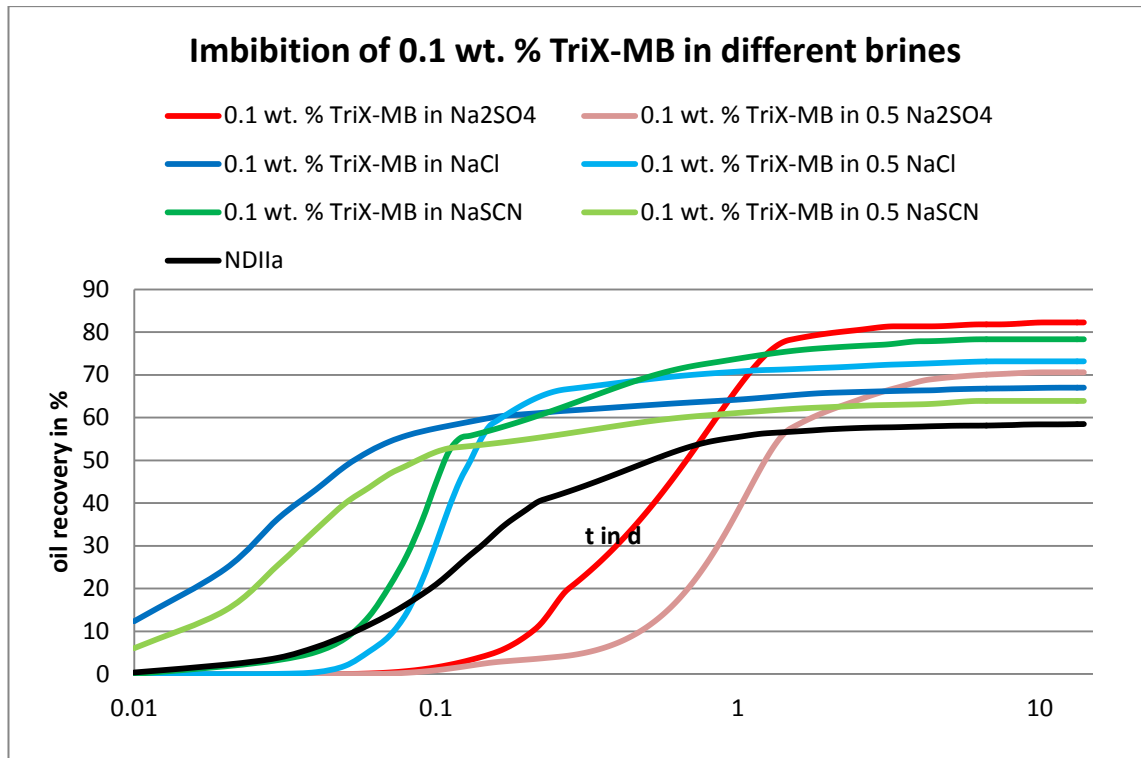


Figure 7-19: Imbibition curves of 0.1 wt. % TriX-MB in different brines

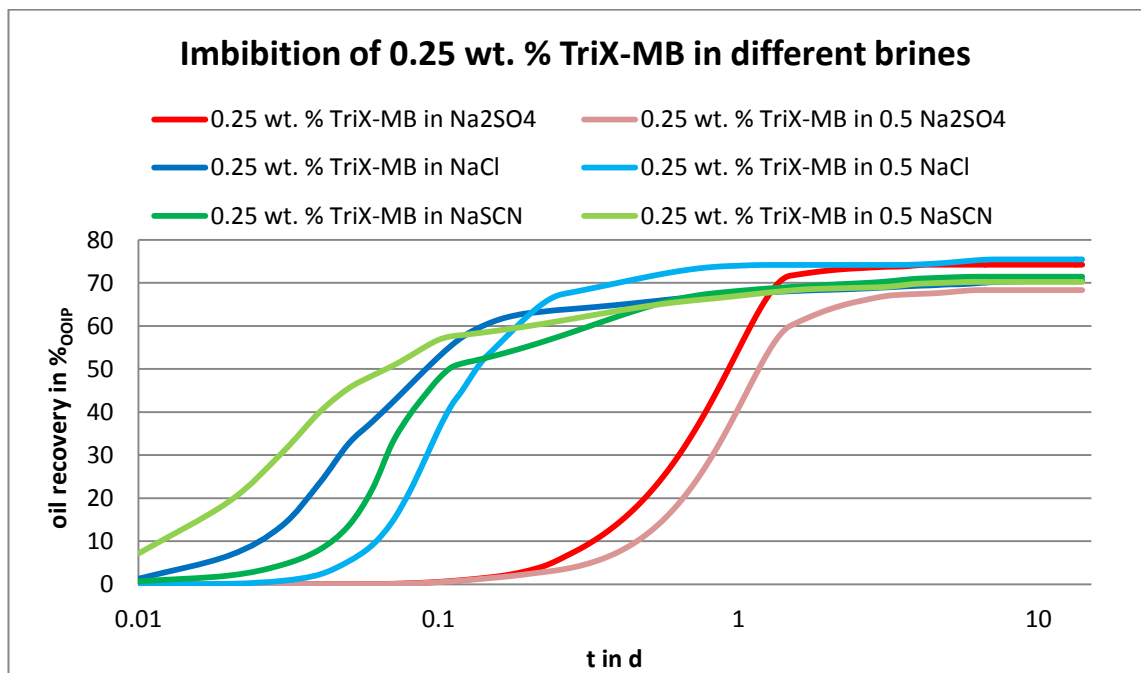


Figure 7-20: Imbibition curves of 0.25 wt. % TriX-MB in different brines

Imbibition with sodium thiocyanate tended to start first, but the difference to sodium chloride was insignificant. The imbibition rate of sodium sulfate solutions was the lowest in every case. This observation correlated with the viscosity of the TriX-MB so-

lutions. However, the fact that 5 of 6 of the sulfate solution imbibition curves showed a very low imbibition rate compared to the other salts, might also be an indication of a detrimental effect on imbibition rate of sodium sulfate alone.

A significant effect of adding TriX-MB to the brines on imbibition rate could not be observed in these experiments. In Figure 7-21 the ultimate recoveries (including the standard deviations) of the imbibition tests with different combinations of brines and TriX-MB are summarized.

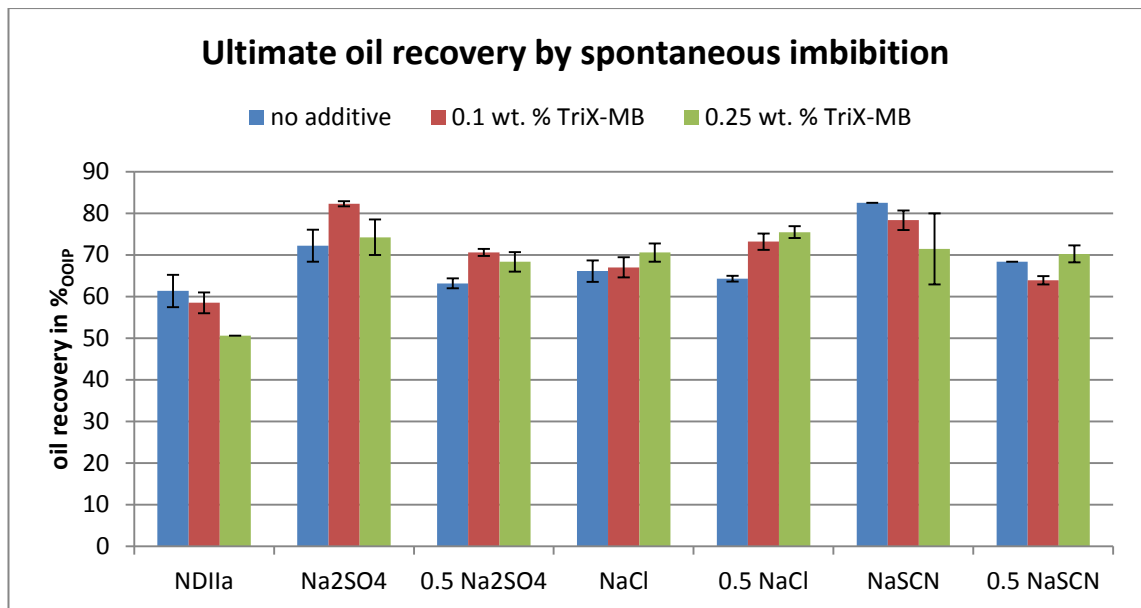


Figure 7-21: Ultimate recoveries of imbibition tests with TriX-MB in different brines

Adding 0.1 wt. % TriX-MB to sodium sulfate solutions led to an increase in oil recovery, probably due to decreasing interfacial tension. At higher concentrations, the oil recovery decreased, because of the high viscosity, which impeded the flow of the TriX solution. In sodium chloride solutions adding TriX-MB leads to a slight increase in oil recovery. This effect grew at higher concentrations. Adding TriX-MB to sodium thiocyanate solutions resulted in lower ultimate oil recoveries.

Summary

The results of the viscosity measurements on TriX-MB in different saline solutions confirm that the *Hofmeister* effects apply for the aggregates of TriX-MB. Pure saline solutions also follow the Hofmeister series with respect to IFT reduction. The imbibition process is very complex and affected by a variety of parameters. The results ob-

tained by the experiments, which have been discussed in this chapter, are too tenuous to make any final statement about how the *Hofmeister* effects influence oil mobilization by TriX-MB solutions. To better understand the interactions between macromolecular structures of TriX-MB and crude oil in the presence of salts, which intensify either hydrophilic or hydrophobic effects, there are more investigations needed. I can even imagine that such investigations must include intensive molecular modeling to understand the mechanisms on the molecular level. NaSCN turned out to have a beneficial effect on oil mobilization, which could be a starting point for new research.

7.6 Injection Tests

7.6.1 Injectivity of 0.1 wt. % TriX-MB in NDIIa solution in high permeable cores (Bentheimer sandstone, $k_{brine} \approx 1.5 D$)

The injectivity of 0.1 wt. % TriX-MB in NDIIa brine was studied by conducting core flooding experiments with Bentheimer sandstone cores. The characteristics of the cores and fluids used are given in Table 7-8.

Table 7-8: Characteristics of cores and fluids of injection tests with NDIIa brine

	#1		#2		#3	
<u>Cores</u>	FC	MC	FC	MC	FC	MC
Type	Bentheimer sandstone					
l in cm	6.03	6.78	4.11	7.11	6.01	29.6
n	0.28	0.26	0.22	0.23	0.25	0.23
PV in ml	19.35	20.3	10.32	18.42	16.87	77.46
k_{NDIIa} in D	1.84	1.52	1.60	1.01	1.13	1.34
<u>Fluids (55°C)</u>						
η_{NDIIa} in mPa·s	0.775		0.776		0.786	
$ \eta_{TriX-MB}^* $ in mPa·s ($\omega = 10$ rad/s, $\gamma = 1$)	10.4		22		8.7	

In experiments #1 and #2 short cores were used for both the filtration and main core. Experiment #3 was conducted with a long main core. Conditioning of TriX-MB in

NDIIa brine was quite difficult because of the complex structure buildup. Prescribed instructions for the proceeding of conditioning were strictly followed, but there still was a great difference in the viscosities of TriX-MB solutions.

The Figures 7-22 and 7-23 show the pressure curves of TriX injection in CF #3 (red points: individual measurements).

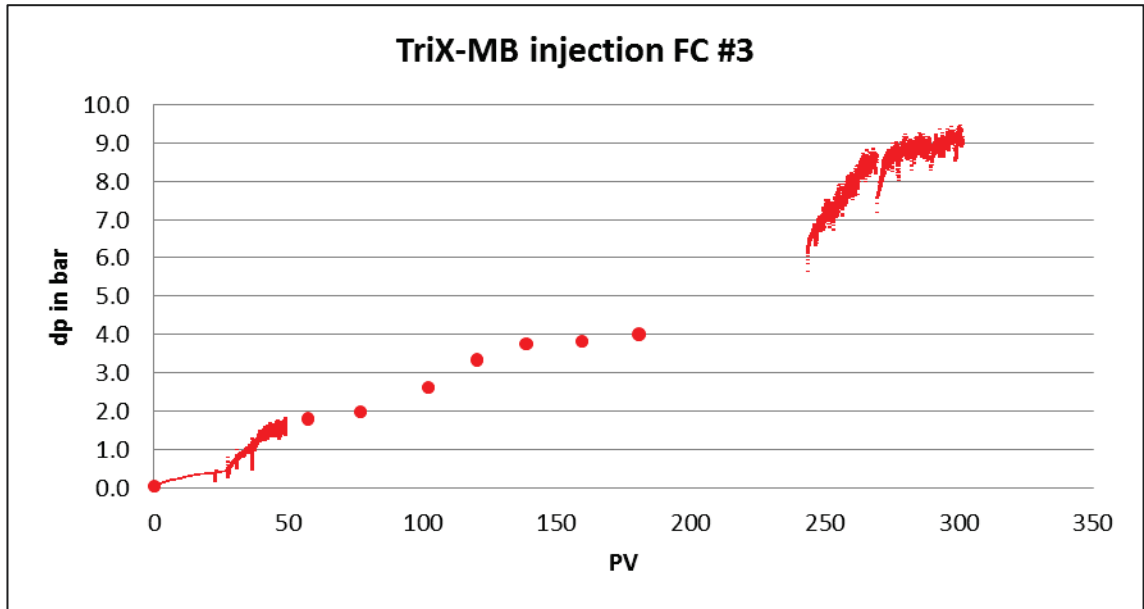


Figure 7-22: Pressure drop over filtration core #3 during injection of 0.1 wt. % TriX-MB in NDIIa brine

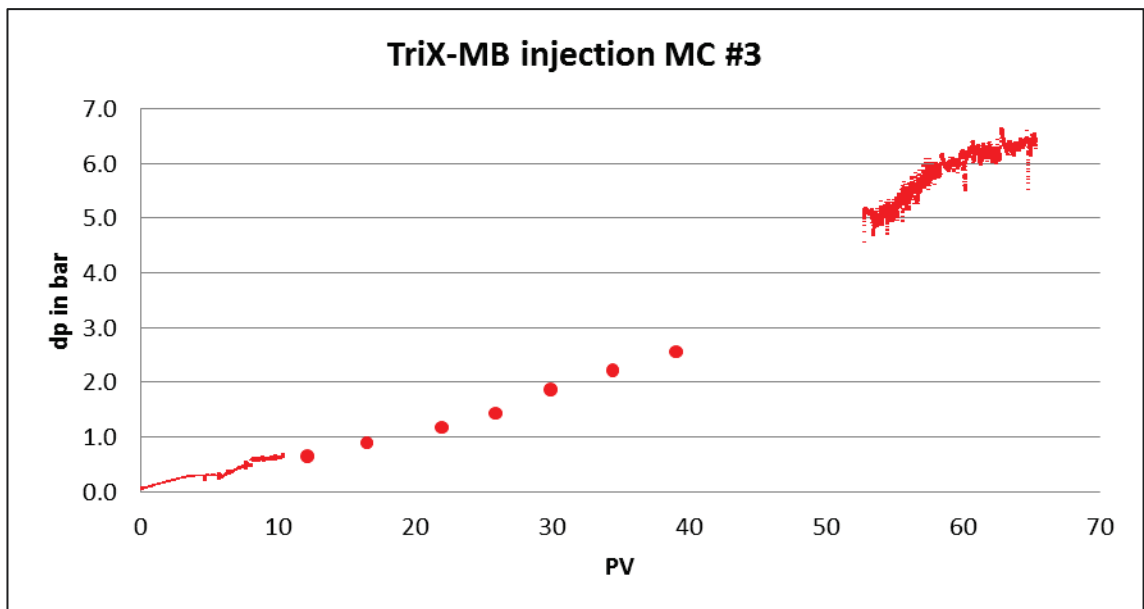


Figure 7-23: Pressure drop over main core #3 during injection of 0.1 wt. % TriX-MB in NDIIa brine

In Table 7-9, the characteristic values of the injection tests #1 to #3 are summarized.

Table 7-9: Characteristic values of injection tests with NDIIa brine

	#1		#2		#3	
<u>Cores</u>	FC	MC	FC	MC	FC	MC
Volume of injected TriX-MB in PV	29.71	27.12	78.69	42.93	300.92	65.25
Steady state?	no	no	no	no	no	yes
<i>RF</i> ($v_D = 1$ ft/d)	>700	>400	>700	> 100	> 1000	> 1000
<i>RRF</i> ($v_D = 1$ ft/d)		370		> 100		> 100

Very high pressure increases could be observed during injection of 0.1 wt. % TriX-MB in NDIIa brine in both the filtration and main cores, which also resulted in high resistance factors. The increase in pressure drops was always greater in the filtration than in the main cores. In the filtration core, no steady differential pressure was reached at all, even after the injection of more than 300 pore volumes of TriX-MB solution. In the main core steady state was reached after injection of ca. 65 pore volumes. The *RF* and *RRF* values were much too high for EOR applications, even in the high permeable sandstone used. These coefficients indicated a kind of blockage inside the cores or at their front faces, caused by the very rigid tertiary network, which TriX-MB was building in the presence of polyvalent ions. After removing the cores from the Hassler cells, gelled material was observed at the inlet and even the outlet of the filtration core (Figure 7-24).



Figure 7-24: Gelled material at front and back face of filtration core #3

The gel-like material was analyzed by BASF. An increased concentration of chrome and iron ions was noticed [109]. Therefore, the gel seemed to be a product of TriX-MB and Cr^{3+} and/or Fe^{3+} ions from high-grade steel parts of the core flood unit. Trivalent ions even intensified the rigidity of the tertiary network of TriX-MB. This should be considered since trivalent ions are also present in the wellbore and possible reservoirs. Complexing of viscoelastic surfactants with iron has already been reported in the literature [110].

After determination of the *RRF* value in experiment #3, it was attempted to remove any material, which was responsible for reversible plugging at the front face and inside the main core by injecting NDIIa brine in the reverse direction. Then the ramp of flow rates was run again. The *RRF* value decreased somewhat but was still very high between 100 and 400 (see: Figure 7-25).

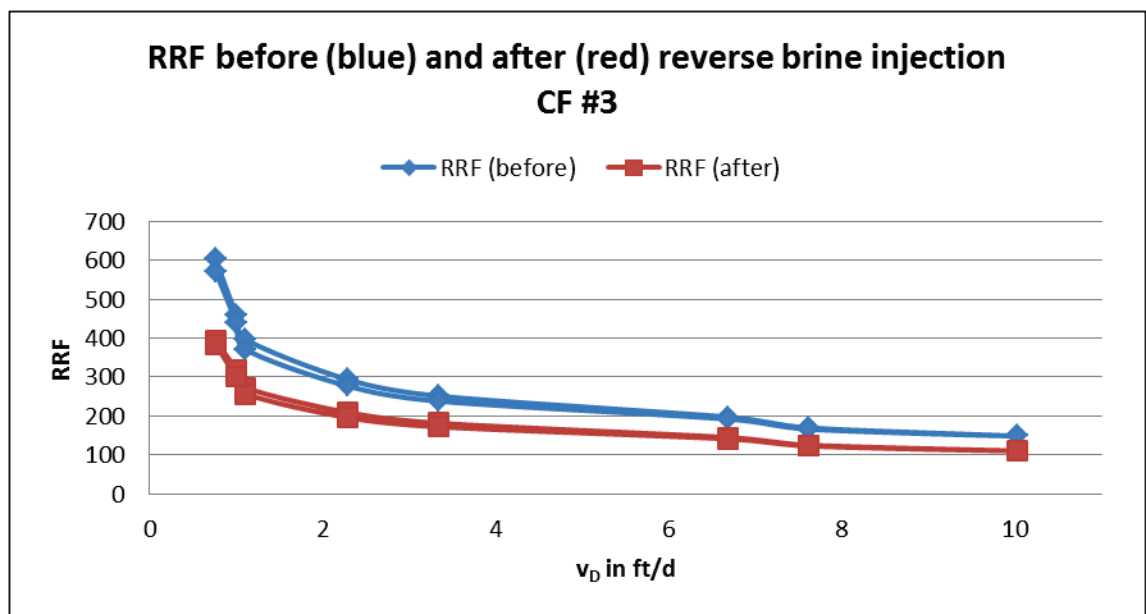


Figure 7-25: RRF before and after reverse brine injection (plugging removal)

In a last step of the experiment fresh water was injected into the main core. Since salt ions are needed to build secondary and tertiary structures, the TriX-MB network broke down, and injectivity improved remarkably. This indicated that the plugging effects were to a large extent a result of the strong tertiary network.

Since the injection tests with TriX-MB in NDIIa solution led to results, which did not contribute to an understanding of the TriX mode-of-action, it was decided to replace NDIIa as brine by NaCl solution with the same ionic strength. In the presence of monovalent ions only, TriX-MB forms similar secondary aggregates in solution, but the ter-

tiary network is less rigid. This was expected to result in lower pressure drops over the cores and less plugging. The experiments with TriX-MB in NaCl should give information about the injectivity and retention of the secondary TriX-MB aggregates.

7.6.2 Injectivity of 0.1 wt. % TriX-MB in NaCl solution in high permeable cores (Bentheimer Sandstone, $k_{brine} \approx 1.5 D$)

The injection tests of 0.1 wt. % TriX-MB in NaCl brine were conducted using a short filtration and a long main core. In experiments #4 and #5, Bentheimer sandstone was used. The characteristics of the cores and fluids used are presented in Table 7-10.

Table 7-10: Characteristics of cores and fluids of injection tests with NaCl

	#4		#5	
<u>Cores</u>	FC	MC	FC	MC
Type	Bentheimer Sandstone			
<i>l</i> in cm	4.08	29.8	6.50	29.8
<i>n</i>	0.27	0.24	0.26	0.29
PV in ml	12.3	80.5	19.0	91.8
k_{NaCl} in D	1.10	1.24	2.47	1.16
<u>Fluids (55°C)</u>				
η_{NaCl} in mPa·s	0.820		0.795	
$\eta_{TriX-MB}^*$ in mPa·s ($\omega = 10$ rad/s, $\gamma = 1$)	10.6		8.5	

Again, the conditioning of TriX-MB in NaCl was performed strictly following the pre-conditioning instructions. The viscosities of the different TriX solutions used in the experiment #4 to #7 were quite uniform.

In the Figures 7-26 and 7-27 the pressure drops over filtration and main core in experiment #4 are given as exemplary presentation for 0.1 wt. % TriX-MB in NaCl brine injection into Bentheimer sandstone.

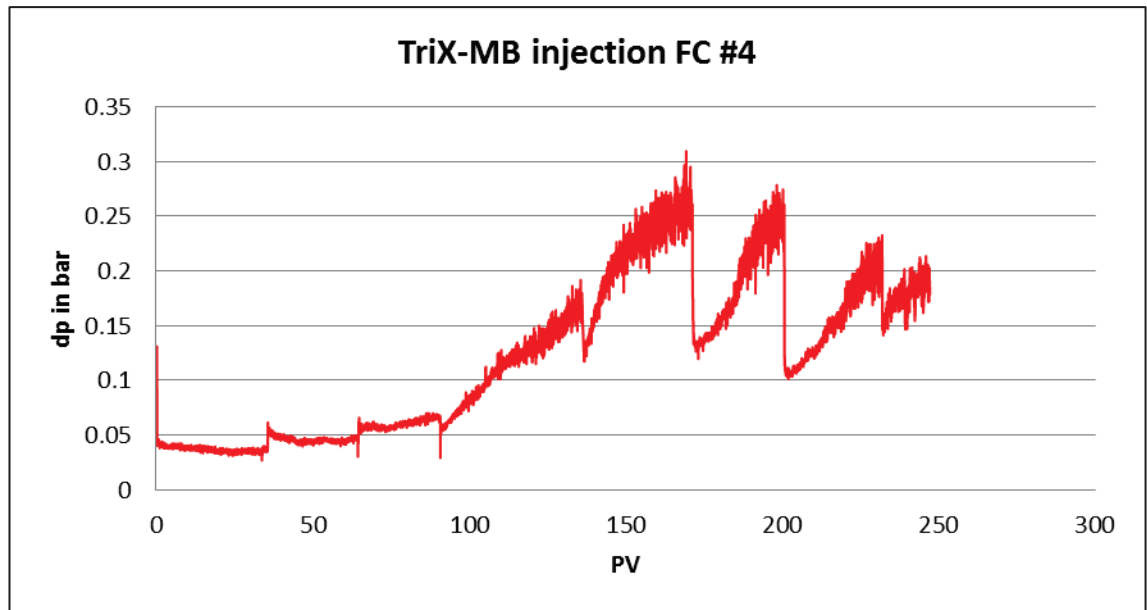


Figure 7-26: Pressure drop over filtration core #4 during injection of 0.1 wt. % TriX-MB in NaCl

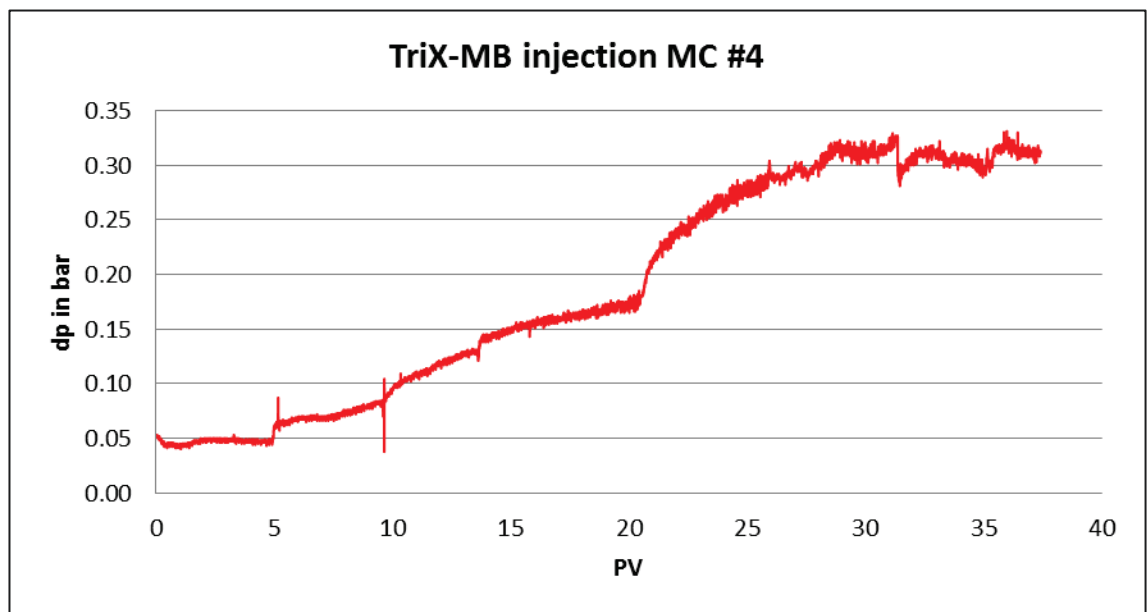


Figure 7-27: Pressure drop over main core #4 during injection of 0.1 wt. % TriX-MB in NaCl

The pressure over the filtration core increased steadily within the first 170 PV injected. After that, it was very unstable. At points of rapid pressure decrease, the injection was interrupted to refill the piston accumulator. After restarting the experiment, the pressure increased again. This could again be caused by rigid tertiary aggregates, which were formed by TriX-MB in combination with trivalent ions. Since the experimental setup was not changed, the presence of Fe^{3+} and Cr^{3+} had to be taken into account. The sharp pressure declines might be indicators for an elastic response of this

network at the front face and inside the core. The pressure drop over the main core steadily increased until, after injection of ca. 30 PV, steady state was reached.

The characteristic values of the injection tests using TriX-MB in NaCl brine are presented in Table 7-11.

Table 7-11: Characteristic values of injection tests with TriX-MB in NaCl (high permeable cores)

<u>Cores</u>	#4		#5	
	FC	MC	FC	MC
Volume of injected TriX-MB in PV	247	37.4	69	14
Steady state?	no	yes (30)	no	yes (4)
$RF (v_D = 1 \text{ ft/d})$	160	28.3	78.8	8.6
$RRF (v_D = 1 \text{ ft/d})$		26.3		7.5

In the two injection tests using TriX-MB in NaCl brine into Bentheimer sandstone steady pressure conditions could be reached in the main cores. Due to filtration effects, no steady state was achieved in the filtration cores. The RF and RRF values were much lower than with NDIIa brine (see: Table 7-9). Especially the RF value of the main core in experiment #5 was at a desirable level. The RF and RRF values of experiment #5 were lower than the values of experiment #4 by a factor 3, which was still a high variation. This might be due to the larger volumes of injected TriX-MB solution and its higher bulk viscosity in experiment #4.

In both experiments, the RRF value was at the same level as the RF value, which was quite surprising, since it has not been reported in the literature by now. The pressure drop over the core was expected to decrease during injection of brine after TriX-MB solution, because of the lower viscosity of the brine.

7.6.3 Injectivity of 0.1 wt. % TriX-MB in NaCl solution in lower permeable cores (Michigan sandstone, $k_{brine} \approx 0.6 \text{ D}$)

Since oil displacement experiments should be conducted in lower permeable sandstone cores, injectivity of TriX-MB under these conditions had to be studied. For

that purpose, Michigan sandstone cores were used in the next injection tests. The characteristics of the cores and fluids used are presented in Table 7-12.

Table 7-12: Characteristics of the cores and fluids of core floods #6 and #7

	#6		#7	
<u>Cores</u>	FC	MC	FC	MC
Type	Michigan Sandstone			
l in cm	5.95	30.0	5.96	30.0
n	0.26	0.22	0.26	0.26
PV in ml	17.6	74.6	17.3	88.9
k_{NaCl} in D	0.32	0.55	0.22	0.66
<u>Fluids (55°C)</u>				
η_{NaCl} in mPa·s	0.799		0.815	
$ \eta_{TriX-MB}^* $ in mPa·s ($\omega = 10$ rad/s, $\gamma = 1$)	10.3		8.5	

Figure 7-28 and Figure 7-29 show the pressure drops during TriX injection into the filtration and main core of experiment #6.

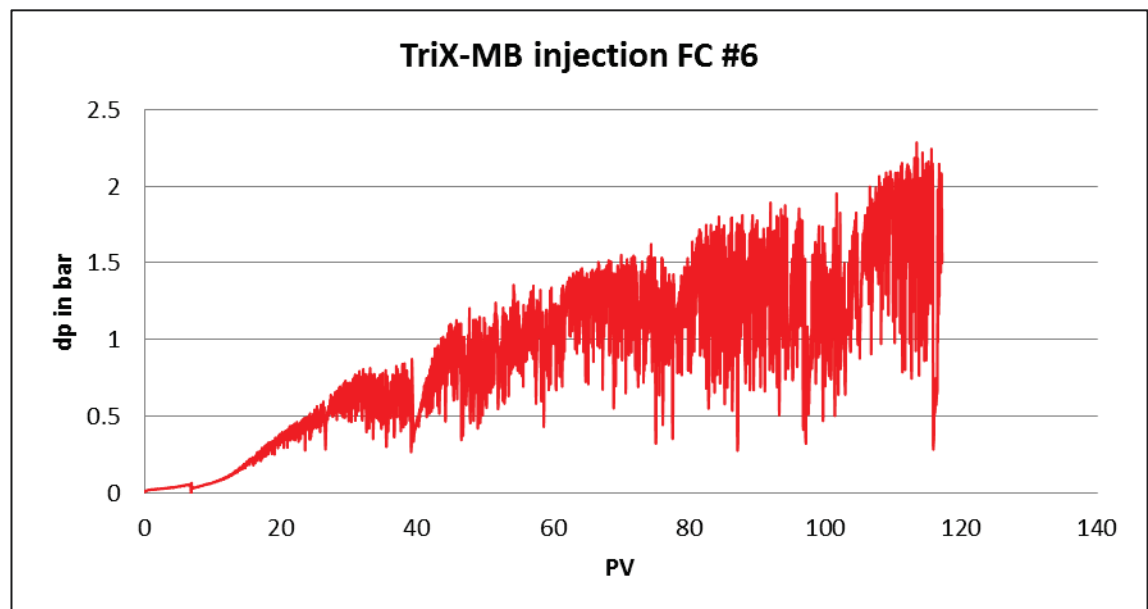


Figure 7-28: Pressure drop over filtration core #6 during injection of 0.1 wt. % TriX-MB in NaCl

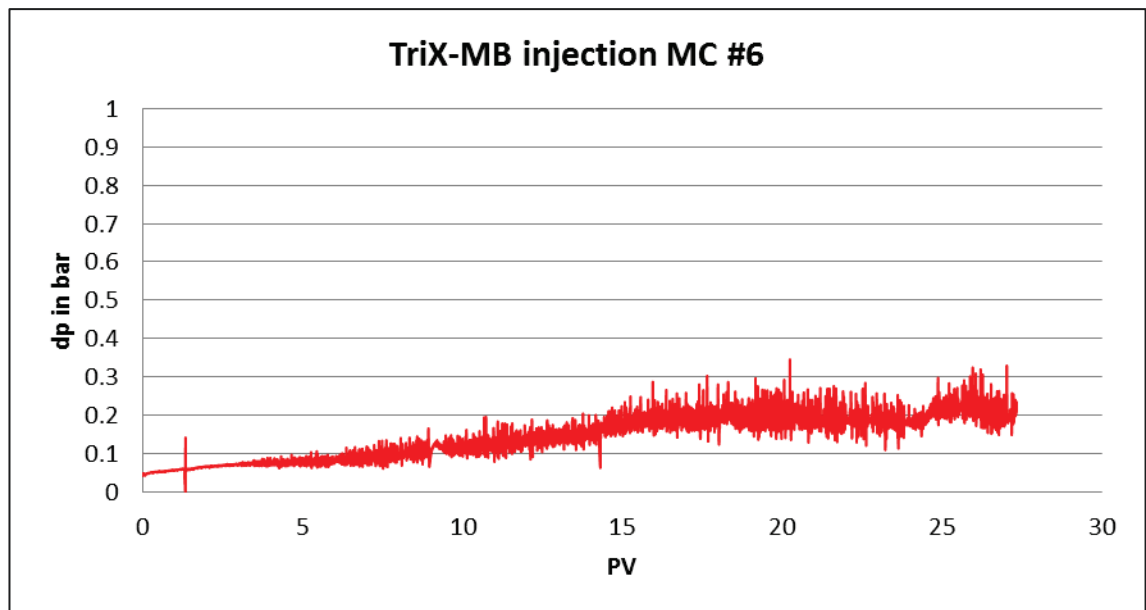


Figure 7-29: Pressure drop over main core #6 during injection of 0.1 wt. % TriX-MB in NaCl

In the filtration cores of the experiments #6 and #7, no steady state was reached, even after the injection of more than 100 PV of the TriX-MB solution. When the filtration cores were removed after completion of the core floods, a thin gel-like layer at the front side of the cores could be observed. Again interaction with trivalent ions took place and the built up network was filtered at the front side of the filtration core. Furthermore, large aggregates of TriX-MB accumulated inside the filtration core.

In the main cores of the experiments #6 and #7 the pressure drop increased very slowly and reached steady state conditions after injection of ca. 16 PV at a comparatively low level of around 0.2 bar. There was no indication for plugging effects in the main cores. The filtrated TriX-MB solution showed good injectivity.

As can be seen in Table 7-13, the *RF* value of the filtration core of core flood #6 was ca. 39, which was a reasonable value for further investigations, considering that the filtration core was simulating the near wellbore area and affected by filtration effects. *RF* and *RRF* of the main cores of the experiments #6 and #7 were on the same level as the values of the core floods #4 and #5. Again both, *RF* and *RRF* values were very similar.

Table 7-13: Characteristic values of injection tests with TriX-MB in NaCl (lower permeable cores)

Cores	#6		#7	
	FC	MC	FC	MC
Volume of injected TriX-MB in PV	117	27.3	131	30.6
Steady state?	no	yes (16)	no	yes (15)
<i>RF</i> ($v_D = 1$ ft/d)	38.8	9.4	N/A	17.6
<i>RRF</i> ($v_D = 1$ ft/d)		5.8		18

In core flood #6 the concentrations of the effluents of both, main and filtration core during TriX-MB injection were determined to assess TriX-MB retention.

7.6.4 Injectivity of 0.1 wt. % TriX-TA in NDIIa solution

The core flooding experiments with TriX-TA were conducted using the synthetic reservoir brine NDIIa. The structure of the TriX-TA molecule is very close to that of TriX-MB. However, it does not form rod-like secondary aggregates, but much smaller spherical micelles and no viscoelastic structure under any conditions. These experiments intended to study the injectivity and retention of this TriX derivative. Furthermore, by using NDIIa, the experimental setup was closer to field conditions.

Injectivity of 0.1 wt. % TriX-TA in NDIIa solution was studied on the filtration cores #14 and #15. The data of the cores are shown in Table 7-14.

Table 7-14: Characteristics of cores and fluids of injection tests with TriX-TA in NDIIa brine

	#14	#15
Cores	FC	FC
Type	Michigan Sandstone	
<i>l</i> in cm	5.95	5.21
<i>n</i>	0.23	0.24
PV in ml	15.4	13.9
<i>k</i>_{NDIIa} in D	0.56	0.65
Fluids (55°C)		
η_{NDIIa} in mPa·s	0.80	0.83
η_{TriX-TA} in mPa·s	0.80	0.82

The preconditioning of 0.1 wt. % TriX-TA in NDIIa solution was conducted following the same proceedings like with TriX-MB solutions.

The TriX-TA concentration in the effluent was determined by UV extinction measurements during the injection test. Figure 7-30 shows the pressure drop over the filtration core #15 and the concentration of the effluent during TriX-TA injection.

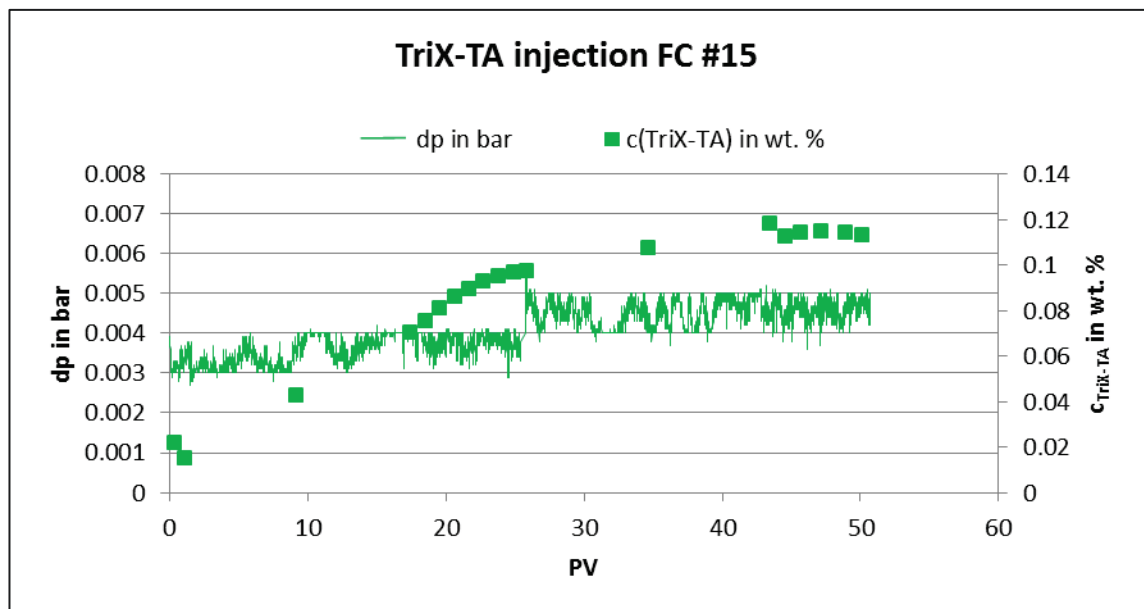


Figure 7-30: Pressure curve and concentration of effluent during TriX-TA in NDIIa brine injection

After injection of ca. 26 PV the piston accumulator had to be refilled. The pressure increase during injection was low compared to TriX-MB injection. Steady pressure conditions were reached instantly, at the latest after injection of around 10 PV. In core flood #14, steady pressure drop over the filtration core was reached a bit later, after around 25 PV, but the total pressure increase was also low, which leads to very favorable RF values of less than 2 in both experiments. The RRF values in both experiments were very similar (around 3), too. This time RRF even slightly exceeded the RF values, which indicated that there is less resistance to the flow of a TriX-TA solution than to the flow of brine alone. The reason might be some kind of a slipping effect between the molecules, which were attracted to the pore walls and the similar molecules in solution. Such effects have already been reported for the flow of several solutions containing macromolecules [111]. Molecular modeling, which has been done by BASF, also indicated that sliding of TriX molecules alongside each other could be possible [112].

The characteristic values of the injection test using TriX-TA in NDIIa brine are presented in Table 7-15. The experiments showed good reproducibility.

Table 7-15: Characteristic values of injection tests with TriX-TA in NDIIa brine

	#14	#15
Cores	FC	FC
Volume of injected TriX-MB in PV	153.9	97.8
Steady state?	yes (25)	yes (10)
RF ($v_D = 1$ ft/d)	1.96	1.52
RRF ($v_D = 1$ ft/d)	3.03	2.82

7.6.5 Injectivity of 0.1 wt. % TriX-M in NDIIa solution

A core flooding experiment with TriX-M was conducted with NDIIa as brine for the same reasons as mentioned above for TriX-TA.

Injectivity of 0.1 wt. % TriX-M into Michigan sandstone was studied on the filtration core of core flood #16. The characteristic values of the core and the used fluids are given in Table 7-16.

Table 7-16: Characteristics of cores and fluids of injection tests with TriX-M in NDIIa brine

#16	
Cores	FC
Type	Michigan Sandstone
<i>l</i> in cm	7.33
<i>n</i>	0.26
PV in ml	21.6
k_{NDIIa} in D	0.74
Fluids (55°C)	
η_{NDIIa} in mPa·s	0.83
η_{TriX-M} in mPa·s	0.82

During injection, the TriX-M concentration in the effluent was determined by means of UV extinction measurements. Figure 7-31 shows the pressure drop over filtration core #16 and the TriX-M concentration in the effluent during injection.

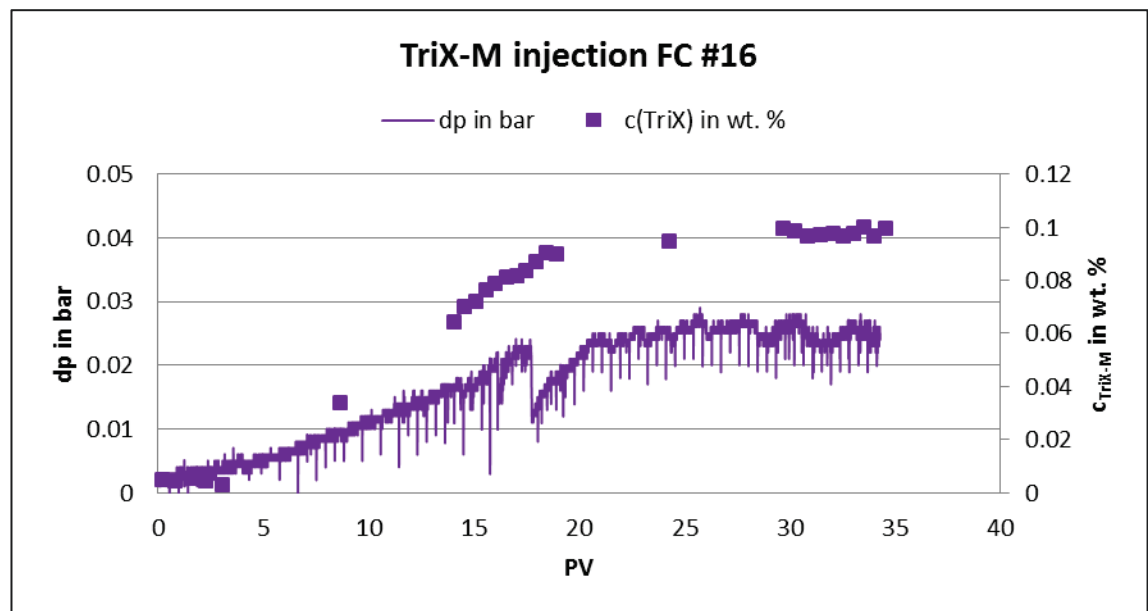


Figure 7-31: Pressure curve and concentration of effluent during TriX-M in NDIIa brine injection

The pressure drop over filtration core #16 increased steadily up to a volume of 20 PV injected. The progression of the pressure curve correlated with the TriX-M concentration in the effluent. After injection of around 20 PV, the flow path in the core

could be considered to be saturated with TriX-M. The pressure increase due to injection of TriX-M was higher compared to TriX-TA, but lower compared to TriX-MB.

Subsequent to the injection test with filtration core #16, an oil displacement test in main core #16 was conducted. In this case additional 63 PV of 0.1 wt. % TriX-M in NDIIa solution passed the filtration core. The *RF* value was determined after total injection of 97.7 PV. *RF* and *RRF* values were slightly higher than for TriX-TA injection but significantly lower than with TriX-MB. Again, the *RRF* slightly exceeded the *RF* value, as can be seen in Table 7-17.

Table 7-17: Characteristic values of injection tests with TriX-M in NDIIa brine

	#16
<u>Core</u>	FC
Volume of injected TriX-MB in PV	97.7
Steady state?	yes (20)
<i>RF</i> ($v_D = 1$ ft/d)	3.40
<i>RRF</i> ($v_D = 1$ ft/d)	4.95

7.6.6 Retention of TriX derivatives in Michigan Sandstone

To investigate retention of TriX in Michigan Sandstone, a mass balance of TriX molecules injected into a core and TriX molecules in the effluent was conducted during core flooding experiments.

For TriX-MB the main core of experiment #6 and the filtration cores of the experiments #6, #9 and #11, for TriX-TA the filtration cores #14 and #15 and for TriX-M filtration core #16 were chosen as subjects to study.

The mass of injected TriX into the filtration cores could easily be determined from the volume of the 0.1 wt. % solution injected. Several samples of the effluent were taken during the core flood (TriX injection and subsequent brine injection). The TriX concentrations of the effluent samples were determined by UV extinction measurements; hence, the mass of TriX in the effluent could be calculated.

The concentration of TriX-MB solution injected into main core #6 was assumed to be the concentration of effluent from the filtration core #6.

Knowing the average molecular weight of the TriX derivatives, the amount of TriX in mmol could be calculated.

Table 7-18 and Figure 7-32 summarize the relevant core data, and the quantities of TriX injected and detected in the effluents, as well as the calculated retention of TriX derivatives in Michigan Sandstone in various units.

Table 7-18: Retention of TriX derivatives during core flooding tests in Michigan sandstone

		TriX-MB (NaCl)				TriX-TA (NDIIa)		TriX-M (NDIIa)
		MC #6	FC #6	FC #9	FC #11	FC #14	FC #15	FC #16
m_{dry}	g	696.0	136.9	133.9	138.0	137.5	120.2	137.9
A_o	m ²	480.24	94.46	92.39	95.22	94.89	82.91	95.18
TriX_{in}	mg	1859.3	2333.7	1301.1	3458.0	1111.0	2292.2	2339.1
	mmol	0.826	1.037	0.578	1.537	0.475	0.980	3.119
TriX_{out}	mg	1432.4	1980.7	997.2	3168.1	927.8	2209.6	2051.0
	mmol	0.637	0.880	0.443	1.408	0.396	0.944	2.735
Retention	mg _{TriX} /g _{rock}	0.613	2.579	2.270	2.101	1.333	0.687	2.088
	mg _{TriX} /m ² _{rock}	0.900	3.737	3.289	3.045	1.931	0.996	3.026
	μmol _{TriX} /g _{rock}	0.273	1.146	1.009	0.934	0.570	0.294	2.784
	μmol _{TriX} /m ² _{rock}	0.395	1.661	1.462	1.353	0.825	0.426	4.035

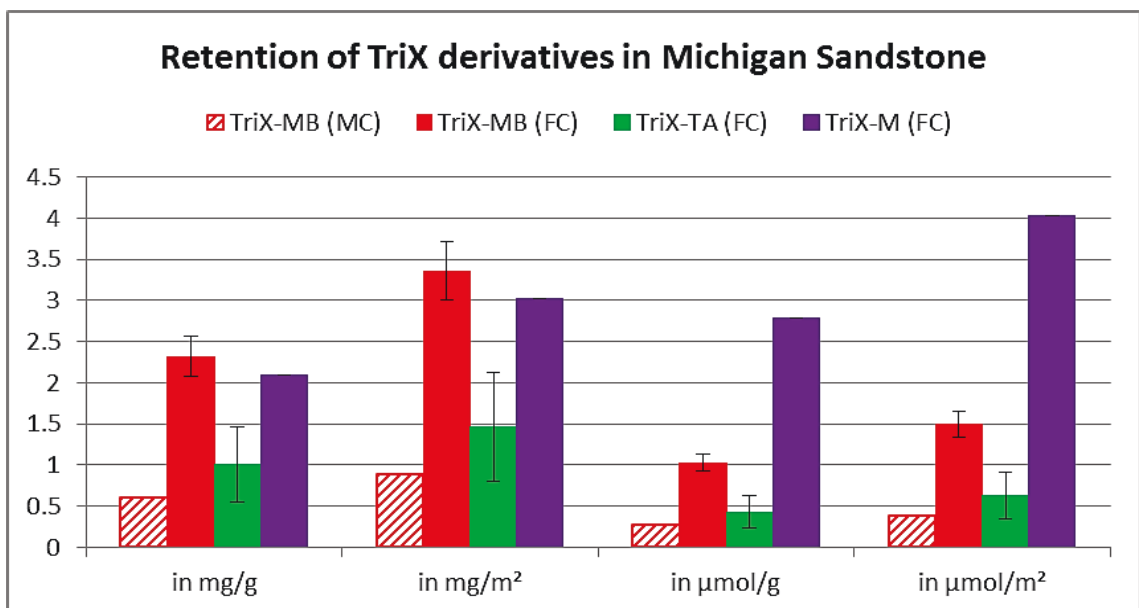


Figure 7-32: Retention of TriX derivatives in Michigan Sandstone in different units

The retention of TriX-MB in the filtration cores was by a factor 3.8 higher than in the main core. This is another proof for the filtration effects, which resulted in the high pressure drops over the filtration cores during TriX-MB injection.

To distinguish adsorption and filtration effects during a core flood and make statements about their proportions, the retention and static adsorption were compared. The values are given in Table 7-19 and the Figures 7-33 and 7-34 (note: logarithmic scale).

Table 7-19: Retention and Adsorption of TriX derivatives

		TriX-MB (NaCl)		TriX-TA (NDIIa)	TriX-M (NDIIa)
		MC	FC	FC	FC
Retention	$\text{mg}_{\text{TriX}}/\text{m}^2_{\text{rock}}$	0.900	3.357	1.464	3.026
	$\mu\text{mol}_{\text{TriX}}/\text{m}^2_{\text{rock}}$	0.395	1.492	0.626	4.035
Adsorption	$\text{mg}_{\text{TriX}}/\text{m}^2_{\text{sand}}$	0.010	0.010	0.018	0.487
	$\mu\text{mol}_{\text{TriX}}/\text{m}^2_{\text{sand}}$	0.004	0.004	0.008	0.650
Adsorption/Retention		1.1 %	0.3 %	0.9 %	16.1 %

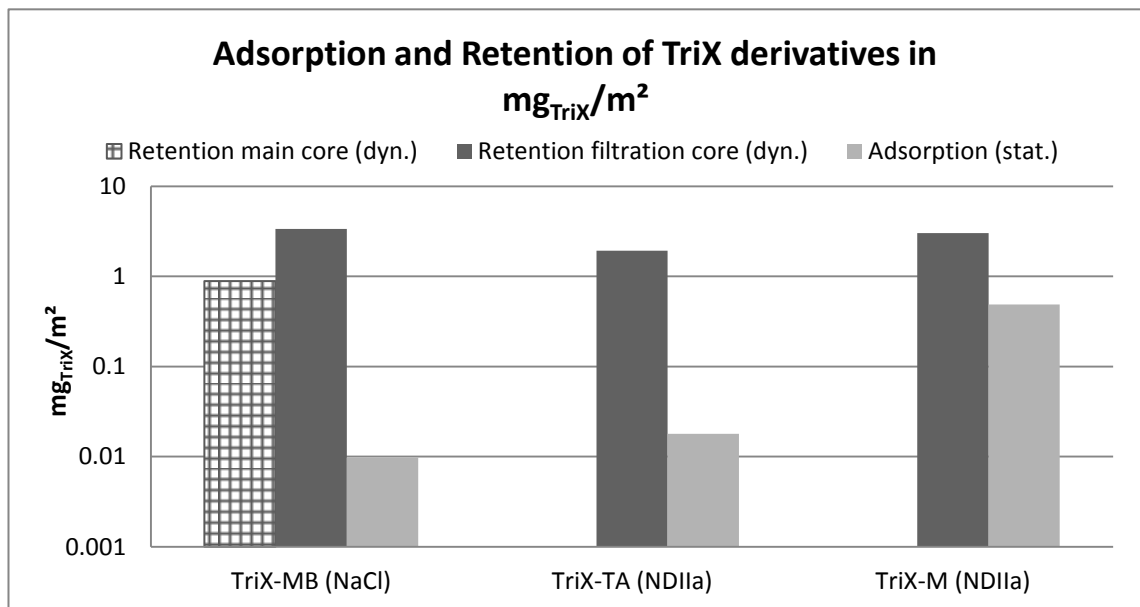
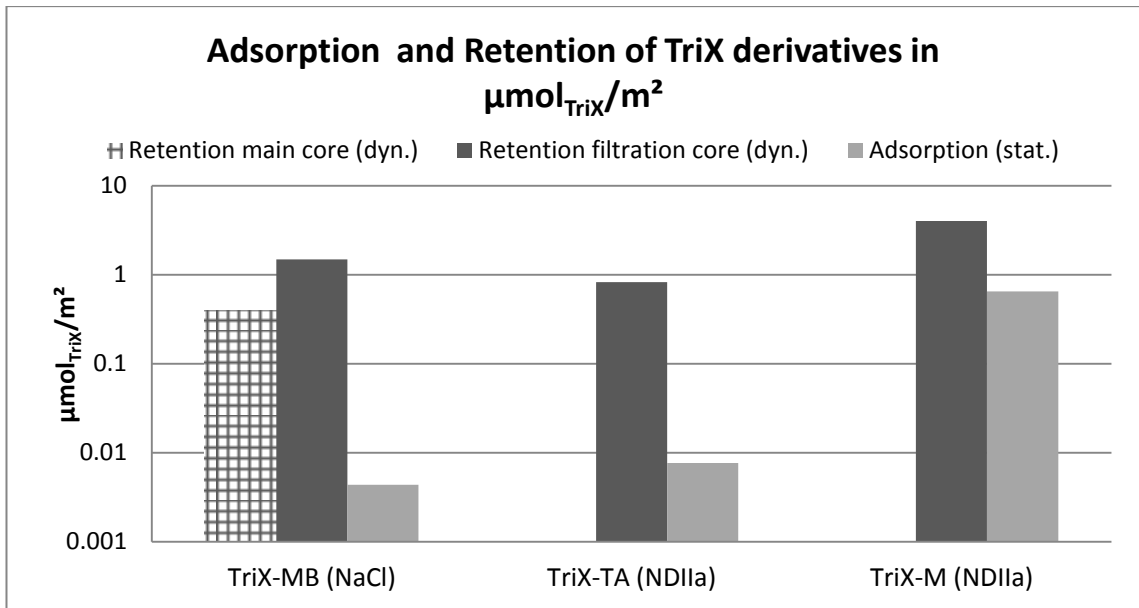


Figure 7-33: Retention and Adsorption of TriX derivatives in mg/m^2

Figure 7-34: Retention and Adsorption of TriX derivatives in $\mu\text{mol}/\text{m}^2$

The retention of TriX-MB is much higher in the filtration core compared to the main core. After filtration the TriX-MB solution shows the lowest retention level of all three derivatives in the main core. For the TriX derivatives with high molecular weight adsorption contributes to retention with only 1 %. Regarding TriX-M the adsorption accounts for around 16 % of total retention.

7.6.7 Summary: Injection tests and Retention of TriX derivatives

In Table 7-20 the results of the injection tests conducted with the different TriX derivatives are summarized.

Table 7-20: Summary of the injection tests

TriX solution	Sandstone type (core)	k_{brine} in D	$RF (v_D = 1 \text{ ft/d})$		$RRF (v_D = 1 \text{ ft/d})$	
			FC	MC	FC	MC
TriX-MB (NDIIa)	Bentheimer	1.4	> 700	> 100	> 100	
TriX-MB (NaCl)	Bentheimer	1.5	79 – 160	9 – 28	8 – 26	
	Michigan	0.4	39	9 – 18	6 – 18	
TriX-TA (NDIIa)	Michigan	0.6	1.7		2.9	
TriX-M (NDIIa)	Michigan	0.7	3.4		5.0	

In the presence of divalent ions, TriX-MB micelles formed a rigid network with a mesh size of 1 μm and more. Due to the long duration of the injection tests with **0.1 % TriX-MB in NDIIa brine**, Cr^{3+} and Fe^{3+} were set free from stainless steel parts of the core flooding unit. The cross-linking between the micelles was reinforced by these trivalent ions, resulting in an even more rigid network. More than 90 % of the pore volume of the cores (Bentheimer sandstone) contained pores with a diameter between 10 and 100 μm . These pore sizes could have easily been passed by single micelles or small tertiary aggregations. However, when injecting the TriX-MB solution into the sandstone cores, the cross-links did not break down due to shear stress and the network associations remained too big. Therefore, parts of this network were filtrated in front of the pores, which could even visually be observed by the formation of a gel-like layer on the front face of the filtration core. It is very likely that those filtration effects also occurred inside the cores to a certain extent. Following associations of TriX-MB micelles were caught in the partially plugged pores which led to a steadily increasing pressure drop over the core. The highly viscoelastic solution of TriX-MB in reservoir brine was found to have poor injectivity.

Injectivity of **0.1 wt. % TriX-MB in NaCl in high permeable Bentheimer sandstone** ($k_{brine} \approx 1.5 \text{ D}$) was much more favorable than in NDIIa brine, because the tertiary network structures built up with monovalent ions were not as strong and rigid as with divalent ions. The cross-links could be broken down by the present shear stresses, which resulted in smaller aggregates and the TriX solution could be injected into the core with moderate pressure buildup. However, the retention of TriX-MB in the filtration core was more than three times higher as in the main core, indicating that TriX-MB structures formed with trivalent cations were filtered out. This led to steady pressure increase and instabilities in the pressure curves of the filtration core. In the main core the differential pressure stabilized after injection of around 30 PV. *RF* and *RRF* values in the main core were on the same level and a little too high for a commercial EOR product.

The injection tests with **0.1 wt. % TriX-MB in NaCl into lower permeable Michigan sandstone** led to results comparable to those of the injection into Bentheimer sandstone. During the injection tests with the concentration of the effluent was analyzed. More than 90 % of injected TriX-MB molecules were found after injection of around

45 PV. The *RF* and *RRF* values are nearly the same in low and high permeable cores. The tertiary network of TriX-MB could again be broken down into smaller networks and secondary rod-like micelles. The smaller pore diameters of the Michigan sandstone had no influence on injection behavior into porous media of secondary aggregates of TriX-MB.

During injection of **0.1 wt. % TriX-TA in NDIIa** into the filtration core ($k_{brine} \approx 0.6 D$) steady state was reached instantly. This is a good result in contrast to TriX-MB, where a steady state, if ever, could be reached after more than 60 PV in the filtration core. The *RF* value was at a very low level of ca. 2, even though over 150 pore volumes of TriX-TA solution were injected. The *RRF* value was also on a low and favorable level of around 3. TriX-TA showed very good injectivity and low reservoir formation damage, which is due to the smaller size of the spherical secondary aggregates (9 – 15 nm) and the fact, that no tertiary structures are formed. TriX-TA showed even lower pressure increase, *RF* and *RRF* values than TriX-M, because of the low level of adsorption and retention.

Injection of **0.1 wt. % TriX-M in NDIIa** resulted in higher pressure increase, *RF* and *RRF* values than TriX-TA, because of higher grade of adsorption inside the core ($k_{brine} \approx 0.6 D$). The pressure curve corresponded to the saturation of the core with TriX-M. Injectivity was much more favorable than with TriX-MB, which was expected because no secondary and tertiary aggregates were formed.

The similarity between *RF* and *RRF* values was observed with all three TriX derivatives. With TriX-TA and TriX-M *RRF* was even slightly higher than the *RF* value in each of the experiments. This is only possible when the mobility of TriX solution in the core is higher than the mobility of brine. An explanation could be a slipping effect between the TriX solution, which was flowing through the pores, and adsorbed TriX molecules on the pore walls. Another conclusion from the fact that *RRF* was similar to *RF* (or even higher) was that permeability reduction due to TriX, though not significant, was irreversible.

The retention of the TriX derivatives was much greater than static adsorption. Granted that retention in the core was the sum of adsorption on pore walls, filtration effects and lost material in dead-end pores, nearly all of retained TriX-MB and TriX-TA was lost because of filtration effects or stuck in dead-end pores. Adsorption was negli-

gible in flooding processes. Retention of TriX-MB in the filtration core was a factor 4 higher than in the main core, indicating the filtration of the tertiary network. For TriX-M adsorption contributed more to loss of material in the core flood, which was expected due to its typical surfactant-like structure. Around 16 % of lost TriX-M molecules were adsorbed on pore walls.

7.7 Oil Displacement Tests

7.7.1 Secondary oil recovery experiments using 0.1 wt. % TriX-MB in NaCl

To investigate the potential of the pre-filtrated solution of 0.1 wt. % TriX-MB in NaCl solution with respect to oil mobilization in secondary mode, TriX solution was injected through the filtration core into the oil-saturated main core. The injection into the main core was sometimes interrupted in experiments #10 and #11 to take samples of the effluent of the filtration core. These samples were included in the retention studies.

The properties of the used cores and fluids for secondary oil displacement tests using TriX-MB in NaCl are presented in Table 7-21.

Table 7-21: Characteristics of cores and fluids of secondary oil displacement tests with TriX-MB

	#10		#11		#12	
Cores	FC	MC	FC	MC	FC	MC
Type	Michigan Sandstone					
<i>l</i> in cm	6.11	29.5	5.99	30	5.92	30.0
<i>n</i>	0.28	0.22	0.23	0.23	0.24	0.23
PV in ml	19.5	73.3	15.2	77.4	15.7	76.7
k_{NaCl} in D	0.26	0.41	0.43	0.89	0.81	0.86
Fluids (55°C)						
η_{oil} in mPa·s	36.8		36.8		36.8	
η_{NaCl} in mPa·s	0.703		0.771		0.760	
$\eta_{TriX-MB}^*$ in mPa·s ($\omega = 10$ rad/s, $\gamma = 1$)	6.2		10.2		7.2	

Core Flooding Experiment #10

4.1 pore volumes of Bockstedt oil were injected into the main core. The oil breakthrough (OBT) could be observed after 0.57 pore volumes. By measuring the amount of water, which was displaced from the main core, an original oil saturation of 59 %_{PV} was determined.

After aging time of one week, injection of 0.1 wt. % TriX-MB in NaCl solution through the filtration into the main core was started. The TriX-MB concentration of the input solution of the main core and the oil production during experiment #10 are shown by the red graphs in Figure 7-35. The concentration of TriX-MB solution entering the main core at the beginning of oil displacement was 0.045 wt. %. After injection of 0.05 pore volumes into the main core, the TriX-MB concentration already increased to 0.066 wt. % and after 0.17 pore volumes to 0.079 wt. %. Water breakthrough occurred after injection of 0.17 pore volumes, and 12.6 ml of oil (equivalent to 29.3 %_{OIP}) were produced up to that point. The remaining oil saturation amounted to 40.0 %_{PV} at water breakthrough. After injection of around two more pore volumes of the TriX-MB solution with a concentration between 0.08 and 0.095 wt. %, additional 8.4 ml of oil were displaced. Overall 51.6 % of original oil in place was produced by then. Further injection of ca. 1.5 pore volumes led to an additional oil production of less than 1 %_{OIP}. Final remaining oil saturation amounted to 28.4 %_{PV}. As the last step of TriX-MB injection, the flow rate was increased stepwise up to *Darcy* velocity of $v_D = 10$ ft/d, but no more oil could be mobilized. Subsequently, 8 pore volumes of NaCl brine were injected. Also in this phase of the core flood no oil was produced anymore.

Core Flooding Experiment #11

After injection of 4.4 pore volumes of Bockstedt oil, the main core had an original oil saturation of 65 %_{PV}. Oil breakthrough was observed after injection of 0.61 pore volumes.

After aging, TriX-MB injection started through the filtration into the main core. Oil production and TriX-MB concentration of the input solution of the main core are presented by the orange graphs in Figure 7-35. To fill the connection pipe between the

cores, 6 ml of 0.1 wt. % TriX-MB in NaCl solution were flooded initially through the filtration core. After that, a sample of the effluent of the filtration core was taken to determine its TriX-MB concentration. At the beginning of oil displacement in the main core, the input solution had a concentration of 0.035 wt. %. Water breakthrough occurred after injection of 0.3 pore volumes. 23.1 ml of oil (equivalent to 46.2 %_{OOIP}) were produced up to then. The remaining oil saturation at water breakthrough amounted to 32.2 %_{PV}. After an overall injection of 0.37 pore volumes of the TriX-MB solution with a concentration between 0.035 and 0.048 wt. %, the oil production amounted to 50.5 %_{OOIP}. After that, less than 1 %_{OOIP} could be mobilized. In total 4.8 pore volumes of TriX-MB solution were injected, and 51.3 % of original oil in place were recovered. The remaining oil saturation after TriX-MB injection at Darcy velocity $v_D = 1$ ft/d was 31.4 %_{PV}. As a last step of TriX-MB injection the injection rates were increased stepwise up to Darcy velocity of $v_D = 10$ ft/d. At injection rates higher than $v_D = 3$ ft/d (flow rate steps: $v_D = 3.3, 6.9$ and 10.0 ft/d) a total volume of 1 ml additional oil could be mobilized. The residual oil saturation amounted to 30.2 %_{PV}. Subsequent to TriX-MB injection, 4.2 pore volumes of brine (NaCl solution) were injected, which did not lead to additional oil production.

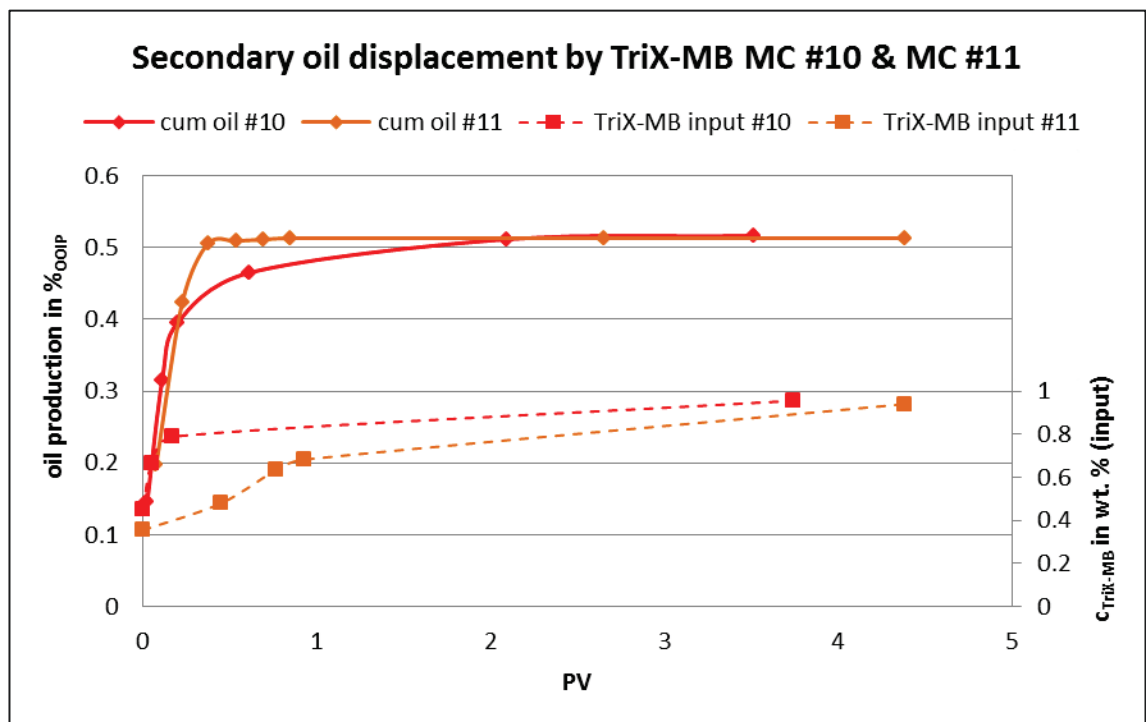


Figure 7-35: Secondary oil recoveries and TriX-MB input concentrations of MC #10 and #11

Secondary oil displacement with 0.1 wt. % TriX-MB in NaCl showed good reproducibility. In Figure 7-37 on page 117, the oil production during brine injection is shown. In experiment #10 and #11 more than 50 %_{OOIP} were mobilized by the TriX-MB solution. The cumulative oil production after NaCl injection only amounted to 23.3 – 26.3 %_{OOIP}. Pre-filtrated TriX-MB in NaCl efficiently increased oil recovery in secondary displacement.

Core Flooding Experiment #12

The aim of experiment #12 was to investigate if TriX-MB mobilizes oil from porous media by adsorption processes, which need more time than given in a typical oil displacement test. The idea was that some oil might cover the pore walls in a reservoir and could not be produced since there are no elastic effects of the TriX-MB solution in the zone of oil contact and the flow velocity near the walls is very low (assuming laminar flow). If TriX-MB molecules would be more likely adsorbed to the pore walls than oil (because of hydrophilic polar tail groups), droplets of oil could have been set free from the pore walls and pushed to an area, where the flow velocity is higher. Thereby, additional oil might be produced. These processes would take some time depending on the adsorption kinetics of the system and the time, which TriX-MB molecules need to diffuse to the pore walls.

After injection of 3.8 pore volumes of Bockstedt oil, an original oil saturation of 65 %_{PV} was reached in the main core. Oil breakthrough occurred after 0.64 pore volumes injected.

After aging the main core for one week, 0.1 wt. % TriX-MB in NaCl solution was injected through the filtration into the main core at a flow rate corresponding to a Darcy velocity of $v_D = 1$ ft/d. Water breakthrough was observed, after injection of 0.31 pore volumes into the main core. Up to that point 24 ml of oil (equivalent to 48 %_{OOIP}) were produced. The remaining oil saturation was 33.9 %_{PV} at water breakthrough. The main production of oil was observed during injection of the first 2.5 pore volumes of TriX-MB solution. After that, less than 1 %_{OOIP} of additional oil was mobilized. During this first TriX-MB injection a total of 4.3 pore volumes were injected, resulting in an oil recovery of 63 %_{OOIP} and a residual oil saturation of 24 %_{PV}.

After the TriX-MB flooding phase of this experiment, the main core was shut in for two weeks, to give time for possible adsorption processes to work. After that time, 0.1 wt. % TriX-MB solution was again injected at a *Darcy* velocity of $v_D = 1$ ft/d. During second TriX-MB injection 4.8 pore volumes were injected, but no additional oil could be produced. Oil mobilization by time-intensive adsorption mechanisms could not be proved. It might also be possible, that all the adsorption took place during the first flooding phase.

The characteristic values of the secondary oil displacement tests using TriX-MB in NaCl brine are summarized in Table 7-22.

Table 7-22: Characteristic values of secondary oil displacement tests with TriX-MB

Main cores		#10	#11	#12
oil injection	Volume of injected oil in PV	4.1	4.4	3.8
	OBT (after ... PV)	0.57	0.61	0.64
	OOIP in %_{PV}	58.7	64.6	65.2
TriX injection	Volume of injected TriX-MB solution in PV	3.9	4.8	4.3+4.8
	WBT (after ... PV)	0.17	0.30	0.31
	S_{OR} at WBT in %_{PV}	40.0	32.2	33.9
	F at WBT in %_{OOIP}	29.3	46.2	48.0
	S_{or} (TriX-MB) in %_{PV}	28.4	30.2	24.0
	F (TriX-MB) in %_{OOIP}	51.6	53.3	63.2

7.7.2 Secondary oil recovery experiments using 0.1 wt. % TriX-TA in NDIIa

Oil recovery experiments with TriX-TA should probe if there are other mechanisms than viscosity increase, which contribute to oil mobilization by the TriX chemical structure. Two secondary oil displacement experiments with TriX-TA were conducted. Core flood #14 was a repro-experiment of #13 to confirm reproducibility of the results. The properties of the cores and fluids used are presented in Table 7-23.

Table 7-23: Characteristics of cores and fluids of secondary oil displacement tests with TriX-TA

	#13		#14	
Cores	FC	MC	FC	MC
Type	Michigan Sandstone			
<i>l</i> in cm	6.04	30	5.95	30
<i>n</i>	0.22	0.22	0.23	0.23
PV in ml	15.1	74.3	15.4	78.3
k_{NDIIa} in D	0.13	0.75	0.56	0.74
Fluids (55°C)				
η_{oil} in mPa·s	36.8		36.8	
η_{NDIIa} in mPa·s	0.783		0.800	
$\eta_{TriX-TA}$ in mPa·s	0.8		0.8	

After injection of 6.1 pore volumes of Bockstedt oil in experiment #13 and 6.9 pore volumes in experiment #14, the cores were shut in for one week. In experiment #14 0.1 wt. % TriX-TA in NDIIa solution was injected into the filtration cores during the aging time to determine retention and resistance factor (see: chapter 7.6.4). Original oil in place amounted to 69.6 %_{PV} in main core #13 and 61.9 %_{PV} in main core #14.

After aging time, TriX-TA was injected through the filtration into the main cores at a flow rate corresponding to a Darcy velocity of $v_D = 1$ ft/d. The concentrations of the effluents of the filtration cores were about 0.1 wt. %; hence, this was the concentration of the solution injected into the main cores. Water breakthrough occurred after 0.15 pore volumes of injected TriX-TA in experiment #13 and after 0.37 pore volumes in experiment #14. Since the permeability of the cores and the mobility ratio between oil and aqueous solution were the same in both core floods, there is no clear explanation for the difference in water breakthrough time. Even the pressure drops over the cores were similar, as can be seen in Figure 7-36.

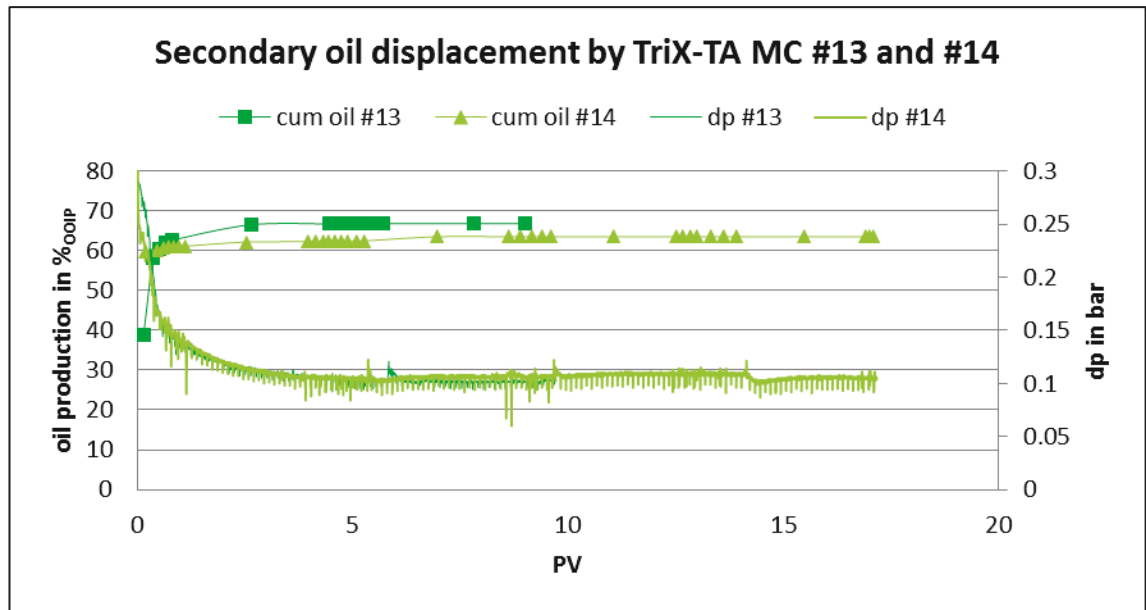


Figure 7-36: Secondary oil recoveries and pressure drops during TriX-TA injection into MC #13 and #14

In experiment #13, 11 ml of oil (equivalent to 21.3 %_{OOIP}) was produced at water breakthrough, resulting in a remaining oil saturation of 54.8 %_{PV}. The main recovery of oil could be observed during the first three pore volumes of injected solution. After that, the recovery became less than 1 %_{OOIP}. In the next step, the flow rates were increased up to a *Darcy* velocity of $v_D = 10$ ft/d. Thereby, additional 0.3 ml of oil could be mobilized. The residual oil saturation in experiment #13 amounted to 22.7 %_{PV}.

In core flood #14, 29 ml of oil were produced up to water breakthrough, which equals to 59.8 %_{OOIP} and resulted in a remaining oil saturation of 24.9 %_{PV}. The main recovery took place during injection of the first 4 pore volumes. Then, less than 1 %_{OOIP} could be mobilized. At the end of TriX-TA injection, the residual oil saturation amounted to 22.6 %_{PV}. It could not be decreased by increasing flow rates. The characteristic values of the secondary oil displacement tests with TriX-TA in NDIIa are given in Table 7-24.

Table 7-24: Characteristic values of secondary oil displacement tests with TriX-TA

Main Cores		#13	#14
oil injection	Volume of injected oil in PV	6.1	6.9
	OBT (after ... PV)	0.71	0.62
	OOIP in %_{PV}	69.6	61.9
TriX injection	Volume of injected TriX-TA solution in PV	10.1	17.2
	WBT (after ... PV)	0.15	0.37
	S_{OR} at WBT in %_{PV}	54.8	24.9
	F at WBT in %_{OOIP}	21.3	59.8
	S_{OR} (TriX-TA) in %_{PV}	22.7	22.6
	F (TriX-TA) in %_{OOIP}	67.4	63.5

7.7.3 Tertiary oil recovery experiments using 0.1 wt. % TriX-MB in NaCl

The ability of TriX-MB in NaCl solution to mobilize remaining oil in a reservoir after water flooding was investigated by performing tertiary oil recovery experiments. For the tests, Michigan sandstone cores ($k_{brine} \approx 0.5 D$) were used and prepared as described in chapter 6.7.2. The main core was then saturated with oil by injecting ca. 4 PV of Bockstedt oil at a flow rate corresponding $v_D = 1$ ft/d. Subsequently, the main core was shut in for 1 week to give time for possible wettability alterations. In Table 7-25 the properties of the cores and fluids used are summarized.

Table 7-25: Characteristics of cores and fluids of tertiary oil displacement tests with TriX-MB

	#8	#9	
Cores	MC	FC	MC
Type	Michigan Sandstone		
l in cm	29.9	5.76	30
n	0.24	0.24	0.23
PV in ml	81.0	15.8	77.6
k_{NaCl} in D	0.63	0.63	0.65
Fluids (55°C)			
η_{oil} in mPa·s	56.5	32.1	
η_{NaCl} in mPa·s	0.831	0.798	
$\eta_{TriX-MB}^*$ in mPa·s ($\omega = 10$ rad/s, $\gamma = 1$)	7.4	8.6	

In experiment #8 a different charge of Bockstedt oil was used. Therefore, the viscosity is different from the other experiments.

Core Flooding Experiment #8

To determine the full potential of TriX-MB in NaCl solution, experiment #8 was conducted using only a main core. TriX-MB has been shown to form spherical oil-in-water-micelles rather than the stiff rod-like micelles after contact with oil (cf. chapter 7.3.2). Therefore, there should be fewer filtration effects in an oil saturated core. After injection of 3.5 PV of Bockstedt oil, the original oil in place amounted to ca. 64 % of the total pore volume.

After aging time NaCl solution was injected at a flow rate corresponding to a Darcy velocity of $v_D = 1$ ft/d. Oil recovery in the brine flooding phase of the experiment is shown by the dark red squares in Figure 7-37. There was early water breakthrough after only 0.1 pore volumes injected. At that time ca. 15 % of the original oil volume in the core was produced. Around 4.1 pore volumes of brine were further injected. Ca. 3.1 ml (equivalent to ≈ 7.5 % of original oil volume in the core) additional oil was mobilized during brine injection after water breakthrough. Overall 12 ml of oil (23.3 %_{OOIP}) could be produced by injection of 4.2 pore volumes of NaCl solution. Most of the oil recovery occurred within the first 1.2 pore volumes of brine injection. After that, the

cumulative oil production could be increased by only 1 % of the original oil volume in the core. The remaining oil saturation after brine flooding was ca. 49 % of the total pore volume. It is quite common to go with higher flow rates at the end of a brine injection phase during a core flooding experiment in the laboratory to approach residual oil saturation. In this experiment it was decided to inject brine at only one flow rate, because it is quite implausible that higher flow rates (by factor 3 or even 10) occur during a real production operation.

Directly after brine flooding 0.1 wt. % TriX-MB in NaCl solution was injected at the same flow rate. After injection of ca. 0.3 pore volumes of TriX-MB an additional oil recovery of ca. 1 %_{OIP} was observed. The major reason for producing this part of the oil might be the pressure pulse when starting TriX injection. After this initial pulse, the oil recovery significantly increased (see: Figure 7-37, red squares) because of TriX-MB injection. By injecting additional 2.3 pore volumes of TriX-MB solution 2.8 ml (equivalent to ≈ 5.4 %_{OIP}) additional oil was produced. After that 1.7 more pore volumes of TriX-MB were injected, but no additional oil was recovered anymore. Overall 3.3 ml of oil could be mobilized by injection of 4.2 pore volumes of 0.1 wt. % TriX-MB in NaCl solution. This equals an additional oil production of 6.3 %_{OIP}. The remaining oil saturation after TriX-MB injection amounted to 44.7 %_{PV} and could not be lowered by injection at (up to a factor 3) higher flow rates.

The pressure drop over the main core steadily decreased during brine injection in experiment #8, as shown by the dark red graph in Figure 7-37. During TriX-MB injection the pressure drop was only slightly higher.

Core Flooding Experiment #9

In experiment #9 a filtration core was used again. During aging of the main core, TriX-MB solution was injected into the filtration core, and the TriX-MB concentration of the effluent was measured. Hence, the core could be used to study the dynamic adsorption of TriX-MB on sandstone. When oil displacement started, the flow path of the TriX-MB solution in the filtration core was considered to be saturated, since a series of UV measurements of the effluent showed an effective concentration of TriX-MB of 0.09 wt. %. The question was if the potential of TriX-MB to mobilize oil in the reservoir is affected by prior filtration of the solution in the reservoir. This should be probed by

comparison of the results of experiment #8 (without filtration core) and experiment #9 (with filtration core).

After injection of 7.5 pore volumes of Bockstedt oil, the original oil in place amounted to ca. 60 %. Oil breakthrough occurred after 0.57 pore volumes of injected oil. Original oil in place and the oil breakthrough were comparable to the values of experiment #8 (cf. Table 7-26).

After aging time NaCl brine was injected into the main core at a flow rate corresponding to a *Darcy* velocity of $v_D = 1$ ft/d. Oil recovery started at a higher level than in experiment #8 and reached its maximum faster, which is shown by the yellow graph in Figure 7-37. This was because of the better mobility ratio of brine to oil in experiment #9, since the oil had lower viscosity than in experiment #8. The water breakthrough was observed after injection of 0.12 pore volumes of brine. Up to then, 20.3 % of the original oil in place had already been produced. The remaining oil saturation at water breakthrough amounted to 47.5 %_{pV}. By injecting ca. 0.7 more pore volumes 26.3 %_{OOIP} were mobilized. After that no more oil was produced by brine flooding. Overall 5 pore volumes of NaCl solution were injected, resulting in a remaining oil saturation of 44 %_{pV}. As in the previous experiment, no higher flow rates were applied.

Subsequently, 0.1 wt. % TriX-MB in NaCl solution was injected through the filtration into the main core. The effective concentration of the solution reaching the main core for oil displacement was around 0.09 wt. %. During TriX-MB injection the pressure drop over the main core increased within the first pore volume injected due to the initially higher viscosity of the TriX-MB solution and then decreased due to oil production until a steady level was reached after injection of ca. 5 pore volumes. After that, no additional oil was mobilized (see: orange squares in Figure 7-37). During injection of the first 0.3 pore volumes, no oil was produced, and only brine was displaced from the core. After that, the effect of TriX could be observed. Within the next 2.6 pore volumes injected the oil production increased steadily and overall 2.9 ml of oil (equivalent to ≈ 6.3 %_{OOIP}) were recovered. Subsequently, further 3.2 pore volumes of TriX-MB solution were injected, but less than 1 %_{OOIP} was produced. Overall 3.2 ml, equivalent to 6.9 %_{OOIP}, additional oil was produced by injecting 5.9 pore volumes of TriX-MB in NaCl solution. The remaining oil saturation after TriX-MB injection amounted to

39.8 %_{PV}. Subsequently, 4 pore volumes of NaCl solution were injected again, but no oil could be mobilized anymore.

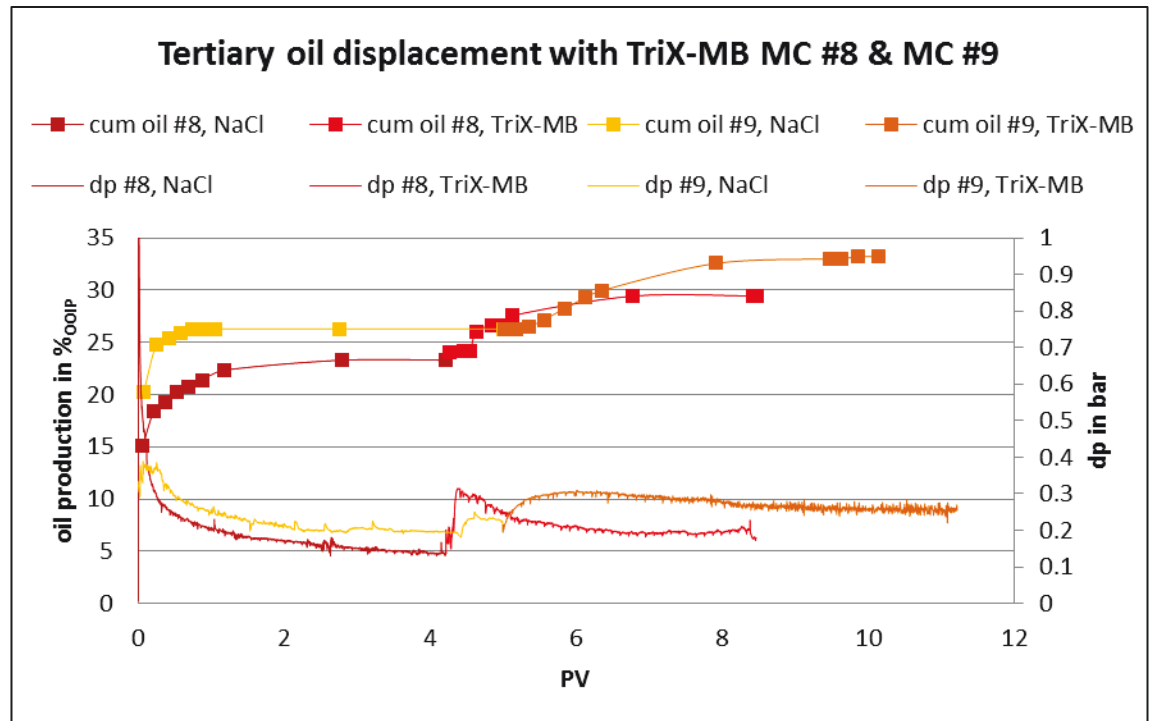


Figure 7-37: Tertiary oil recoveries and pressure drops during TriX-MB injection into MC #8 and #9

The pressure drop over the filtration core of experiment #9 was constant during TriX-MB injection through the filtration into the main core. At the end of TriX injection, a final sample of the effluent of the filtration core was taken. The concentration of TriX-MB was equal to the concentration, determined before starting TriX-MB injection into the main core (0.09 wt. %). The difference of 0.01 wt. % of TriX-MB in concentration measurements between the inlet and the outlet of the filtration core indicates that the TriX-MB solution undergoes alteration to a certain extent on its way through the core. Despite this alteration and the lower effective concentration of TriX-MB in oil displacement test #9, both experiments (#8 and #9) showed very similar results with respect to oil displacement by TriX-MB. The additional oil productions amounted 6.3 %_{OOIP} (#8) and 6.9 %_{OOIP} (#9). A detrimental effect on TriX-MB solutions by filtration could not be attested. The higher pressure, during TriX-MB injection in the main cores compared to brine injection was proof for the higher viscosity of the TriX-MB solution and thus, an improved mobility ratio. The viscoelastic network of the TriX-MB solution might not fully break down during oil displacement.

A summary of the characteristic values of the tertiary mode oil displacement tests using TriX-MB in NaCl brine is given in Table 7-26.

Table 7-26: Characteristic values of tertiary oil displacement tests with TriX-MB

Main Cores		#8	#9
oil injection	Volume of injected oil in PV	3.5	7.5
	OBT (after ... PV)	0.60	0.57
	OOIP in %_{PV}	63.6	59.6
brine injection	Volume of injected brine in PV	4.2	5.0
	WBT (after ... PV)	0.10	0.12
	S_{OR} at WBT in %_{PV}	54.1	47.5
	F at WBT in %_{OOIP}	15.0	20.3
	S_{OR} after brine injection in %_{PV}	48.7	44.0
	F (brine) in %_{OOIP}	23.3	26.3
TriX injection	Volume of injected TriX-MB solution in PV	4.2	24.8
	S_{OR} (TriX-MB) in %_{PV}	44.7	39.8
	F (TriX-MB) in %_{OOIP}	29.6	33.2

7.7.4 Tertiary oil recovery experiment using 0.1 wt. % TriX-TA in NDIIa

Core Flooding Experiment #15

In secondary oil displacement tests, TriX-TA showed the ability to mobilize more oil than brine or even TriX-MB. Since TriX-TA has a similar viscosity as brine, better oil recovery is not caused by increasing water viscosity. Therefore, the efficiency of TriX-TA to mobilize oil was tested in tertiary mode to get more information about the mode-of-action of oil displacement.

The characteristics of the cores and fluids used in this experiment are shown in Table 7-27.

Table 7-27: Characteristics of cores and fluids of tertiary oil displacement test with TriX-TA

#15		
Cores	FC	MC
Type		
<i>l</i> in cm	5.21	29.95
<i>n</i>	0.24	0.22
PV in ml	13.9	75.9
k_{NDIIa} in D	0.65	1.01
Fluids (55°C)		
η_{oil} in mPa·s	32.1	
η_{NDIIa} in mPa·s	0.825	
$\eta_{TriX-TA}$ in mPa·s	0.8	

After core preparation, 6.4 PV Bockstedt oil were injected into the main core at a flow rate corresponding to a Darcy velocity $v_D = 1$ ft/d. Oil breakthrough occurred after 0.61 PV. After that, no water was displaced from the core anymore, i.e., original oil in place amounted to 60.6 %_{PV}.

The main core was shut in for one week after oil injection. Then 6.8 PV NDIIa were injected into the main core at $v_D = 1$ ft/d. The pressure and oil recovery curves are given in Figure 7-38. Water breakthrough of NDIIa occurred after 0.1 PV (7.7 ml). At this point the oil saturation amounted to 50.5 %_{PV}. After injection of 0.6 PV NDIIa no oil was produced anymore, even by application of higher flow velocities up to $v_D = 10$ ft/d. At the end of brine flooding, the residual oil saturation was 49.2 %_{PV}. Subsequently, injection of 0.1 wt. % TriX-TA in NDIIa solution was started. 5.7 PV were injected at a flow rate resulting in $v_D = 1$ ft/d. After injection of 0.5 PV oil production increased significantly. Oil mobilization also led to a slight pressure decrease over the core. At the end of TriX-TA flooding the oil saturation amounted to 39.4 %_{PV}, meaning that additional 16.2 %_{OIP} were produced. Again application of higher flow rates did not lead to further oil mobilization.

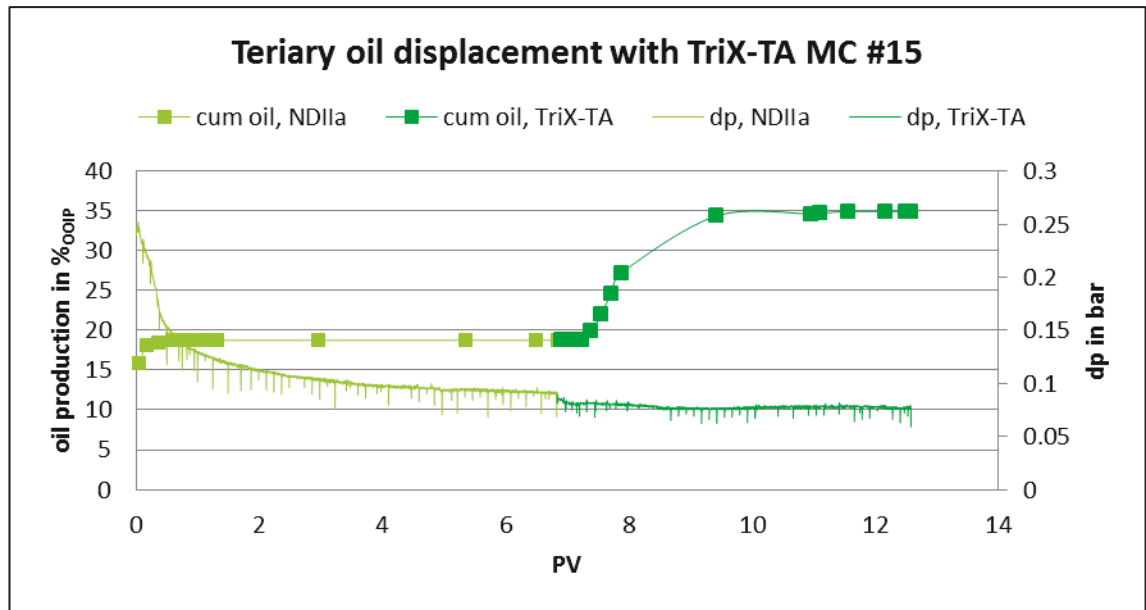


Figure 7-38: Tertiary oil recovery and pressure drop during TriX-TA injection into MC #15

The characteristic values for oil recovery in core flood #15 are given in Table 7-28.

Table 7-28: Characteristic values of tertiary oil displacement test with TriX-TA

<u>Main Core</u>		#15
oil injection	Volume of injected oil in PV	6.4
	OBT (after ... PV)	0.61
	OOIP in %_{PV}	60.6
brine injection	Volume of injected brine in PV	6.8
	WBT (after ... PV)	0.10
	S_{or} at WBT in %_{PV}	50.5
	F at WBT in %_{OOIP}	16.7
	S_{or} after brine injection in %_{PV}	49.2
	F (brine) in %_{OOIP}	18.9
TriX injection	Volume of injected TriX-TA solution in PV	5.7
	S_{or} (TriX-TA) in %_{PV}	39.4
	F (TriX-TA) in %_{OOIP}	35.1

7.7.5 Tertiary oil recovery experiment using 0.1 wt. % TriX-M in NDIIa

Core Flooding Experiment #16

The core flood with 0.1 wt. % TriX-M in NDIIa solution was conducted in tertiary mode since TriX-M has the structure of a conventional surfactant. It has been shown that IFT reduction to oil by TriX-M is not sufficient to mobilize oil. However, there are other factors, e.g., wettability change, which might contribute to an increase in the capillary number and therefore, to additional oil production. This should be probed by this experiment.

The properties of the used cores and fluids are given in Table 7-29.

Table 7-29: Characteristics of cores and fluids of tertiary oil displacement test with TriX-M

#16		
Cores	FC	MC
Type		
<i>l</i> in cm	7.33	29.95
<i>n</i>	0.26	0.23
PV in ml	21.6	78.8
k_{NDIIa} in D	0.74	0.71
Fluids (55°C)		
η_{oil} in mPa·s	32.1	
η_{NDIIa} in mPa·s	0.825	
η_{TriX-M} in mPa·s	0.82	

6.5 pore volumes of Bockstedt oil were injected into the main core at a flow rate corresponding to *Darcy* velocity of $v_D = 1$ ft/d. After that the main core was shut in for one week. The original oil in place amounted to 60 % of the pore volume.

During the aging time, an injection test was conducted with the filtration core. This is described in the chapters 6.7.3 and 7.6.5.

After aging time ca. 7.2 pore volumes of NDIIa were injected into the main core at $v_D = 1$ ft/d. The pressure drop over the main core during that phase of the experiment is shown by the light violet; the oil recovery by squares in the same color in Figure 7-39. Water breakthrough occurred after 0.1 pore volumes. Up to that point, 17.4 % of

original oil in place was produced. The remaining oil saturation at water breakthrough amounted to 49.3 %_{PV}. After injection of 0.8 pore volumes, no more oil was produced anymore. Increasing the flow rates up to $v_D = 10$ ft/d did not lead to oil production, either. The residual oil saturation after injection of NDIIa amounted to 47.3 %_{PV}.

Subsequently, 0.1 wt. % TriX-M in NDIIa solution was injected through the filtration into the main core. The pressure drop over the filtration core was constant at around 0.25 bar during injection. The pressure drop over the main core is shown by the dark violet line in Figure 7-39. After injection of around 0.3 pore volumes of TriX-M solution oil recovery increased significantly, as can be seen from the dark violet squares in the Figure below. The main recovery occurred within injection of 5 pore volumes. Oil recovery was almost doubled by TriX-M. The residual oil saturation could be lowered from 47.3 %_{PV} to 35.0 %_{PV}. The recovery factor was increased by 20.6 %_{OIP} by the TriX-M solution.

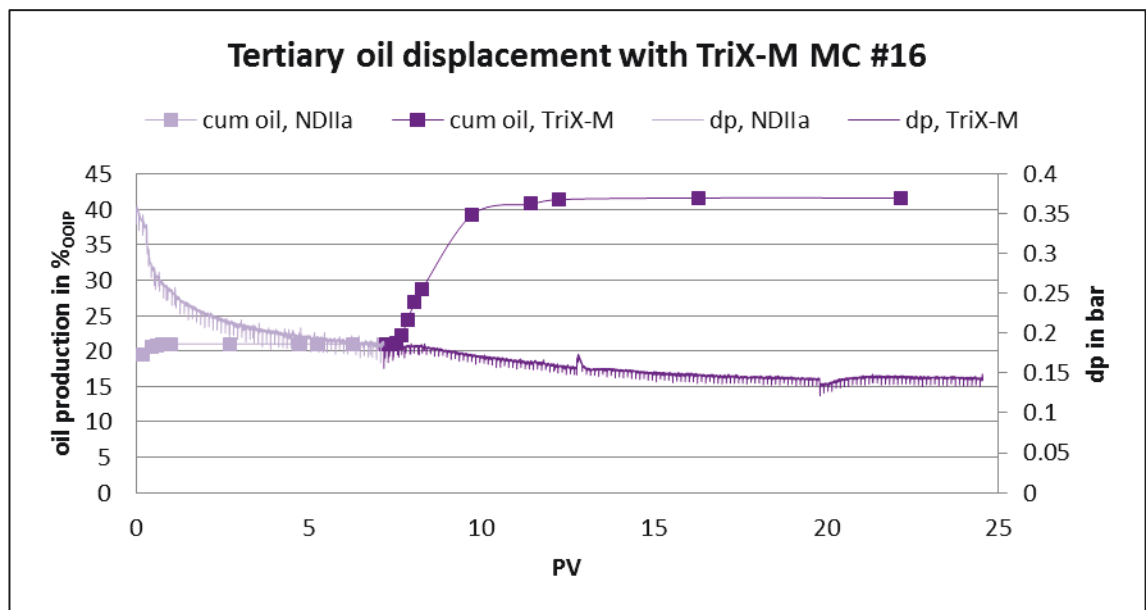


Figure 7-39: Tertiary oil recovery and pressure drop during TriX-MB injection into MC #16

In Table 7-30 the characteristic values of core flood #16 are given.

Table 7-30: Characteristic values of tertiary oil displacement test with TriX-M

Main Core		#16
oil injection	Volume of injected oil in PV	6.5
	OBT (after ... PV)	0.58
	OOIP in %_{PV}	59.7
brine injection	Volume of injected brine in PV	7.2
	WBT (after ... PV)	0.10
	S_{OR} at WBT in %_{PV}	49.3
	F at WBT in %_{OOIP}	17.4
	S_{OR} after brine injection in %_{PV}	47.3
	F (brine) in %_{OOIP}	21.0
TriX injection	Volume of injected TriX solution in PV	17.4
	S_{OR} (TriX-M) in %_{PV}	35.0
	F (TriX-M) in %_{OOIP}	41.6

7.7.6 Summary: Oil Displacement Tests

Secondary oil displacement

In Table 7-31 the oil saturations at different times during secondary oil displacements with TriX-MB and TriX-TA solutions are summarized.

Table 7-31: Remaining oil saturation in secondary oil displacement experiments

	NaCl		NDIIa		0.1 wt. % TriX-MB in NaCl			0.1 wt. % TriX-TA in NDIIa	
	#8	#9	#15	#16	#10	#11	#12	#13	#14
OOIP in %_{PV}	63.6	59.6	60.6	59.7	58.7	64.6	65.2	69.6	61.9
WBT in PV	0.10	0.12	0.10	0.10	0.17	0.3	0.31	0.15	0.37
S_{oR} @ WBT in %_{PV}	54.1	47.5	50.5	49.3	40.0	32.2	33.9	54.8	24.9
F @ WBT in %_{OOIP}	15.0	20.3	16.7	17.4	29.3	46.2	48.0	21.3	40.2
S_{oR} after inj. of 1 PV in %_{PV}	49.6	44.0	49.2	47.3	30.7	31.4	28.2	25.7	24.1
F after inj. of 1 PV in %_{OOIP}	21.7	26.3	18.9	21.0	47.7	51.3	56.8	67.4	61.1
S_{oR} in %_{PV}	48.7	44.0	49.2	47.3	28.4	30.2	24.0	22.7	22.6
F in %_{OOIP}	23.3	26.3	18.9	21.0	51.6	53.3	63.2	67.4	63.5

Both TriX-MB and TriX-TA showed higher oil recovery than brine only. The water breakthrough was delayed by application of both molecules.

In Table 7-32 the average values of secondary oil displacements with NDIIa and TriX-MB from another laboratory are given.

Table 7-32: Core flooding results for cores ($k_{brine} = 2$ D) at S_{wi} at 55 °C and a flow rate of 9 ml/h (corresponding Darcy's velocity of 1 ft/d) in the Wintershall laboratory [88]

		NDIIa	TriX-MB in NDIIa
brine/TriX injection	WBT in PV	0.35	0.59
	S_{oR} @ WBT in %_{PV}	53.6	33.6
	S_{oR} after inj. of 1 PV in %_{PV}	38.7	25.0
	S_{oR} in %_{PV}	29.1	18.4

The experiments conducted in the scope of this thesis showed earlier water breakthroughs and higher remaining oil saturations compared to the core floods of the other laboratory. This could be due to the shorter cores (7 – 8 cm) in the Wintershall laboratory. The effect of viscous fingering is more pronounced the higher the distance

between injector and producer, i.e., the longer the core. Therefore, the volumetric sweep efficiency should be lower in the core floods conducted in the scope of this thesis compared to the tests in Table 7-32. In the Wintershall laboratory the oil saturation at the end of TriX-MB in NDIIa injection was reduced by 10.2 % compared to brine flooding.

0.1 wt. % TriX-MB in NaCl reduced S_{OR} by around 19 %, compared to NaCl flooding, which might be due to fewer filtration effects, since the tertiary network is not as large and stiff in NaCl compared to NDIIa. Therefore, more parts of the oil saturated core could be penetrated by TriX-MB in NaCl solution to mobilize oil.

Figure 7-40 shows the fractional flow of the aqueous phases during the oil displacement tests as a function of water saturation in the core.

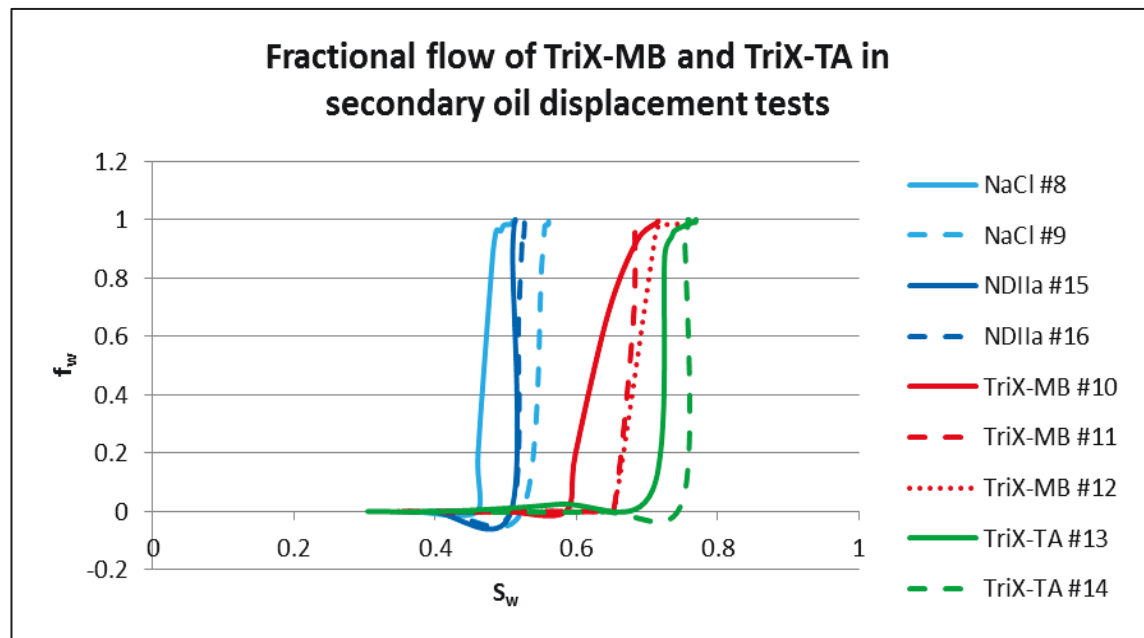


Figure 7-40: Fractional flow of secondary oil displacement tests

By application of the *Buckley-Leverett* model, the water breakthrough point of the displacement tests was fitted by modifying the *Corey* parameters for the relative permeability functions. The resulting relative permeability curves are given in the Figures 7-41 and 7-42.

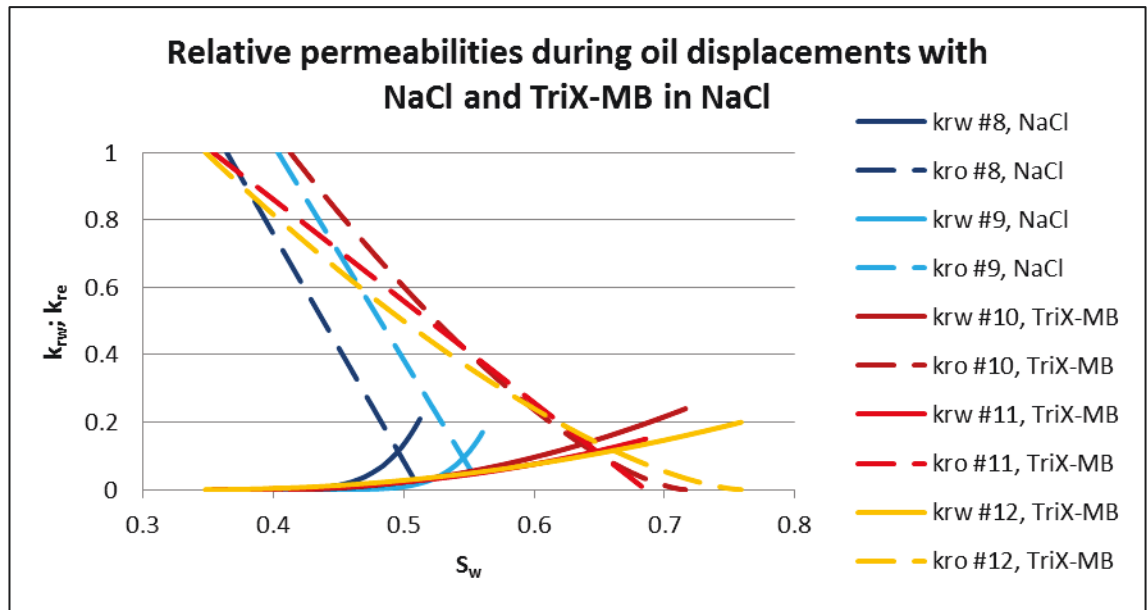


Figure 7-41: Relative permeabilities during oil displacements with NaCl and 0.1 wt. % TriX-MB in NaCl

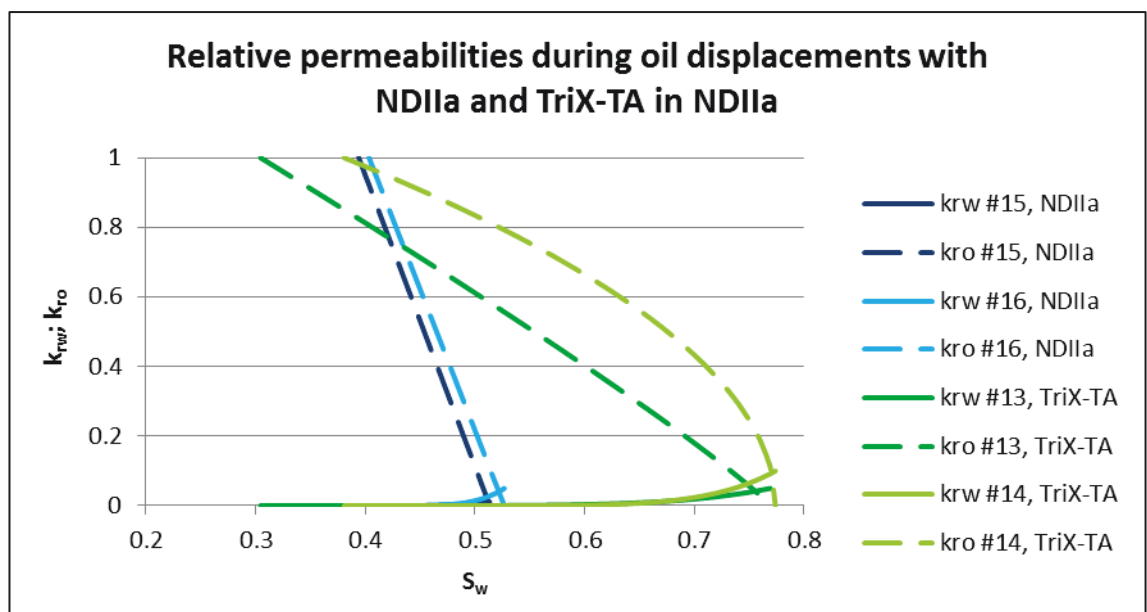


Figure 7-42: Relative permeabilities during oil displacements with NDIIa and 0.1 wt. % TriX-TA in NDIIa

Injection of **0.1 wt. % TriX-MB in NaCl** was more efficient in reducing the oil saturation compared to brine injection. Main oil production occurred within the first injected pore volume. A delayed water breakthrough in the oil displacement tests and the shift of the fractional flow curves in Figure 7-40 to higher water saturations indicated a more uniform displacement front as a typical result of an improved mobility ratio for TriX-MB solutions compared to brine. The crossover of oil and water relative permeability curves was shifted to higher water saturation by using TriX-MB solution

for oil displacement. This suggested that TriX-MB made the rock more water-wet during oil displacement. Residual oil saturation was significantly decreased compared to brine flooding.

The results of secondary oil displacement tests with **0.1 wt. % TriX-TA in NDIIa** exceeded the results obtained with TriX-MB. Main oil recovery occurred within the first 4 PV, which is a little more compared to TriX-MB injection. The water breakthrough in experiment #13 was only a little later compared to water breakthrough during brine injection. In core flood #14 water breakthrough was delayed. Since TriX-TA does not increase the viscosity of the displacement fluid, a delayed water breakthrough might be caused by a highly viscoelastic interface between water and oil at the displacement front. This would also explain that TriX-TA shows best mobility ratio compared to TriX-MB solutions and pure brines, based on the graphs in Figure 7-40. Unfortunately, interfacial rheology was not investigated within the project. TriX-TA showed an even greater effect on residual oil saturation and the crossover of the relative permeability curves than observed with TriX-MB. Secondary aggregates of TriX-TA are smaller than the rod-like micelles built up by TriX-MB. Therefore, TriX-TA molecules could penetrate lower permeable parts of the core and contribute to oil displacement, even better than TriX-MB in NaCl. Low adsorption of TriX-TA on the pore walls led to sufficient concentration of TriX-TA throughout the core. Plugging effects can be excluded.

Regarding oil mobilization by **brine injection**, NaCl was slightly more effective than NDIIa, which correlates with the results of the imbibition tests.

Tertiary oil displacement

In Table 7-33 the characteristic values of the tertiary oil displacement tests are summarized. Figure 7-43 shows the pressure curves and oil recovery for all tertiary oil displacement tests.

Table 7-33: Remaining oil saturation in tertiary oil displacement experiments

	TriX-MB in NaCl		TriX-TA in NDIIa	TriX-M in NDIIa
	#8	#9	#15	#16
OOIP in %_{PV}	63.6	59.6	60.6	59.7
WBT in PV	0.10	0.12	0.10	0.10
S_{OR} @ WBT in %_{PV}	54.1	47.5	50.5	49.3
F @ WBT in %_{OOIP}	15.0	20.3	16.7	17.4
S_{OR} after inj. of 1 PV in %_{PV}	49.6	44.0	49.2	47.3
F after inj. of 1 PV in %_{OOIP}	21.7	26.3	18.9	21.0
$S_{or,brine}$ in %_{PV}	48.7	44.0	49.2	47.3
F_{brine} in %_{OOIP}	23.3	26.3	18.9	21.0
S_{OR} after inj. of 1 PV in %_{PV}	47.3	42.5	44.5	43.1
F after inj. of 1 PV in %_{OOIP}	27.7	28.8	26.6	27.8
$S_{or,TriX}$ in %_{PV}	44.7	39.8	39.4	35.0
F_{TriX} in %_{OOIP}	29.6	33.2	35.1	41.3

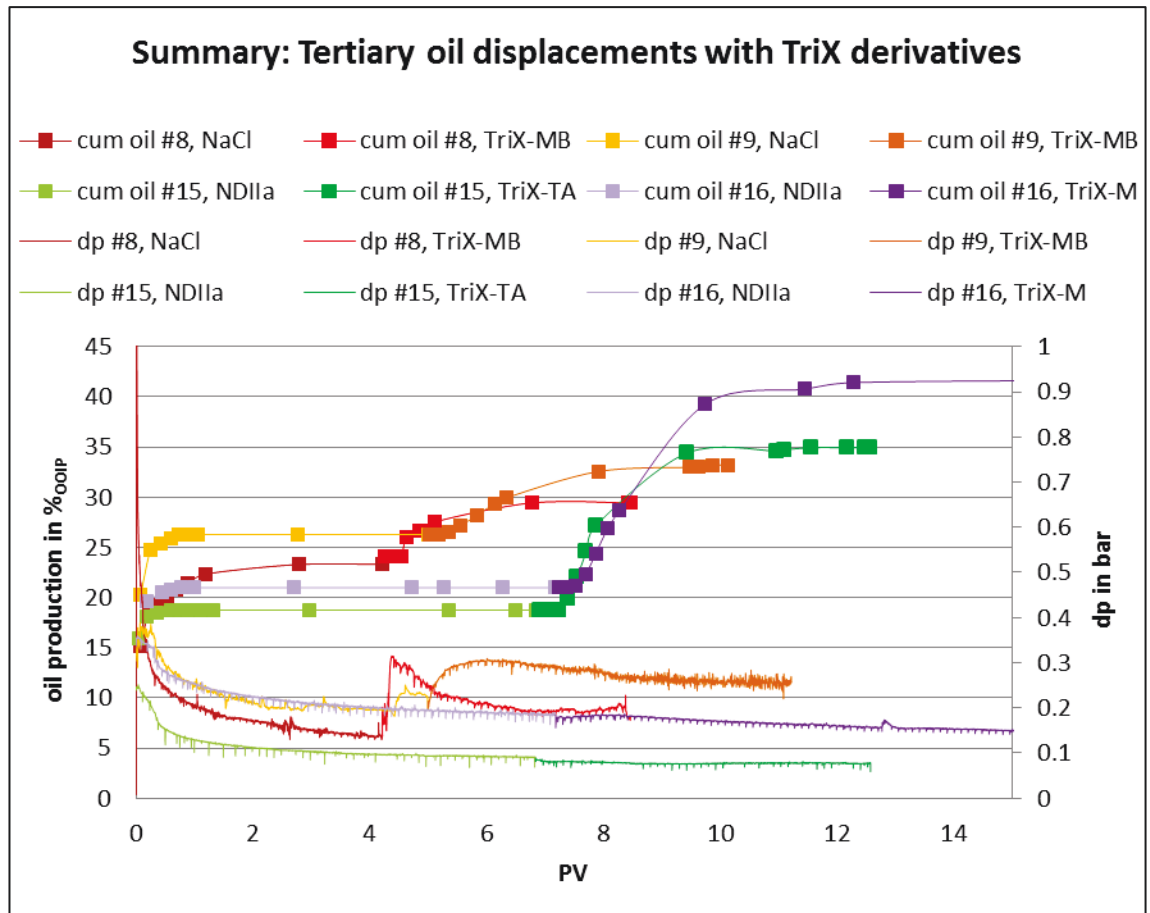


Figure 7-43: Summary of tertiary oil displacement tests with TriX-MB, TriX-TA, and TriX-M

All TriX derivatives led to additional oil production. Significant production of additional oil after brine flooding (especially when higher flow rates have been applied) was an indication that residual oil has been mobilized.

In the laboratory of a project partner, a tertiary oil displacement test was conducted with 0.23 wt. % TriX-MB in NDIIa. The pressure and oil production curves were reported in 2014 and are shown in Figure 7-44 [88].

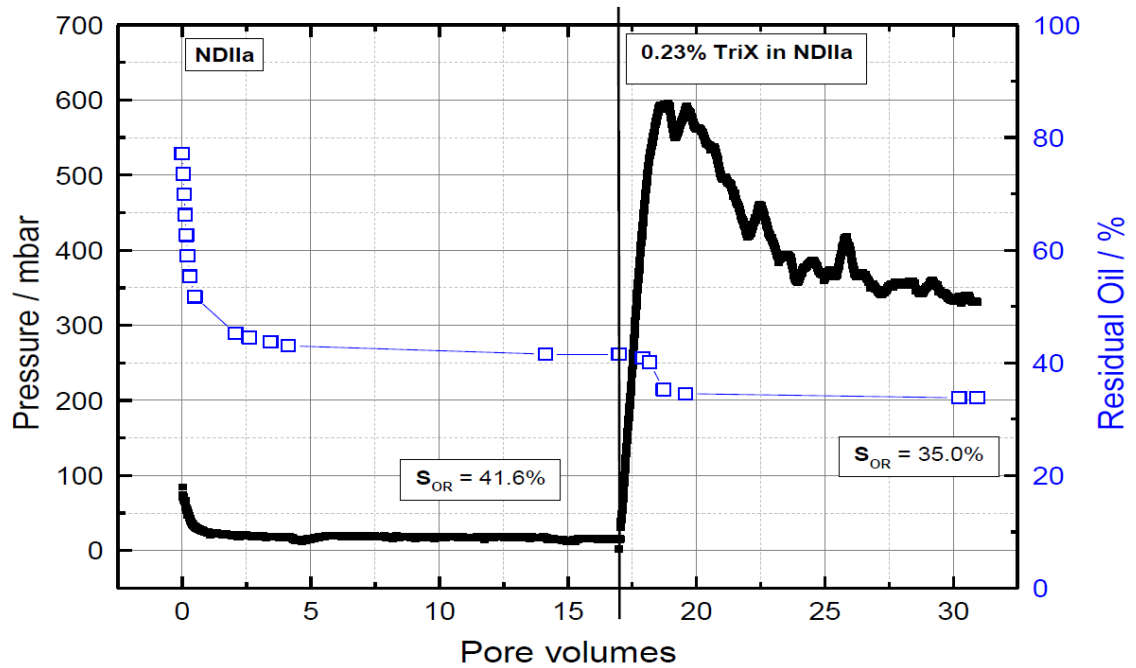


Figure 7-44: Mobilization of residual oil by TriX-MB in a 2 D Gildehaus Sandstone core [88]

In the core flooding test with TriX-MB in NDIIa the remaining oil saturation could also be reduced by 6 %. The pressure increase at the beginning of the injection of TriX-MB is around 0.6 bar. The higher pressure increase in a core with even higher permeability, which occurs when starting TriX-MB injection in NDIIa (Figure 7-44) compared to TriX-MB in NaCl (Figure 7-73), is very likely a result of the stronger network TriX-MB forms in NDIIa. TriX-MB in NaCl could mobilize a moderate the same amount of residual oil at lower concentrations and shows better injectivity than in NDIIa.

0.1 wt. % TriX-MB in NaCl led to a S_{OR} reduction after brine flooding of 8 % in experiment #8 and 9.5 % in core flood #9. TriX-MB mobilized 6 %_{OOIP} more oil after NaCl injection in both experiments. This is a moderate amount compared to the other published data regarding oil recovery with viscoelastic surfactant solutions (12 – 17 %_{OOIP}; cf. chapter 4.2). However, the oil viscosity in the experiments conducted in the scope of this thesis was higher compared to that formerly reported by other research groups and TriX-MB works at high salinity. Injection of TriX-MB led to an increase in differential pressure at first, which is an indicator, that the TriX-MB solution had a higher viscosity than brine only. Later, pressure decreases due to oil production. Mobility enhancement was contributing to oil mobilization by TriX-MB.

0.1 wt. % TriX-TA in NDIIa and **0.1 wt. % TriX-M in NDIIa** had the same viscosity as NDIIa. Therefore, the pressure decreased steadily due to oil production. Both TriX derivatives were more efficient in mobilizing additional oil than TriX-MB. TriX-TA mobilized 16 %_{OOIP} additional oil (S_{or} reduction: 20 %_{PV}). TriX-M showed highest additional oil production of 21 %_{OOIP} (S_{or} reduction: 26 %_{PV}). Around 5 pore volumes had to be injected for main oil recovery. TriX-TA and TriX-M produced a substantial amount of additional oil after brine flooding. These molecules efficiently mobilized residual oil. The reduction of the interfacial tension was shown not to be sufficient enough to contribute to oil recovery.

8. Summary

The aims of this study were to investigate the behavior of TriX-MB, TriX-TA, and TriX-M in porous media. The experimental procedure, which was conceived to first understand the interaction of TriX molecules with the single components of an oil reservoir and include the obtained results into the analysis of oil displacement tests, proved to be reasonable. By pursuing this strategy, a comprehensive investigation on the mode-of-action of the TriX molecules with respect to oil mobilization was carried out in the scope of this thesis.

8.1 Bulk Studies on TriX Derivatives and Triton-X-100

TriX-MB forms stiff, rod-like micelles in saline solutions with high persistence lengths at very low concentrations. These micelles are linked by salt bridges forming a viscoelastic network. The strength of the cross-linking increases with the valence of the cations, which are present in solution. TriX-MB builds a very rigid viscoelastic network with di- and trivalent ions. The TriX molecules consist of a compact hydrophobic group and a large hydrophilic part. By designing the hydrophobic core of Triphenoxymethane micelles as compact as possible, it was thought that the accumulation of oil inside a micelle could be prevented, which would cause the loss of viscoelasticity of the TriX-MB solution. TriX-TA forms spherical micelles at low concentrations in solution and develops no viscoelastic behavior. TriX-M has a surfactant-like structure, but with a compact hydrophobic “head” and a long hydrophilic “tail”.

The adsorption of TriX derivatives on sand resulted in adsorption values of 10 – 30 $\mu\text{g}_{\text{TriX}}/\text{g}_{\text{sand}}$ for TriX-MB and TriX-TA in highly saline brines. These values are much lower than the values, which were reported for viscoelastic surfactants in other publications in brines with low salt concentrations (cf. chapter 4.2). High salinity is a critical parameter for many EOR chemicals. Therefore, the adsorption level TriX-MB and TriX-TA is of even higher quality. TriX-MB exhibited slightly higher adsorption values in NDIIa than in NaCl, which can be explained by the fact, that the tertiary network with divalent ions is more rigid and stronger than in NaCl solution. TriX-M, as a surfactant, exhibited static adsorption values of around 470 $\mu\text{g}_{\text{TriX}}/\text{g}_{\text{sand}}$, which is a moderate value

for surfactant adsorption. Compared to the adsorption of Triton-X-100 ($780 \mu\text{g}_{\text{TriX}}/\text{g}_{\text{sand}}$) this is a promising result. Both molecules are structurally very similar, but TriX-M is an anionic and Triton-X-100 a nonionic surfactant. This difference is probably the reason for the advantage of TriX-M.

Different anions in aqueous solution affected the micellar network of TriX-MB solutions in a way that contributes to the *Hofmeister* series. An effect of different salt anions on TriX-MB in contact with oil could not be observed in this study.

The reduction of interfacial tension to Bockstedt oil was not sufficient to increase the capillary number significantly for TriX-MB, TriX-TA and TriX-M. The TriX derivatives did not dissolve into the oil phase, but promoted oil-in-water emulsions. In contact with oil, TriX-MB micelles became spherical and the viscoelastic properties of the solution are lost.

In contrast to TriX-M, Triton-X-100 is lost from the aqueous phase after oil contact. In comparison to Triton-X-100, TriX-M exhibited similar IFT reduction in highly saline brine and remarkably better adsorption values on sand (Triton-X-100 seemed to adsorb twice as much as TriX-M). Furthermore, Triton-X-100 showed great interactions in contact with oil and even vanished from aqueous solution. A decrease in TriX-M concentration in brine after oil contact was not observed. TriX-M is an interesting and promising alternative for Triton-X-100 in EOR applications and should be further studied.

8.2 Imbibition Tests

TriX-MB in NDIIa did not lead to additional oil recovery in spontaneous imbibition tests. The tertiary network might be too strong for the aqueous solution to be soaked into the core by capillary forces. In NaCl, TriX-MB increased imbibition rate and ultimate recovery. The decisive factor is the weaker cross-linking between secondary aggregates. The network can be broken down into structures, which are smaller than the pore necks of the sandstone.

TriX-TA exhibited the best results in imbibition tests. Due to the small size of the spherical micelles (9 – 15 nm), TriX-TA in NDIIa solution penetrated the core well. The

lowest level of adsorption of all tested molecules resulted in highest effective concentration inside the core.

Highest imbibition rate at the beginning of spontaneous imbibition tests exhibited TriX-M. Due to higher adsorption, TriX-M increased ultimate recovery significantly only at higher concentrations (0.25 wt. %, instead of 0.1 wt. %).

Triton-X-100 had no significant effect on ultimate oil recovery due to high adsorption on sand and the fact that it got attracted to the oil phase.

8.3 Injectivity and Retention

The critical property of the behavior of TriX in porous media is the type of association of TriX molecules.

TriX-MB forms a strong and rigid network with divalent ions, which are present in NDIIa. The network size can be greater than 1 μm . During injection tests, it led to poor injectivity of TriX-MB in NDIIa. Even in high permeable cores ($k_{brine} \approx 1.5 \text{ D}$) plugging was observed. In the presence of only monovalent ions the network of TriX-MB is smaller, and cross-linking between secondary aggregates is weaker, which contributed to lower pressure drops during injection. TriX-MB shows shear thinning behavior. The injectivity of TriX-MB in NaCl was not affected by reduced permeability of the core samples. The main part of the pores of the sandstones used had diameters, which could be passed by small parts of the tertiary network of TriX-MB. Some of the experiments were affected by trivalent ions from the stainless steel parts of the core flooding unit. The cross-linking between the rod-like micelles was reinforced and TriX-MB formed a gel-like material. This effect should be considered for further tests on this molecule.

TriX-TA does not form rod-like tertiary aggregates, but only spherical micelles 9 – 15 nm in size. Adsorption is on a low level. Therefore, low pressure gradients were observed for TriX-TA injection.

Injectivity of TriX-M was not affected by the formation of aggregates, but by adsorption of TriX-M molecules on the pore walls.

During all injection tests, the resistance factor and the residual resistance factor were on the same level. This was explained by a slipping effect between TriX solution,

which is flowing through the pores, and on the pore walls adsorbed TriX molecules. It is also an indication for irreversible permeability reduction by TriX.

The retention of TriX molecules inside the core was much higher than adsorption. Ca. 99 % of retained TriX-MB and TriX-TA was lost because of filtration effects or stuck in dead-end pores. Adsorption was negligible for these molecules. For TriX-M the adsorption had a higher effect on retention (16 %), which was expected, due to its surfactant-like structure.

8.4 Oil displacement

All TriX derivatives mobilized additional oil in secondary and tertiary mode, even after flowing through a filtration core.

TriX-M led to highest additional oil recovery, followed by TriX-TA and TriX-MB. These results correlate with the observations from the imbibition tests.

TriX derivatives lead to an IFT reduction by only a factor 4 to 10, which is not enough to increase the capillary number sufficiently. Lowering the interfacial tension between water and oil is a positive effect in any case, but the tested molecules are not able to mobilize additional oil by that mechanism alone. Oil mobilization due to adsorption could not be found during this study.

In secondary oil recovery tests, TriX-MB in NaCl resulted in an increased oil production of around 31 %_{OOIP}, compared to brine flooding. In tertiary oil recovery tests TriX-MB in NaCl showed better results than TriX-MB in NDIIa and mobilized 6 %_{OOIP} additional oil. The strong network of TriX-MB formed with divalent ions might have a detrimental effect on the propagation of the solution in the reservoir. It seems that the volumetric sweep efficiency is affected by plugging mechanisms. Hence, this molecule could be applied in reservoirs with low content of divalent ions and maybe at lower TriX-MB concentrations. During injection of TriX-MB in NaCl a higher pressure drop over the core and a delayed water breakthrough were observed compared to brine injection. This indicated that there was an effective improvement of the mobility ratio. TriX-MB also showed a beneficial effect on relative permeabilities. Even though the rod-like micelles transformed to spherical ones in contact with oil, and the viscoelastic

properties of the solution got lost to a great extent, there still might be a viscoelastic phase behind the zone of water-oil contact, contributing to mobility control.

After injection of TriX-TA in secondary mode the recovery factor was around 45 %_{OOIP} higher compared to brine injection. TriX-TA also produced a considerable amount of additional oil (16 %_{OOIP}) after brine flooding in tertiary oil displacement experiments. This molecule efficiently mobilized residual oil. The advantageous effect on relative permeabilities was greater for TriX-TA than for TriX-MB, which correlates with higher oil production. TriX-TA did not develop any viscoelasticity. The effect on relative permeabilities could be a result of wettability changes to more water-wet conditions during the core flood. Another possibility might be that the rheological properties of the oil-water interface are influenced in a beneficial way. The higher the elasticity of the interface between water and oil, the more snap-off of oil droplets is prevented. This could have resulted in a more uniform water front and thus to better oil production.

For TriX-M it can be stated, that there is no viscosity increase in bulk phase and IFT reduction is not significant enough to reduce residual oil. Since there was only one tertiary displacement experiment conducted for TriX-M, no statements about relative permeability changes with respect to this derivative can be made. However, this molecule showed the best results in tertiary oil displacement. The additional oil production amounted to 21 %_{OOIP}. This might be an indication for an even more pronounced effect on relative permeabilities than with TriX-TA, maybe by alteration of interfacial viscosity or wettability.

All in all the positive effect of the basic chemical structure of Triphenoxymethanes on oil displacement was proved by the investigations in the scope of this thesis. The main mode-of-action was most likely wettability alteration to strong water-wet systems. Triphenoxymethanes are very promising chemicals for enhanced oil recovery in highly saline reservoir brine.

9. Outlook

The TriX derivatives, which were studied in the scope of this thesis, efficiently mobilized additional oil in secondary and tertiary mode. Their great advantage over all so far reported viscoelastic surfactant solutions for EOR application is, that they are effective in high saline (up to 20 % TDS) and hard brine at low surfactant concentrations of 0.1 wt. %. Therefore, further investigations on these new class of (viscoelastic) surfactant solutions could lead to a commercial EOR product for many mature oil reservoirs.

To get an even better understanding of the mode-of-action of the TriX derivatives, investigations on their influence on the wettability of the reservoir and oil-water-interfacial rheology are recommended. The theory of mobility enhancement by increased interfacial viscosity has not been reported in the literature so far, and would need extensive laboratory investigations concerning interfacial viscosity, emulsification properties, and oil displacement to be probed.

The effect of alkaline or co-surfactants on TriX solutions and their interaction with oil was not studied in the context of this thesis. However, such formulations can have very beneficial properties for chemical EOR. The screening of suitable alkalines or co-surfactants in combination with TriX should be considered for future research projects.

Investigations on the applicability of TriX-MB as a foaming agent could also be taken into account, since the formation of stable foam because of the great size of the formed micelles is imaginable.

A very interesting result of the investigations, which have been conducted in the framework of this thesis, was the very favorable effect of a chaotropic salt (NaSCN) on oil recovery in imbibition tests. Taking advantage of salts, which intensify hydrophilicity, on oil recovery might be an interesting new approach for research.

Bibliography

- [1] International Energy Agency, 2012, *World Energy Outlook 2012* (OECD Publishing)
- [2] Birol, F., 2014, *World Energy Outlook* (Rotterdam: International Energy Agency)
- [3] U.S. Energy Information Administration, 2016, *International Energy Outlook 2016: With Projections to 2040* (Washington DC: U.S. Energy Information Administration)
- [4] Gravsholt, S., 1976, *Viscoelasticity in highly dilute aqueous solutions of pure cationic detergents*, *Journal of Colloid and Interface Science* **57**, pp.: 575–7
- [5] Kefi, S.; Lee, J.; Pope, T. L.; Sullivan, P.; Nelson, E.; Hernandez, A. N.; Olsen, T.; Palar, M.; Powers, B.; Roy, A.; Wilson, A. and Twynam, A., 2004/05, *Expanding Applications for Viscoelastic Surfactants*, *Oilfield Review 2004/2005*
- [6] Yang, J., 2002, *Viscoelastic wormlike micelles and their applications*, *Current Opinion in Colloid & Interface Science* **7**, pp. 276–81
- [7] Chang, F.; Love, T.; Affeld, C. J. B. B, Thomas, R. and Fu, D., 1999, *Case Study of a Novel Acid-Diversion Technique in Carbonate Reservoirs*, *SPE Annual Technical Conference and Exhibition*
- [8] Samuel, M.; Polson, D.; Graham, D.; Kordziel, W.; Waite, T.; Waters, G.; Vinod, P. S.; Fu, D. and Downey, R., 2000, *Viscoelastic Surfactant Fracturing Fluids: Applications in Low Permeability Reservoirs*, *SPE Rocky Mountain Regional/Low-Permeability Reservoirs Symposium and Exhibition*
- [9] Reinoso, G. M.; Oetter, G.; Kurkal-Siebert, V.; Heinz, B.; Bittner, C.; Hansch, M. and Raether, R. B., 2013, *Derivatives of tris(2-hydroxyphenyl)methane, and preparation and use thereof*, patent: WO 2011144643 A1
- [10] Terry, R. E., 2001, *Enhanced Oil Recovery*, *Encyclopedia of Physical Science and Technology*, pp. 503–18
- [11] Muggeridge, A.; Cockin, A.; Webb, K.; Frampton, H.; Collins, I.; Moulds, T. and Salino, P., 2014, *Recovery rates, enhanced oil recovery and technological limits*, *Philosophical transactions. Series A, Mathematical, physical, and engineering sciences* **372**

- [12] Lakatos, I.; Janos, T.; Bodi, T. and Lakatos-Szabo, J., 2007, *Application of Viscoelastic Surfactants as Mobility-Control Agents in Low-Tension Surfactant Floods*, SPE International Symposium on Oilfield Chemistry (Houston, Texas, USA, 28.02. - 02.03.2007)
- [13] Buckley, S. E. and Leverett, M. C., 1942, *Mechanism of Fluid Displacement in Sands* (New York: A.I.M.E.)
- [14] Sheng, J., 2011, *Modern Chemical Enhanced Oil Recovery* (Elsevier)
- [15] Lake, L. W., 2010, *Enhanced oil recovery* (Richardson, Tex.: Society of Petroleum Engineers)
- [16] Stegemeier, G. L., 1974, *Relationship of Trapped Oil Saturation to Petrophysical Properties of Porous Media*, Improved Oil Recovery Symposium of the Society of Petroleum Engineers of AIME 1974
- [17] Lake, L. W.; Johns, R. T.; Rossen, W. R. and Pope, G. A., 2014, *Fundamentals of enhanced oil recovery* (Richardson, Tex.: Soc. of Petroleum Engineers)
- [18] Cârcoană, A., 1992, *Applied enhanced oil recovery* (Englewood Cliffs, NJ: Prentice Hall)
- [19] Bogdanov, I.; Torres, J.; Kamp, A. M. and Corre, B., 2013, *Comparative Analysis of Electromagnetic Methods for Heavy Oil Recovery*, SPE Heavy Oil Conference and Exhibition SPE Heavy Oil Conference and Exhibition (Kuwait City, Kuwait, 2011-12-12) (Society of Petroleum Engineers)
- [20] Vermeulen, F. and McGee, B., 2000 *In Situ Electromagnetic Heating for Hydrocarbon Recovery and Environmental Remediation*, *Journal of Canadian Petroleum Technology*, August 2000, vol. 39
- [21] Santoso, R. K.; Rachmat, S.; Putra, W. D. K.; Resha, A. H. and Hartowo, H., 2016, *Numerical Modeling of Nanoparticles Transport in Porous Media for Optimisation in Well Stimulation and EOR Using Electromagnetic Heating*, SPE Asia Pacific Oil & Gas Conference and Exhibition SPE Asia Pacific Oil & Gas Conference and Exhibition (Perth, Australia, 2016-10-25)
- [22] Kostrov, S. and Wooden, W., 2008, *Possible Mechanisms and Case Studies for Enhancement of Oil Recovery and Production Using In-Situ Seismic Stimulation*, SPE/DOE Improved Oil Recovery Symposium 2008, Tulsa, Oklahoma, USA

- [23] Hamida, T., 2006, *The Influence of Ultrasonic Energy on Capillary Fluid Displacement*, Proceedings of SPE Annual Technical Conference and Exhibition SPE Annual Technical Conference and Exhibition (24.09.2006 - 27.09.2006)
- [24] Kurawle, I. B.; Kaul, M.; Mahalle, N. A.; Carvalho, V. H.; Nath, N. and Amin, Z. M., 2013, *Seismic EOR—The Optimization of Aging Waterflood Reservoirs, Off-shore Europe Offshore Europe (Aberdeen, UK, 2009-09-08)*
- [25] Degré, G.; Morvan, M.; Bouillot, J.; Zaitoun, A.; Al-Maamari, R. S.; Al-Hashmi, A. R. and Al-Sharji, H. H., 2011, *Viscosifying Surfactants for Chemical EOR, IOR 2011 - 16th European Symposium on Improved Oil Recovery (Cambridge, UK) (Proceedings)* (EAGE Publications BVNetherlands)
- [26] Sydansk, R. D. and Romero-Zerón, L., 2011, *Reservoir conformance improvement* (Richardson, TX: Society of Petroleum Engineers)
- [27] Liu, S., 2007, *Alkaline Surfactant Polymer Enhanced Oil Recovery Process*, Dissertation, Rice University
- [28] Alvarado, V.; Moradi Bidhendi, M.; Garcia-Olvera, G.; Morin, B. and Oakey, J. S., 2014, *Interfacial Visco-Elasticity of Crude Oil - Brine: An Alternative EOR Mechanism in Smart Waterflooding, SPE Improved Oil Recovery Symposium 2014*
- [29] Garcia-Olvera, G. and Alvarado, V., 2016, *The Potential of Sulfate as Optimizer of Crude Oil-Water Interfacial Rheology to Increase Oil Recovery During Smart Water Injection in Carbonates, SPE Improved Oil Recovery Conference 2016*
- [30] Green, D. W. and Willhite, G. P., 2008, *Enhanced oil recovery (SPE textbook series vol 6)*, 4th edn. (Richardson, Tex.: Henry L. Doherty Memorial Fund of AIME Society of Petroleum Engineers)
- [31] Aoudia, M.; Al-Harhi, Z.; Al-Maamari, R. S.; Lee, C. and Berger, P., 2010, *Novel Alkyl Ether Sulfonates for High Salinity Reservoir: Effect of Concentration on Transient Ultralow Interfacial Tension at the Oil–Water Interface, J. Surfact. Deterg.***13**, pp.: 233–42
- [32] Ezrahi, S.; Tuval, E. and Aserin, A., 2006, *Properties, main applications and perspectives of worm micelles, Advances in colloid and interface science* **128-130**, pp. 77–102

- [33] Hamberger, A. and Landfester, K., 2011, *Influence of size and functionality of polymeric nanoparticles on the adsorption behavior of sodium dodecyl sulfate as detected by isothermal titration calorimetry*, *Colloid Polym Sci* **289**, pp. 3–14
- [34] USA KINO Industry CO. Ltd., 2014, *Determining Critical Micelle Concentration of surfactant*, <http://www.surface-tension.org/news/58.html> (accessed 13 Mar 2017)
- [35] Yu, X., 2004, *Gegenseitige Beeinflussung von mizellaren Strukturen und Photodimerisierung von Cumarinderivaten*, *Dissertation*, Technische Universität Dresden
- [36] Romsted, L. S., *Surfactant Science and Technology: One Hundred Years of Micelles* (CRC Press)
- [37] Acharya, D. P. and Kunieda, H., 2006, *Wormlike micelles in mixed surfactant solutions*, *Advances in colloid and interface science* **123-126**, pp. 401–13
- [38] Cates, M. E. and Candau, S. J., *Statics and dynamics of worm-like surfactant micelles*, *Journal of Physics: Condensed Matter* **1990**, pp.: 6869–92
- [39] Candau, S. J. and Oda, R., 2001, *Linear viscoelasticity of salt-free wormlike micellar solutions*, *Colloids and Surfaces A: Physicochemical and Engineering Aspects* **183-185**, pp.: 5–14
- [40] Mezger, T. G., 2012, *Das Rheologie-Handbuch: Für Anwender von Rotations- und Oszillations-Rheometern (Farbe und Lack Edition)*, 4th edn., (Hannover: Vincentz Network)
- [41] Dreiss, C. A., 2007, *Wormlike micelles: Where do we stand? Recent developments, linear rheology and scattering techniques*, *Soft Matter* **3**, pp. 956-70
- [42] Rehage, H. and Hoffmann, H., 1991, *Viscoelastic surfactant solutions: Model systems for rheological research*, *Molecular Physics* **74**, pp. 933–73
- [43] Schramm, G., 2000, *A Practical Approach to Rheology and Rheometry*, 2nd edn., (Karlsruhe, Germany)
- [44] Roylance, D., 2001, *Engineering Viscoelasticity*, Department of Materials Science and Engineering, Massachusetts Institute of Technology
- [45] Koh, H., 2015, *Experimental investigation of the effect of polymers on residual oil saturation*, *Dissertation*, University of Texas at Austin

- [46] Dong, B.; Zhang, J.; Zheng, L.; Wang, S.; Li, X. and Inoue, T., 2008, *Salt-induced viscoelastic wormlike micelles formed in surface active ionic liquid aqueous solution*, *Journal of Colloid and Interface Science* **319**, pp. 338–43
- [47] Afsharpoor, A., 2014, *Pore-Scale Modeling of Viscoelastic Flow and the Effect of Polymer Elasticity on Residual Oil Saturation*, Dissertation, University of Texas at Austin
- [48] Datta, S. S., *Rheology of Soft Materials Tutorial* (Department of Physics, Harvard University)
- [49] Morvan, M.; Degre, G.; Beaumont, J.; Dupuis, G.; Zaitoun, A.; Al-maamari, R. S.; Al-Hashmi, A.-A. R. and Al-Sharji, H. H., 2012, *Optimization of Viscosifying Surfactant Technology for Chemical EOR*, *SPE Improved Oil Recovery Symposium (Tulsa, Oklahoma, USA, 2012-04-14)*
- [50] Wang, D.; Wang, G.; Wu, W.; Xia, H. and Yin, H., 2007, *The Influence of Viscoelasticity on Displacement Efficiency-From Micro- to Macroscale* *SPE Annual Technical Conference and Exhibition, 11-14 November, Anaheim, California, U.S.A.*
- [51] Goodwin, J. W. and Hughes, R. W., 2008, *Rheology for Chemists: An introduction, 2nd edn.*, (Cambridge, UK: Royal Soc. of Chemistry)
- [52] Sharma, S. C.; Shrestha, R. G.; Shrestha, L. K. and Aramaki, K., 2009, *Viscoelastic wormlike micelles in mixed nonionic fluorocarbon surfactants and structural transition induced by oils*, *The journal of physical chemistry. B* **113**, pp. 1615–22
- [53] Zhang, Y. and Cremer, P. S., 2006, *Interactions between macromolecules and ions: The Hofmeister series*, *Current opinion in chemical biology* **10**, pp. 658–63
- [54] Raghavan, S. R. and Kaler, E. W., 2001, *Highly Viscoelastic Wormlike Micellar Solutions Formed by Cationic Surfactants with Long Unsaturated Tails*, *Langmuir* **17**, pp. 300–6
- [55] Hofmeister, F., 1888, *Zur Lehre von der Wirkung der Salze: zweite Mittheilung* (Pharmakologisches Institut der deutschen Universität zu Prag)
- [56] Hardy, J. G.; Römer, L. M. and Scheibel, T. R., 2008, *Polymeric materials based on silk proteins*, *Polymer* **49**, pp. 4309–27

- [57] Leontidis, E., 2002, *Hofmeister anion effects on surfactant self-assembly and the formation of mesoporous solids*, *Current Opinion in Colloid & Interface Science* **7**, pp. 81–91
- [58] Kunz, W.; Lo Nostro, P. and Ninham, B. W., 2004, *The present state of affairs with Hofmeister effects*, *Current Opinion in Colloid & Interface Science* **9**, pp. 1-18
- [59] Oelschlaeger, C.; Suwita, P. and Willenbacher, N., 2010, *Effect of counterion binding efficiency on structure and dynamics of wormlike micelles*, *Langmuir: the ACS journal of surfaces and colloids* **26**, pp. 7045–53
- [60] Manet, S.; Karpichev, Y.; Bassani, D.; Kiagus-Ahmad, R. and Oda, R., 2010, *Counteranion effect on micellization of cationic gemini surfactants 14-2-14: Hofmeister and other counterions*, *Langmuir: the ACS journal of surfaces and colloids* **26**, pp. 10645–56
- [61] Maiti, K.; Mitra, D.; Guha, S. and Moulik, S. P., 2009, *Salt effect on self-aggregation of sodium dodecylsulfate (SDS) and tetradecyltrimethylammonium bromide (TTAB): Physicochemical correlation and assessment in the light of Hofmeister (lyotropic) effect*, *Journal of Molecular Liquids* **146**, pp. 44–51
- [62] Kuperkar, K.; Abezgauz, L.; Prasad, K. and Bahadur, P., 2010, *Formation and Growth of Micelles in Dilute Aqueous CTAB Solutions in the Presence of NaNO₃ and NaClO₃*, *J Surfact Deterg* **13**, pp. 293–303
- [63] Ho, P. C. and Kraus, K. A., 1982, *The Effect of Hydrotropic Salts on Phase Relationships Involving Hydrocarbons, Water, and Alcohols*, *Society of Petroleum Engineers Journal*, June 1982
- [64] Jovancicevic, V.; Ramachandran, S. and Ahn, Y. S. and Oude Alink, B. A. M., 2001, *Corrosion Inhibition and Drag Reduction in Multiphase Flow*, *CORROSION 2001*, Paper No. 01052
- [65] Zakin, J. L. and Chang, J. L., 1972, *Non-ionic Surfactants as Drag Reducing Additives*, *Nature Physical Science* **239**, pp. 24–8
- [66] Zakin, J. L. and Lui, H.-L., 2007, *Variables Affecting Drag Reduction By Nonionic Surfactant Additives†*, *Chemical Engineering Communications* **23**, pp. 77–88
- [67] Tadros, T. F., 2011, *Self-Organized Surfactant Structures, 4th edn.*, (Hoboken: John Wiley & Sons)

- [68] Wang, D.; Li, Q.; Gong, X. and Wang, Y., 2000, *The Engineering and Technical Aspects of Polymer Flooding in Daqing Oil Field, International Oil and Gas Conference and Exhibition in China, 7-10 November, Beijing, China*
- [69] Jiang, H.; Wu, W.; Wang, D.; Zeng, Y.; Zhao, S. and Nie, J., 2008, *The Effect of Elasticity on Displacement Efficiency in the Lab and Results of High Concentration Polymer Flooding in the Field, SPE Annual Technical Conference and Exhibition (Denver, Colorado, USA, 2008-09-21)*
- [70] Wang, D.; Xia, H.; Yang, S. and Wang, G., 2010, *The Influence of Visco-Elasticity on Micro Forces and Displacement Efficiency in Pores, Cores and in the Field SPE EOR Conference at Oil & Gas West Asia, 11-13 April, Muscat, Oman*
- [71] Urbissinova, T.; Trivedi, J. and Kuru, E., 2002, *Effect of Elasticity During Viscoelastic Polymer Flooding: A Possible Mechanism of Increasing the Sweep Efficiency, SPE Western Regional Meeting (Lafayette, Louisiana, USA)*
- [72] Wang, D. and Wang, G., 2012, *New Insights on the Mechanism of Displacement Efficiency of Natural Cores by Chemical Flooding and Its Influence on the Development and Selection of Chemicals for EOR, SPE Improved Oil Recovery Symposium 2012*
- [73] Oliveira, P. J., 2002, *An exact solution for tube and slit flow of a FENE-P fluid, Acta Mechanica* **158**, pp. 157–67
- [74] Wang, D.; Cheng, J.; Yang, Q.; Gong, W.; Li, Q. and Chen, F., 2000, *Viscous Elastic Polymer Can Increase Microscale Displacement Efficiency in Cores, SPE Annual Technical Conference 2000*
- [75] Wang, D.; Wang, G. and Xia, H., 2011, *Large Scale High Visco-Elastic Fluid Flooding in the Field Achieves High Recoveries, SPE Enhanced Oil Recovery Conference (Kuala Lumpur, Malaysia, 2011-07-19)*
- [76] Brown, J.; Lee, R.; Nelson, E. and Ali, S., 1996, *Use of a Viscoelastic Carrier Fluid in Frac-Pack Applications SPE Formation Damage Control Symposium, 14-15 February, Lafayette, Louisiana*
- [77] Stewart, B. R.; Mullen, M. E.; Howard, W. J. and Norman, W. D., 1995, *Use of a Solids-free Viscous Carrying Fluid in Fracturing Applications: An Economic and Productivity Comparison in Shallow Completions SPE European Formation Damage Conference, 15-16 May, The Hague, Netherlands*

- [78] Nehmer, W. L., 1988, *Viscoelastic Gravel-Pack Carrier Fluid*, SPE Formation Damage Control Symposium, Bakersfield, California, February 8-9, 1988
- [79] Chang, F. F.; Acock, A. M.; Geoghagan, A. and Huckabee, P. T., 2001, *Experience in Acid Diversion in High Permeability Deep Water Formations Using Viscoelastic-Surfactant SPE European Formation Damage Conference*, 21-22 May, The Hague, Netherlands
- [80] Morvan, M.; Moreau, P.; Degre, G.; Leng, J.; Masselon, C.; Bouillot, J. and Zaitoun, A., 2009, *New Viscoelastic Fluid for Chemical EOR*, SPE International Symposium on Oilfield Chemistry (The Woodlands, Texas, 2009-04-20)
- [81] Morvan, M.; Degre, G.; Beaumont, J.; Colin, A.; Dupuis, G.; Zaitoun, A.; Al-maamari, R. S.; Al-Hashmi, A.-A. R. and Al-Sharji, H. H., 2012, *Viscosifying Surfactant Technology for Heavy Oil Reservoirs*, SPE Heavy Oil Conference Canada (Calgary, Alberta, Canada, 2012-06-12)
- [82] Zhu, Y.; Fan, J.; Liu, X. and Li, J., 2016, *Studies on Viscoelastic Surfactants for its Potential EOR Application in the Low Permeability Reservoirs*, SPE Improved Oil Recovery Conference (Tulsa, Oklahoma, USA, 2016-04-11)
- [83] Casiraghi, G.; Casnati, G. and Cornia, M., 1973, *Regiospecific Reactions of Phenol Salts: Reaction-Pathways of Alkylphenoxy-Magnesiumhalides with Triethylorthoformate*, *Tetrahedron Letters* **9**, pp. 679–82
- [84] Dinger, M. B. and Scott, M. J., 1999, *Selective binding of substrates using sodium salts of linked C3 symmetric aryl oxides*, *Chem. Commun.*, pp. 2525–6
- [85] Dinger, M. B. and Scott, M. J., 2000, *Extended Structures Built on a Triphenoxymethane Platform –C3-Symmetric, Conformational Mimics of Calix[n]arenes*, *Eur. J. Org. Chem.* 2000, pp. 2467–78
- [86] Siggel, L.; Santa, M.; Hansch, M.; Nowak, M.; Ranft, M.; Weiss, H.; Hajnal, D.; Schreiner, E.; Oetter, G. and Tinsley, J., 2012, *A New Class of Viscoelastic Surfactants for Enhanced Oil Recovery*, SPE Improved Oil Recovery Symposium (Tulsa, Oklahoma, USA, 2012-04-14)

- [87] Rodriguez-Abreu, C.; Aramaki, K.; Tanaka, Y.; Lopez-Quintela, M. A.; Ishitobi, M. and Kunieda, H., 2005, *Wormlike micelles and microemulsions in aqueous mixtures of sucrose esters and nonionic cosurfactants*, *Journal of Colloid and Interface Science* **291**, pp. 560–9
- [88] Siggel, L.; Radloff, M.; Reimann, S.; Hansch, M.; Nowak, M.; Ranft, M.; Weiss, H.; Schreiner, E. and Brand, F., 2014, *TPM's: A New Class of Viscoelastic Solutions for Enhanced Oil Recovery*, *SPE EOR Conference at Oil and Gas West Asia (Muscat, Oman, 2014-03-31)*
- [89] Oetter, G.; Heinz, B.; Hansch, M.; Weiss, H.; Deglmann, P.; Kurkal-Siebert, V.; Heilmann, F.; Aglave, R.; Siggel, L. and Wenzke, B., 2013, *Verwendung von tris(2-hydroxyphenyl)-methan-derivaten für die tertiäre Erdölförderung*, patent: *WO 2013057044 A1*
- [90] Siggel, L., 2017, personal communication (aggregation of TriX), 2017-01-19
- [91] Siggel, L., 2017, personal communication (size of TriX-TA micelles, DLS measurements done by V. Boyko (BASF)), email 2017-03-11
- [92] Siggel, L., 2014, personal communication (TriX properties), email 2014-12-04
- [93] Lawson, J. B., 1978, *The Adsorption of Non-ionic and Anionic Surfactants on Sandstone and Carbonate*, 5. *Symposium on Improved Methods for Oil Recovery of SPE and AIME, Tulsa, Oklahoma, USA, 16. - 19. April 1978*
- [94] Corp S-A Triton™ X-100 (T8532) - Product Information Sheet
- [95] Magnus, M., 2017, *Qualitative und quantitative mikroskopische Beschreibung an Dünnschliffen: Analysenberichte (Bentheimer und Michigan Sandstein)*, (Institut für Geologie, TU Bergakademie Freiberg)
- [96] Siggel, L., 2016, personal communication (UV-Detection of TriX), email 2016-08-23
- [97] Schechter, D.; Zhou, D. and Orr, F., 1994, *Low IFT drainage and imbibition*, *Journal of Petroleum Science and Engineering* **11**, pp. 283–300
- [98] Baldwin, B. and Spinler, E., 2002, *In situ saturation development during spontaneous imbibition*, *Journal of Petroleum Science and Engineering* **35**, pp. 23–32

- [99] Chauveteau, G. and Kohler, N., 1974, *Polymer Flooding: The Essential Elements for Laboratory Evaluation, Improved Oil Recovery Symposium of the Society of Petroleum Engineers of AIME 1974*, pp. 115–30
- [100] Hirasaki, G. J.; Miller, C. A. and Puerto, M., 2008, *Recent Advances in Surfactant EOR, SPE Annual Technical Conference and Exhibition 2008*
- [101] Ruiz, C. C.; Molina-Bolívar, J. A.; Aguiar, J.; Maclsaac, G.; Moroze, S. and Palepu, R., 2001, *Thermodynamic and Structural Studies of Triton X-100 Micelles in Ethylene Glycol–Water Mixed Solvents, Langmuir* **17**, pp. 6831–40
- [102] Alam, S.; Siddiq, A. M. and Mandal, A. B., 2015, *The Micellization and Clouding of Nonionic Surfactant, Poly(Ethylene Glycol) t -Octylphenyl Ether (Triton X-100): Effect of Halide Ions of (Sodium Salt) Electrolytes, Journal of Dispersion Science and Technology* **37**, pp. 1385–94
- [103] Trogus, F. J.; Sophany, T.; Schechter, R. S. and Wade, W. H., 1977, *Static and Dynamic Adsorption of Anionic and Nonionic Surfactants, Society of Petroleum Engineers Journal* **17**, pp. 337–44
- [104] Bera, A.; Kumar, T.; Ojha, K. and Mandal, A., 2013, *Adsorption of surfactants on sand surface in enhanced oil recovery: Isotherms, kinetics and thermodynamic studies, Applied Surface Science* **284**, pp.: 87–99
- [105] Ramirez, W. F.; Shuler, P. J. and Friedman, F., 1980, *Convection, Dispersion, and Adsorption of Surfactants in Porous Media, Society of Petroleum Engineers Journal* **20**, pp. 430–8
- [106] Siggel, L., 2016, personal communication (Final Report Revision), email 2016-10-04
- [107] dos Santos, A. P. and Levin, Y., 2013, *Surface and interfacial tensions of Hofmeister electrolytes, Faraday Discuss* **160**, pp. 75–87
- [108] Xie, W. J. and Gao, Y. Q., 2013, *A Simple Theory for the Hofmeister Series, The journal of physical chemistry letters* **4**, pp. 4247–52
- [109] Hansch, M., 2015, personal communication (Analysis of gelled samples from core floods with TriX-MB), email 2015-03-24
- [110] Li, L.; Nasr-El-Din, H. A. and Cawiezel, K. E., 2013, *Rheological Properties of a New Class of Viscoelastic Surfactant, SPE Production & Operations* **25**, pp. 355-66

- [111] Hatzikiriakos, S. G., 2015, *Slip mechanisms in complex fluid flows*, *Soft Matter* **11**, pp. 7851–6
- [112] Schreiner, E., 2014, personal communication (Molecular modelling of TriX) (Kassel, Germany), R&D meeting 2014-10-30
- [113] Kleppe, J., TPG4150 *Reservoir Recovery Techniques 2016, Hand-out note 4: Buckley-Leverett Analysis* (Norwegian University of Science and Technology, Dep. of Petroleum Engineering and Applied Geophysics) 31.08.16
- [114] Craig Jr., F., 1971, *The Reservoir Engineering Aspects of Waterflooding* (Society of Petroleum Engineers of AIME, New York)
- [115] Corey, A. T., 1956, *The Interrelation Between Gas and Oil Relative Permeabilities* http://www.discovery-group.com/pdfs/Corey_1954.pdf (accessed: 8. Nov. 2016)
- [116] Brooks, R. H. and Corey, A. T., 1966, *Properties of Porous Media Affecting Fluid Flow, Journal of the IRRIGATION AND DRAINAGE DIVISION, Proceedings of the American Society of Civil Engineers*, pp. 61–88
- [117] Goda, H. M. and Behrenbruch, P., 2004, *Using a Modified Brooks-Corey Model to Study Oil-Water Relative Permeability for Diverse Pore Structures SPE Asia Pacific Oil and Gas Conference and Exhibition, 18-20 October, Perth, Australia*
- [118] Amro, M., 2012, University Lecture: Enhanced Oil Recovery (TU Bergakademie Freiberg)

List of Figures

	<u>Page</u>
Figure 1-1: Total world energy consumption by energy source, 1990–2040 (in 10 ¹⁵ Btu), (CPP = Clean Power Plan) [3]	1
Figure 2-1: Relative permeability curves for water (k_{rw}) and oil (k_{ro}) as a function of the water saturation of the reservoir (S_w) [8]	5
Figure 2-2: Schematic representation of volumetric sweep efficiency (adapted from [9])	7
Figure 2-3: Categories of enhanced oil recovery methods	9
Figure 2-4: Water flooding with unfavorable mobility ratio, $M < 1$ (left) and polymer flooding with increased mobility ratio (right) [20]	12
Figure 3-1: Critical micelle concentration (schematic) [33, 34]	18
Figure 3-2: Energetic contributions of different phenomena during micellization in a surfactant solution	18
Figure 3-3: Parameters in Packing Factor [8]	19
Figure 3-4: Schematic representation of contour length (L), persistence length (l_p) and cross section diameter (D_{cs}) of a worm-like micelle [41]	20
Figure 3-5: Viscoelastic deformation of a Maxwell fluid	23
Figure 3-6: Normal stresses on a Newtonian and a viscoelastic fluid under shear [8]	24
Figure 3-7: First normal stress differences of different HPAM solutions as a function of shear rate (1: $MW = 21 * 10^6$, highest elasticity; 2: $MW = 12 * 10^6$; 3: $MW = 7.5 * 10^6$, lowest elasticity) [8]	25

Figure 3-8::	Principle using a frequency sweep to determine the relaxation time [48]	26
Figure 3-9:	Hofmeister series of cat- and anions and effects in aqueous solution [53, 56]	29
Figure 4-1:	Velocity profiles in tube flow for varying Deborah numbers [73]	32
Figure 4-2:	Velocity profile of different fluids and on residual oil film on oil wet pore wall [70]	33
Figure 4-3:	Mobilization of oil film [70]	33
Figure 4-4:	Recovery of residual oil from dead-end pores by water, viscous glycerin and viscoelastic polyacrylamide [74]	34
Figure 5-1:	Generic chemical structure of a Triphenoxymethane [86]	41
Figure 5-2:	Results of a frequency sweep of TriX-MB in NDIIa at 55 °C with constant deformation of 100 % [86]	43
Figure 6-1:	Amott cell	56
Figure 6-2:	Scheme of the core flooding unit	58
Figure 6-3:	Photo of the core flooding unit	58
Figure 7-1:	Surface tensions of TriX derivatives and Triton-X-100, concentration in ppm	65
Figure 7-2:	Surface tensions of TriX derivatives and Triton-X-100, concentration in mmol/l	65
Figure 7-3:	Surface tensions of TriX-M and Triton-X-100 as a function of concentration in ppm	66
Figure 7-4:	Changes in surfactant concentration after sand contact	67
Figure 7-5:	Static adsorption of surfactants on sand in $\text{mg}_{\text{surf}}/\text{g}_{\text{sand}}$	68

Figure 7-6:	Static adsorption of TriX derivatives and Triton-X-100 on sand in $\mu\text{mol}_{\text{surf}}/\text{g}_{\text{sand}}$	69
Figure 7-7:	Adsorption of TriX derivatives and Triton-X-100 in $\text{mg}_{\text{surf}}/\text{m}^2_{\text{sand}}$	70
Figure 7-8:	Adsorption of TriX derivatives and Triton-X-100 in $\mu\text{mol}_{\text{surf}}/\text{m}^2_{\text{sand}}$	71
Figure 7-9:	Interfacial tensions of TriX derivatives and Triton-X-100 to Bockstedt oil (c in ppm)	72
Figure 7-10:	Interfacial tensions of TriX derivatives and Triton-X-100 to Bockstedt oil (c in $\mu\text{mol}/\text{l}$)	73
Figure 7-11:	Apparent changes in concentration in wt. % of bulk solutions after oil contact	74
Figure 7-12:	Apparent changes in concentration in mmol/l of bulk solutions after oil contact	75
Figure 7-13:	Imbibition curves of TriX derivatives and Triton-X-100 in NDIIa brine	77
Figure 7-14:	Imbibition curves of TriX-MB and Triton-X-100 in NaCl	79
Figure 7-15:	Ultimate recoveries of imbibition tests	80
Figure 7-16:	Viscosity of TriX-MB solutions in different brines	82
Figure 7-17:	Interfacial tension to Bockstedt oil of TriX-MB solutions in different brines	83
Figure 7-18:	Imbibition curves of different brines	84
Figure 7-19:	Imbibition curves of 0.1 wt. % TriX-MB in different brines	85
Figure 7-20:	Imbibition curves of 0.25 wt. % TriX-MB in different brines	85

Figure 7-21:	Ultimate recoveries of imbibition tests with TriX-MB in different brines	86
Figure 7-22:	Pressure drop over filtration core #3 during injection of 0.1 wt. % TriX-MB in NDIIa brine	88
Figure 7-23:	Pressure drop over main core #3 during injection of 0.1 wt. % TriX-MB in NDIIa brine	88
Figure 7-24:	Gelled material at front and back face of filtration core #	89
Figure 7-25:	RRF before and after reverse brine injection (plugging removal)	90
Figure 7-26:	Pressure drop over filtration core #4 during injection of 0.1 wt. % TriX-MB in NaCl	92
Figure 7-27:	Pressure drop over main core #4 during injection of 0.1 wt. % TriX-MB in NaCl	92
Figure 7-28:	Pressure drop over filtration core #6 during injection of 0.1 wt. % TriX-MB in NaCl	94
Figure 7-29:	Pressure drop over main core #6 during injection of 0.1 wt. % TriX-MB in NaCl	95
Figure 7-30:	Pressure curve and concentration of effluent during TriX-TA in NDIIa brine injection	97
Figure 7-31:	Pressure curve and concentration of effluent during TriX-M in NDIIa brine injection	99
Figure 7-32:	Retention of TriX derivatives in Michigan Sandstone in different units	101
Figure 7-33:	Retention and Adsorption of TriX derivatives in mg/m^2	102
Figure 7-34:	Retention and Adsorption of TriX derivatives in $\mu\text{mol}/\text{m}^2$	103

Figure 7-35:	Secondary oil recoveries and TriX-MB input concentrations of MC #10 and #11	108
Figure 7-36:	Secondary oil recoveries and pressure drops during TriX-TA injection into MC #13 and #14	112
Figure 7-37:	Tertiary oil recoveries and pressure drops during TriX-MB injection into MC #8 and #9	117
Figure 7-38:	Tertiary oil recovery and pressure drop during TriX-TA injection into MC #15	120
Figure 7-39:	Tertiary oil recovery and pressure drop during TriX-MB injection into MC #16	122
Figure 7-40:	Fractional flow of secondary oil displacement tests	125
Figure 7-41:	Relative permeabilities during oil displacements with NaCl and 0.1 wt. % TriX-MB in NaCl	126
Figure 7-42:	Relative permeabilities during oil displacements with NDIIa and 0.1 wt. % TriX-TA in NDII	126
Figure 7-43:	Summary of tertiary oil displacement tests with TriX-MB, TriX-TA, and TriX-M	129
Figure 7-44:	Mobilization of residual oil by TriX-MB in a 2 D Gildehaus Sandstone core [88]	130
Figure A3-1:	Pore size distribution of Bentheimer sandstone	163
Figure A3-2:	Pore size distribution of Michigan sandstone	163
Figure A4-1	Typical relative permeability curves (left) and corresponding fractional flow (right) [113]	164
Figure A4-2	Fractional flow (f_w) as a function of water saturation (S_w) and mobility ratio (M) [15]	165

Figure A4-3: Typical relative permeability curves for strongly water-wet (left) and strongly oil-wet (right) conditions [114]	167
---	-----

List of Tables

	<u>Page</u>
Table 4-1: additional oil production in core floods conducted by Lakatos et al. [6]	35
Table 6-1: Composition of NDIIa	47
Table 6-2: Designation and compositions of saline solutions	47
Table 6-3: Density and Viscosity of Bockstedt oil	50
Table 6-4: Concentration of used surfactants	52
Table 6-5: Wavelength for extinction measurements	53
Table 7-1: Surface tension measurements of TriX derivatives and Triton-X-100 dilution series	66
Table 7-2: Changes in surfactant concentration after sand contact	67
Table 7-3: Static adsorption of surfactants on sand	68
Table 7-4: Static adsorption related to surface area	70
Table 7-5: Interfacial tension measurements of TriX derivatives and Triton-X-100 dilution series to Bockstedt oil	72
Table 7-6: Apparent changes of concentration in bulk solutions of TriX derivatives and Triton-X-100 after oil contact	74
Table 7-7: Inverse <i>Bond</i> numbers of imbibition tests	76
Table 7-8: Characteristics of cores and fluids of injection tests with NDIIa brine	87
Table 7-9: Characteristic values of injection tests with NDIIa brine	89
Table 7-10: Characteristics of cores and fluids of injection tests with NaCl	91

Table 7-11:	Characteristic values of injection tests with TriX-MB in NaCl (high permeable cores)	93
Table 7-12:	Characteristics of the cores and fluids of core floods #6 and #7	94
Table 7-13:	Characteristic values of injection tests with TriX-MB in NaCl (lower permeable cores)	96
Table 7-14:	Characteristics of cores and fluids of injection tests with TriX-TA in NDIIa brine	97
Table 7-15:	Characteristic values of injection tests with TriX-TA in NDIIa brine	98
Table 7-16:	Characteristics of cores and fluids of injection tests with TriX-M in NDIIa brine	99
Table 7-17:	Characteristic values of injection tests with TriX-M in NDIIa brine	100
Table 7-18:	Retention of TriX derivatives during core flooding tests in Michigan sandstone	101
Table 7-19:	Retention and Adsorption of TriX derivatives	102
Table 7-20:	Summary of the injection tests	103
Table 7-21:	Characteristics of cores and fluids of secondary oil displacement tests with TriX-MB	106
Table 7-22:	Characteristic values of secondary oil displacement tests with TriX-MB	110
Table 7-23:	Characteristics of cores and fluids of secondary oil displacement tests with TriX-TA	111
Table 7-24:	Characteristic values of secondary oil displacement tests with TriX-TA	112
Table 7-25:	Characteristics of cores and fluids of tertiary oil displacement tests with TriX-MB	114

Table 7-26:	Characteristic values of tertiary oil displacement tests with TriX-MB	118
Table 7-27:	Characteristics of cores and fluids of tertiary oil displacement test with TriX-TA	119
Table 7-28:	Characteristic values of tertiary oil displacement test with TriX-TA	120
Table 7-29:	Characteristics of cores and fluids of tertiary oil displacement test with TriX-M	121
Table 7-30:	Characteristic values of tertiary oil displacement test with TriX-M	123
Table 7-31:	Remaining oil saturation in secondary oil displacement experiments	124
Table 7-32:	Core flooding results for cores ($k_{brine} = 2 D$) at S_{wi} at 55 °C and a flow rate of 9 ml/h (corresponding Darcy's velocity of 1 ft/d) in another laboratory [88]	124
Table 7-33:	Remaining oil saturation in tertiary oil displacement experiments	128
Table A1-1:	Griffin scale of HLB values	159
Table A2-1:	Densities and viscosities of the used aqueous solutions	160
Table A4-1:	Corey factors for water and oil for different wettability conditions [116]	166
Table A4-2:	Values to define wettability from relative permeability curves [117]	167

Appendix

A1 The hydrophilic-lipophilic balance

A2 Densities and viscosities of the used aqueous solutions (Table)

A3 Pore size distributions of Bentheimer and Michigan sandstone

A4 The Buckley-Leverett model and Corey relative permeability functions

A1 The hydrophilic-lipophilic balance (HLB)

The HLB value is a measure to quantify the hydrophilic and lipophilic character of a surfactant molecule. This concept is often used to describe emulsification processes. A high HLB value is characteristic for surfactants with a pronounced hydrophilic character, which propagate the formation of oil-in-water emulsions. In presence of surfactants with low HLB values, water-in-oil emulsions are more likely formed.

A wide-spread mean to rate the hydrophilic or lipophilic effect of a surfactant by its HLB value is the Griffin scale, as shown in Table A1-1. It facilitates the screening of different surfactants for practical applications.

Table A1-1: Griffin scale of HLB values

HLB range	Use
4 – 6	w/o emulsifiers
7 – 9	wetting agents
8 – 18	o/w emulsifiers
13 – 15	detergents
15 – 18	solubilizer

A2 Densities and viscosities of the used aqueous solutions

Table A2-1: Densities and viscosities of the used aqueous solutions

	20 °C		55 °C		room temp.
	Density in g/cm ³	dyn. Viscosity in mPa·s	Density in g/cm ³	dyn. Viscosity in mPa·s	pH-value
saline solutions					
NDIIa	1.1266 ± 0.0029	1.481 ± 0.024	1.1094 ± 0.0029	0.7977 ± 0.0385	5.7 ± 0.2
NaCl	1.1406 ± 0.0056	1.486 ± 0.156	1.1223 ± 0.0055	0.8073 ± 0.0204	5.6 ± 0.4
0.5 NaCl	1.0694 ± 0.0039	1.009 ± 0.473	1.0530 ± 0.0047	0.6642 ± 0.0442	5.8 ± 0.2
Na₂SO₄	1.1450 ± 0.0007	1.825 ± 0.115	1.1277 ± 0.0004	0.8977 ± 0.0583	5.9 ± 0.1
0.5 Na₂SO₄	1.0724 ± 0.0043	1.301 ± 0.026	1.0558 ± 0.0042	0.6685 ± 0.0191	5.8 ± 0.2
NaSCN	1.1451 ± 0.0018	1.483 ± 0.008	1.1207 ± 0.0010	0.7935 ± 0.0169	5.7 ± 0.1
0.5 NaSCN	1.0644 ± 0.0141	1.132 ± 0.035	1.0457 ± 0.0130	0.6025 ± 0.0021	5.6 ± 0.2

Table A2-1: Densities and viscosities of the used aqueous solutions (continued)

	20 °C		55 °C		room temp.
	Density g/cm ³	dyn. Viscosity mPa·s	Density g/cm ³	complex Viscosity mPa·s	pH-value
TriX-MB in different saline solutions					
0.1 wt. % TriX-MB in NDIIa	1.1225 ± 0.0111	N/A	1.1100 ± 0.0031	12.3 ± 3.9	6.0 ± 0.3
0.1 wt. % TriX-MB in NaCl	1.1405 ± 0.0062	N/A	1.1222 ± 0.0060	8.5 ± 1.8	5.9 ± 0.6
0.25 wt. % TriX-MB in NaCl	1.1393 ± 0.0001	N/A	1.1218 ± 0.0008	20.7 ± 0.4	5.8 ± 0.0
0.1 wt. % TriX-MB in 0.5 NaCl	1.0693 ± 0.0000	N/A	1.0526 ± 0.0064	5.6 ± 0.0	5.9 ± 0.4
0.25 wt. % TriX-MB in 0.5 NaCl	1.0721 ± 0.0009	N/A	1.0567 ± 0.0006	5.6 ± 0.9	6.1 ± 0.1
0.1 wt. % TriX-MB in Na₂SO₄	1.1438 ± 0.0002	N/A	1.1265 ± 0.0006	9.7 ± 0.1	5.7 ± 0.3
0.25 wt. % TriX-MB in Na₂SO₄	1.1440 ± 0.0003	N/A	1.1263 ± 0.0008	30.6 ± 0.5	5.8 ± 0.5
0.1 wt. % TriX-MB in 0.5 Na₂SO₄	1.0762 ± 0.0030	N/A	1.0589 ± 0.0005	8.1 ± 0.0	5.1 ± 0.1
0.25 wt. % TriX-MB in 0.5 Na₂SO₄	1.0763 ± 0.0030	N/A	1.0589 ± 0.0004	7.0 ± 0.2	5.4 ± 0.2
0.1 wt. % TriX-MB in NaSCN	1.1492 ± 0.0010	N/A	1.1227 ± 0.0030	7.3 ± 0.2	6.0 ± 0.3
0.25 wt. % TriX-MB in NaSCN	1.1435 ± 0.0009	N/A	1.1191 ± 0.0003	7.3 ± 0.6	5.9 ± 0.3
0.1 wt. % TriX-MB in 0.5 NaSCN	1.0748 ± 0.0007	N/A	1.0549 ± 0.0015	6.6 ± 0.1	5.7 ± 0.1
0.25 wt. % TriX-MB in 0.5 NaSCN	1.0730 ± 0.0006	N/A	1.0533 ± 0.0013	6.3 ± 0.1	5.9 ± 0.1

Table A2-1: Densities and viscosities of the used aqueous solutions (continued)

	20 °C		55 °C		room temp.
	Density g/cm ³	dyn. Viscosity mPa·s	Density g/cm ³	dyn. Viscosity mPa·s	pH-value
TriX-TA, TriX-M, and Triton-X-100 in NDIIa					
0.1 wt. % TriX-TA in NDIIa	1.1266 ± 0.0009	1.486 ± 0.000	1.1096 ± 0.0009	0.805 ± 0.012	5.9 ± 0.4
0.25 wt. % TriX-TA in NDIIa	1.1275 ± 0.0011	1.508 ± 0.003	1.1108 ± 0.0013	0.863 ± 0.006	5.8 ± 0.1
0.1 wt. % TriX-M in NDIIa	1.1282 ± 0.0012	N/A	1.1110 ± 0.0009	0.785 ± 0.003	5.6 ± 0.1
0.25 wt. % TriX-M in NDIIa	1.1275 ± 0.0006	N/A	1.1111 ± 0.0013	0.842 ± 0.083	5.8 ± 0.0
0.1 wt. % Triton X 100 in NDIIa	1.1308 ± 0.0029	1.439 ± 0.022	1.1155 ± 0.0072	0.720 ± 0.015	5.9 ± 0.1
0.25 wt. % Triton X 100 in NDIIa	1.1264 ± 0.0000	1.542 ± 0.000	1.1095 ± 0.0000	0.927 ± 0.000	5.5 ± 0.0
0.1 wt. % Triton X 100 in NaCl	1.1383 ± 0.0047	1.452 ± 0.032	1.1204 ± 0.0046	0.811 ± 0.002	5.6 ± 0.1

A3 Pore size distributions of Bentheimer and Michigan sandstone

Bentheimer sandstone

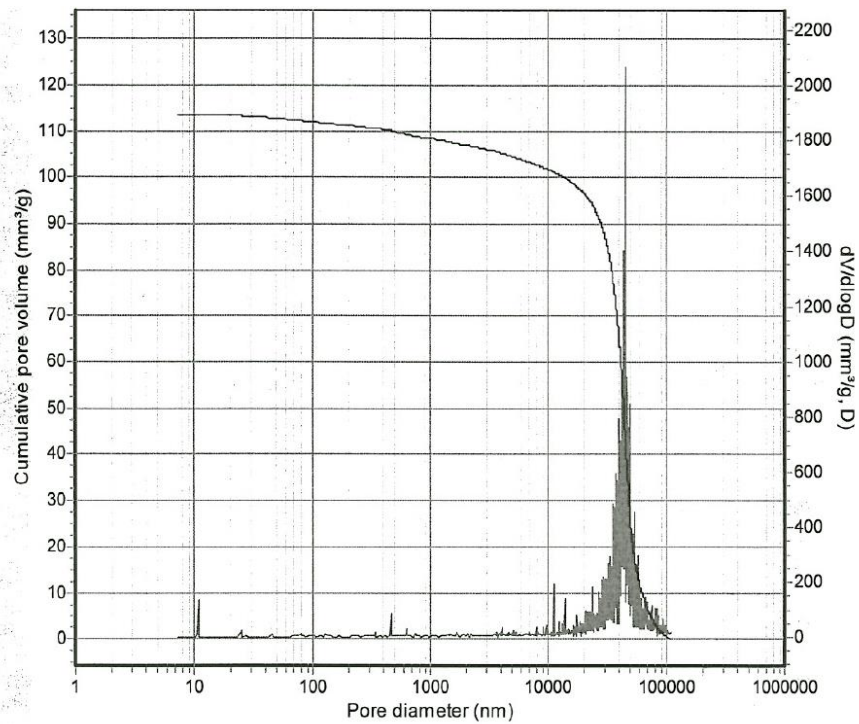


Figure A3-1: Pore size distribution of Bentheimer sandstone

Michigan sandstone

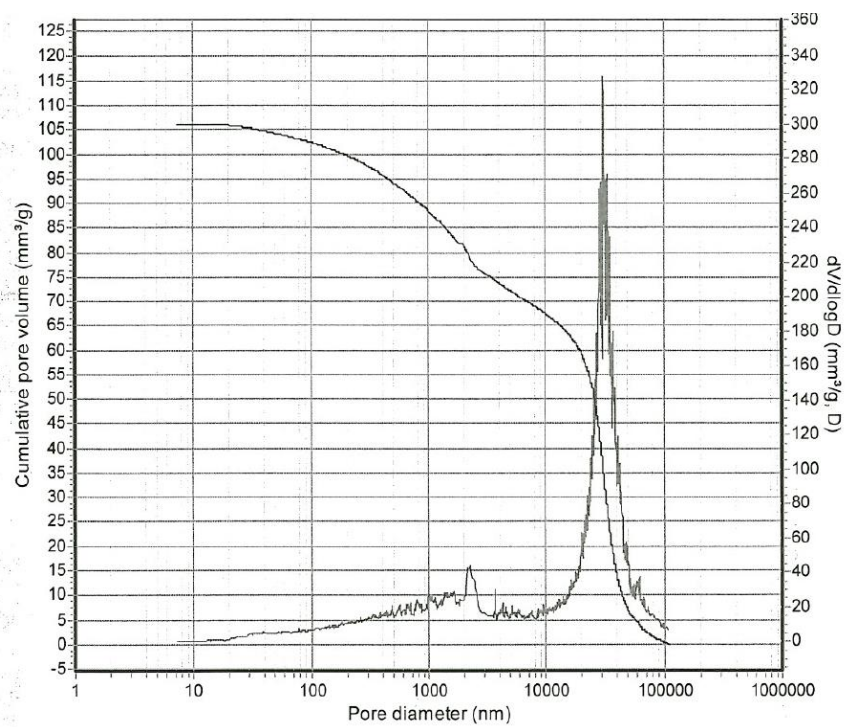


Figure A3-2: Pore size distribution of Michigan sandstone

A4 The Buckley-Leverett model and Corey relative permeability functions

The *Buckley-Leverett* model is a simple analytical tool to analyze oil displacement in a porous medium. Under the assumptions displaced (oil) and displacing (water) fluids are immiscible, incompressible and gravity effects and capillary forces are neglectable, the fractional flow of the water (f_w) is described as a function of saturation of the porous medium [13, 113].

$$f_w = \frac{1}{1 + \frac{k_{ro}(S_w)}{\eta_o} * \frac{\eta_w}{k_{rw}(S_w)}} \quad \text{Eq. A4-1}$$

f_w	–	fractional flow of water
$k_{ro}(S_w)$	–	relative permeability for oil
η_o	–	dynamic viscosity of oil in Pa·s
η_w	–	dynamic viscosity of water in Pa·s
$k_{rw}(S_w)$	–	relative permeability for water

Typical relative permeability curves with corresponding fractional flow diagram are given in Figure A4-1.

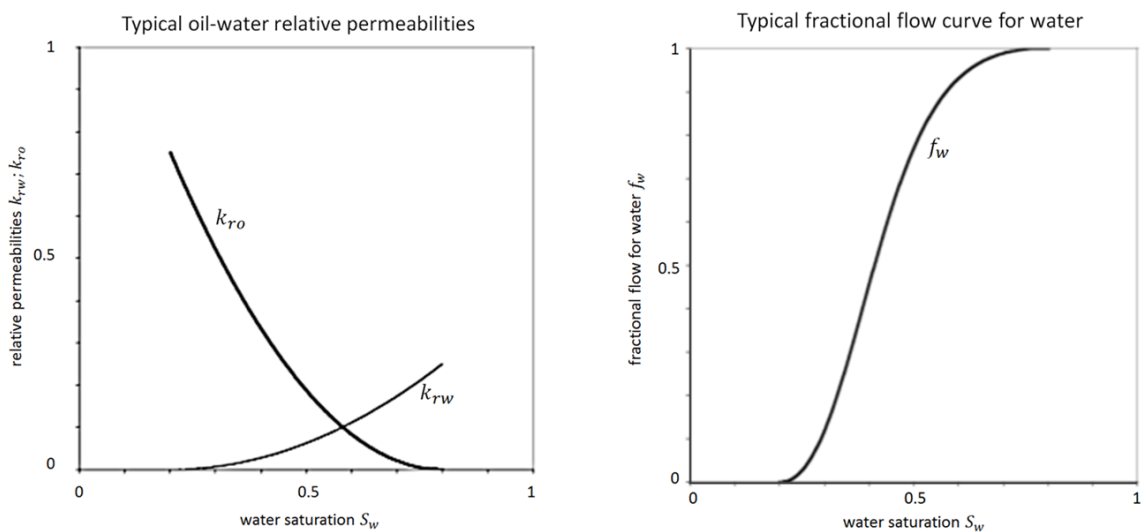


Figure A4-1: Typical relative permeability curves (left) and corresponding fractional flow (right) [113]

The fractional flow depends on the mobility ratio between water and oil. Hence, statements about the mobility ratio in each experiment could be made on the basis of the observed fractional flow of water and oil phase. Figure A4-2 shows fractional flow curves as a function of water saturation in the core at different mobility ratios M . The lower the mobility ratio, the more efficient is the oil displacement.

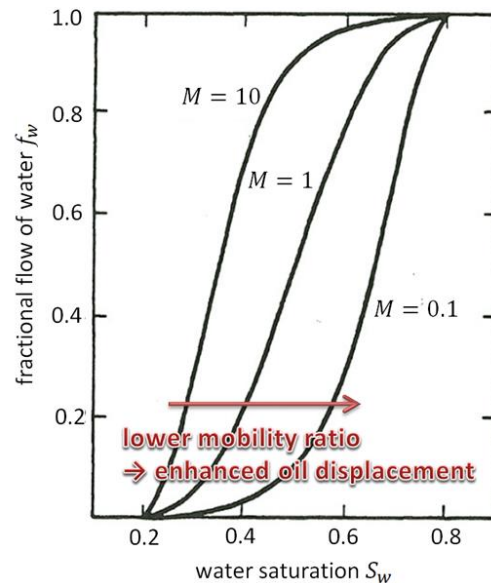


Figure A4-2: Fractional flow (f_w) as a function of water saturation (S_w) and mobility ratio (M) [15]

A. T. Corey conducted a large number of experiments on relative permeabilities [115, 116]. He specified the relation between relative permeabilities and saturations with respect to capillary effects by the introduction of an exponent (κ), which influences the shape of the relative permeability curves. Relative permeabilities can be calculated as follows.

$$k_{rw}(S_w) = \left(\frac{S_w - S_{wi}}{1 - S_{wi} - S_{or}} \right)^{\kappa_w} * k_{rw}(S_{or}) \quad \text{Eq. A4-2}$$

$$k_{ro}(S_w) = \left(\frac{1 - S_w - S_{or}}{1 - S_{wi} - S_{or}} \right)^{\kappa_o} * k_{ro}(S_{wi}) \quad \text{Eq. A4-3}$$

$k_{rw}(S_w)$	–	relative permeability for water
S_w	–	water saturation
S_{wi}	–	irreducible water saturation
S_{or}	–	residual oil saturation
κ_w	–	<i>Corey</i> exponent for water
$k_{rw}(S_{or})$	–	relative permeability for water at residual oil saturation
$k_{ro}(S_w)$	–	relative permeability for oil
κ_o	–	<i>Corey</i> exponent for oil
$k_{ro}(S_{wi})$	–	relative permeability for oil at irreducible water saturation

The *Corey* factors typically range between 2 and 8, depending on the wettability of the porous medium (Table A4-1).

Table A4-1: *Corey* factors for water and oil for different wettability conditions [117]

	κ_o	κ_w
oil wet	6 – 8	2 – 3
slightly oil wet	2 – 6	2 – 4
slightly water wet	2 – 6	4 – 6
water wet	2 - 4	6 – 8

Relative permeability curves for water wet and oil wet conditions are shown in Figure A4-3.

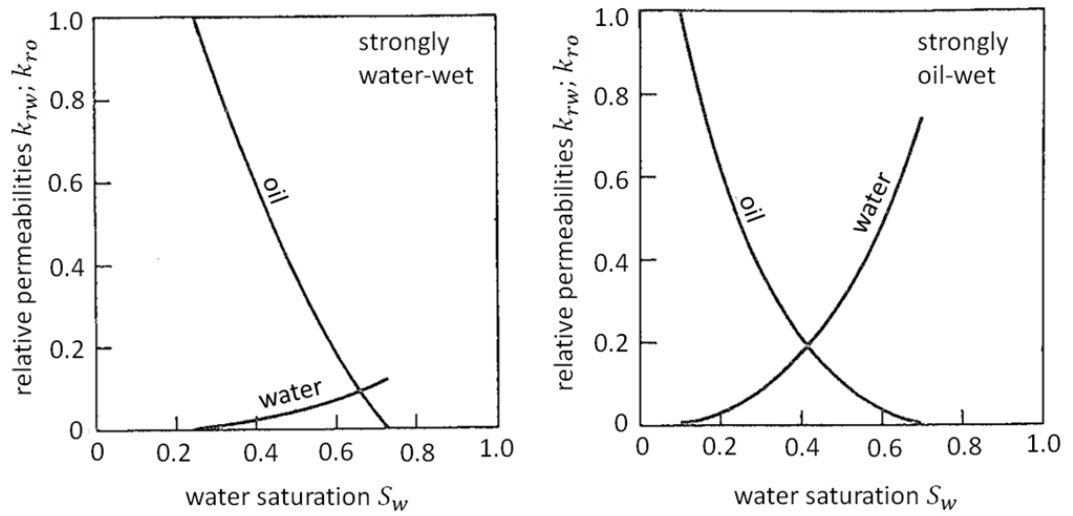


Figure A4-3: Typical relative permeability curves for strongly water-wet (left) and strongly oil-wet (right) conditions [114]

Table A4-2 shows critical values to define wettability from relative permeability curves (rules of thumb) [118].

Table A4-2: Values to define wettability from relative permeability curves [118]

	water-wet	oil-wet
S_{wc}	> 0.2	< 0.15
S_{or}	< 0.3	> 0.3
$S_w (k_{rw} = k_{ro})$	> 0.5	< 0.5
$k_{rw}(S_{or})$	< 0.3	> 0.5